

Quick Muonjets Write-up

Jim Pivarski

July 25, 2010

Contents

1	Introduction	1
1.1	Target signatures	2
2	Acceptance and efficiency	3
2.1	Acceptance region	3
2.2	Efficiency of track-reconstruction	3
2.3	Trigger efficiency	23
2.4	Efficiency of track cuts	32
2.5	Efficiency for displaced muon-jets	32
3	Grouping muons	45
3.1	Muon-grouping efficiency	45
3.2	Muon-jet merging	45
3.3	Extra muons in muon-jets	45
4	Backgrounds	53
4.1	Pair-pair mass constraint	58

1 Introduction

This is just for me to organize my own results. It's about physics results, not technical or framework issues (for that, see the twiki page:

<https://twiki.cern.ch/twiki/bin/view/CMS/ExoticaMuonJets>).

Definition: a “muon-jet” is a group of nearby muons produced by an as-yet undiscovered low-mass boson produced by a top-down decay accessible only in high collision energies (7 TeV). Due to their low mass and high boost, the muons from the decay of the new boson are typically close to each other. Examples: “dark photon” (γ_{dark}) inspired by the PAMELA result: $\gamma_{\text{dark}} \rightarrow \mu^+ \mu^-$ with a small opening angle, “dark higgs” (h_{dark}): $h_{\text{dark}} \rightarrow \gamma_{\text{dark}} \gamma_{\text{dark}} \rightarrow \mu^+ \mu^- \mu^+ \mu^-$ also with a small opening angle. Muon-jets are unrelated to hadronic jets or quark-gluon fragmentation.

FIXME: On second thought, eliminate all references to “muon-jet” and say “muon-group” instead. For 90% of the collaboration, “muon-jet” sounds like “muon-plus-jet” and would just be confusing.

1.1 Target signatures

We want to find beyond-the-Standard Model signatures with any of the following properties:

1. single muon-jet containing a large number of muons (at least 3): “mega-muon-jet”;
2. event with more than one muon-jet: “multi-muon-jet”;
3. muon jet accompanied by missing energy: “muon-jet plus missing energy”;
4. muon jet with a highly displaced vertex: “displaced muon-jet”.

These are different ways in which muon-jet physics can distinguish itself from background (including misreconstructed background). These signatures should be chosen such that they overlap, so that there are no artificial cracks in our search.

2 Acceptance and efficiency

2.1 Acceptance region

For a single muon-jet: $pT_2 > 5 \text{ GeV}/c$ and $|\eta_1| < 2.4$

For two muon-jets: $pT_4 > 5 \text{ GeV}/c$ and $|\eta_1| < 2.4$

2.2 Efficiency of track-reconstruction

GlobalMuons require StandAloneMuons

Overlapping muons in muon system can confuse StandAloneMuon-finding algorithm

GlobalMuon efficiency is less than or equal to StandAloneMuon efficiency, because the global algorithm requires a StandAloneMuon. This is not evident in the plots that require an MC match (because of the StandAloneMuon resolution), but it is evident in the plots that only require two reconstructed muons.

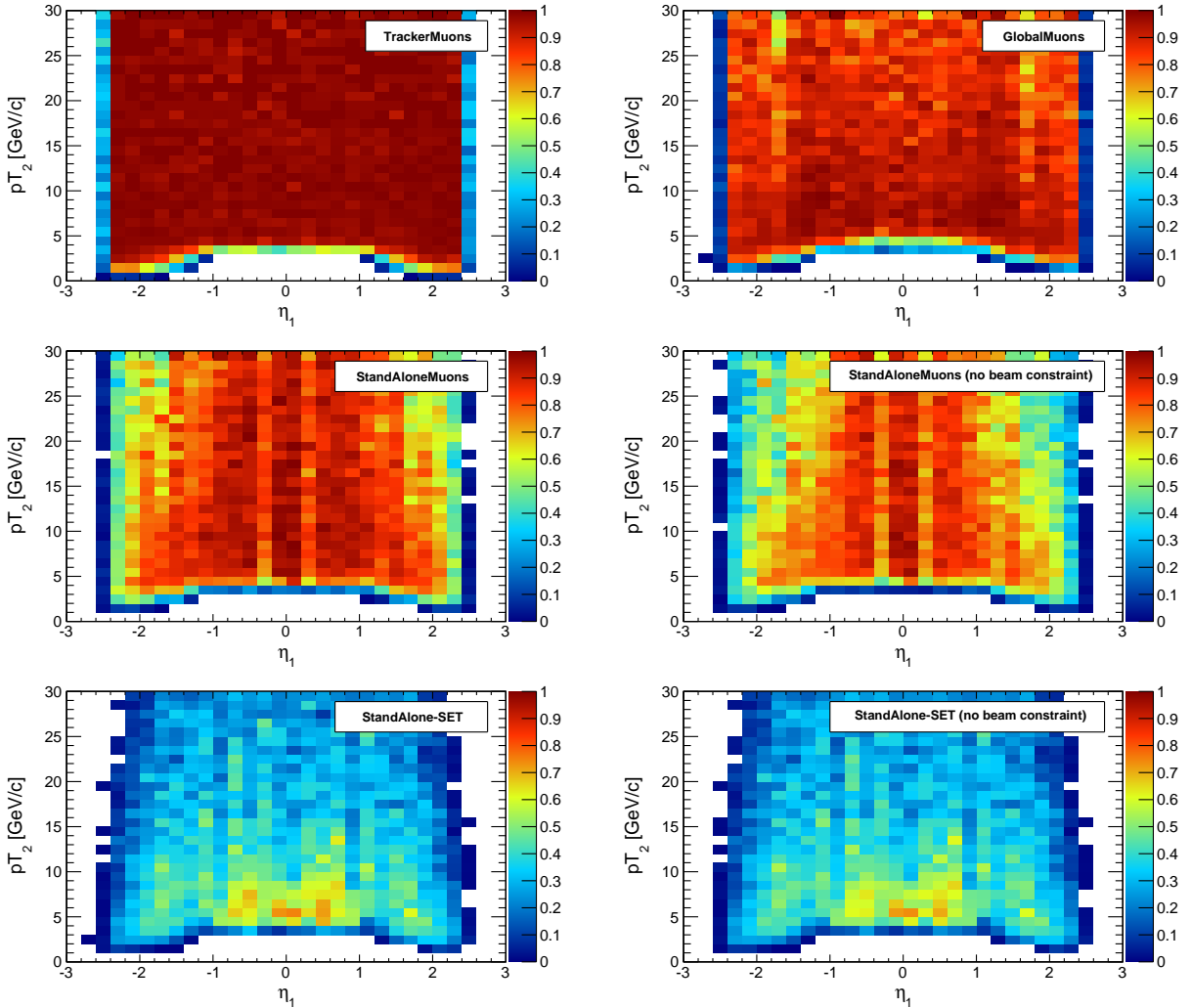


Figure 1: Acceptance region and efficiency for different reconstruction methods. pT_2 is the second-highest p_T muon in the event, η_1 is the largest-magnitude pseudorapidity in the event. Denominator: all generated events; numerator: reconstructed and MC-matched μ^+ and μ^- .

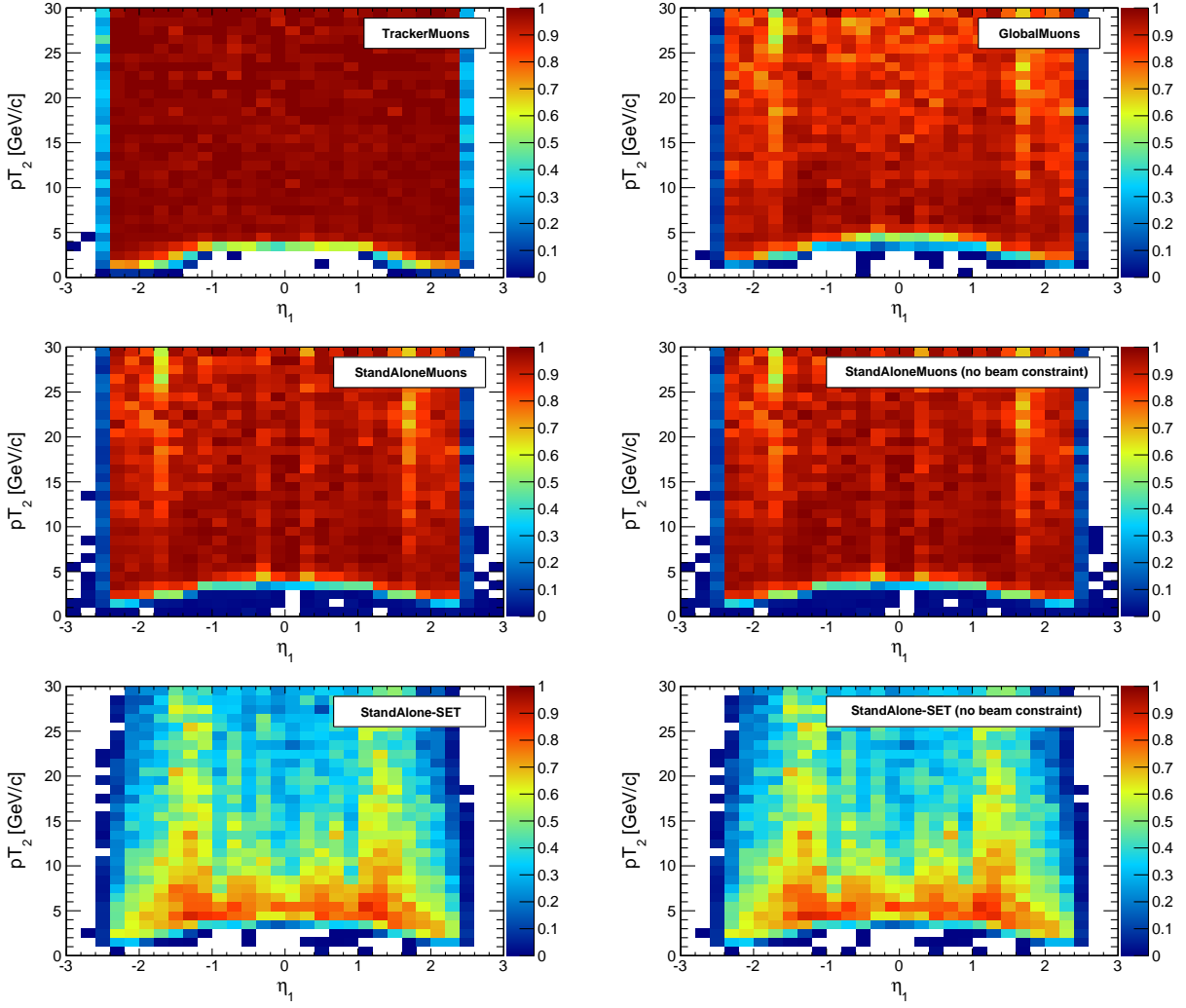


Figure 2: Same as Fig. 1, except that numerator only requires two reconstructed muons (no MC-matching).

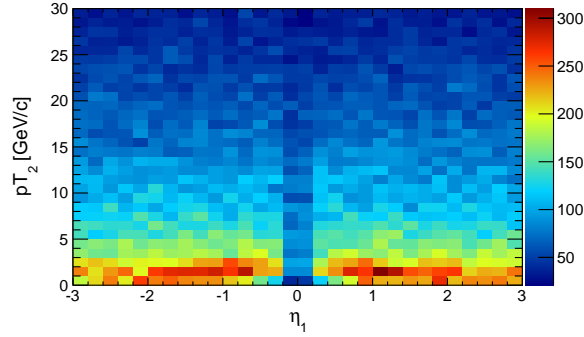


Figure 3: Denominator of Figs. 1 and 2.

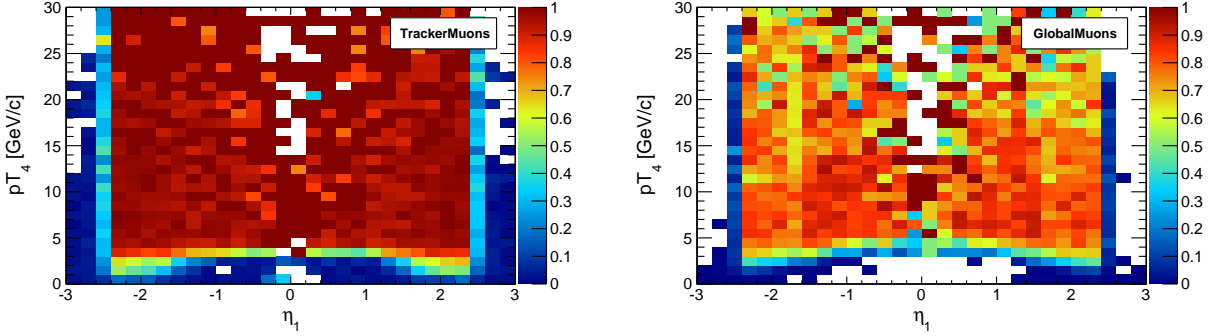


Figure 4: Acceptance region and efficiency for four muons. pT_4 is the fourth-highest p_T muon in the event, η_1 is the largest-magnitude pseudorapidity in the event. Denominator: all generated events; numerator: events with four reconstructed muons.

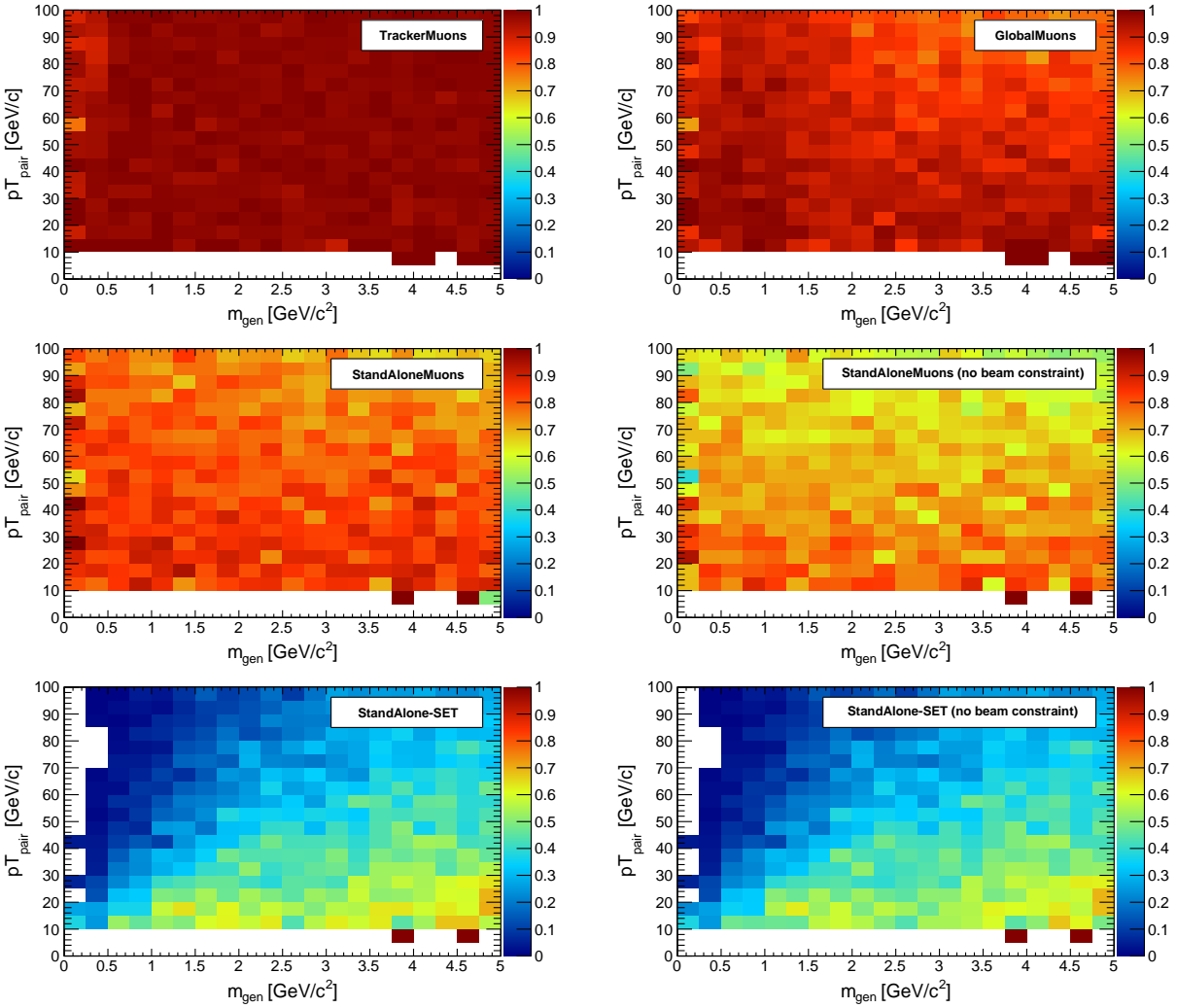


Figure 5: Efficiency as a function of physics-relevant variables: p_T and invariant mass of the $\mu^+ - \mu^-$ pair. Denominator: generated events with $pT_2 > 5 \text{ GeV}/c$ and $|\eta_1| < 2.4$; numerator: reconstructed and MC-matched μ^+ and μ^- .

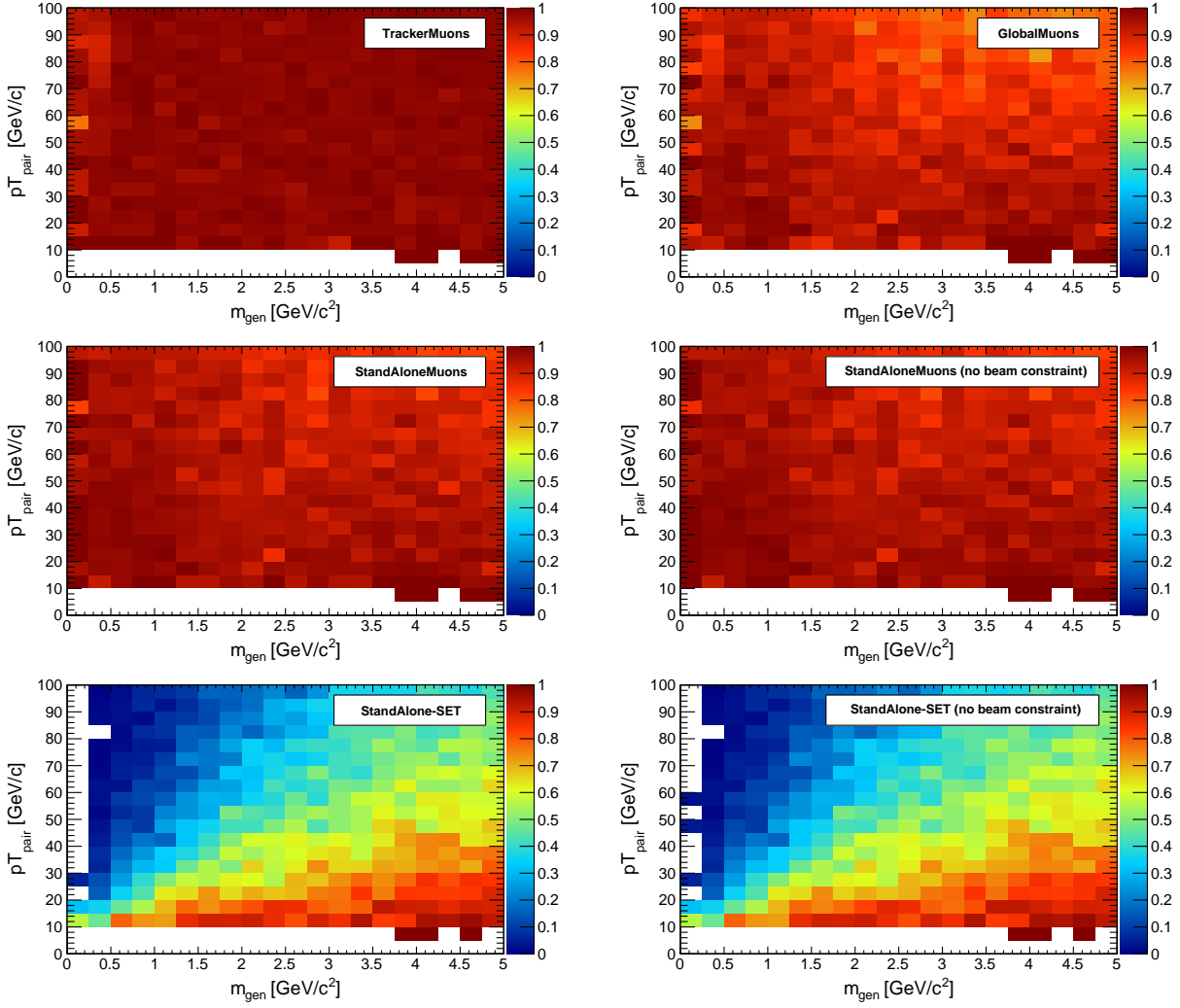


Figure 6: Same as Fig. 5, except that numerator only requires two reconstructed muons (no MC-matching).

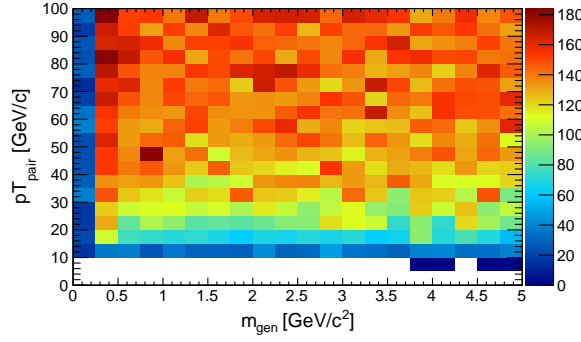


Figure 7: Denominator of plots in Figs. 5 and 6.

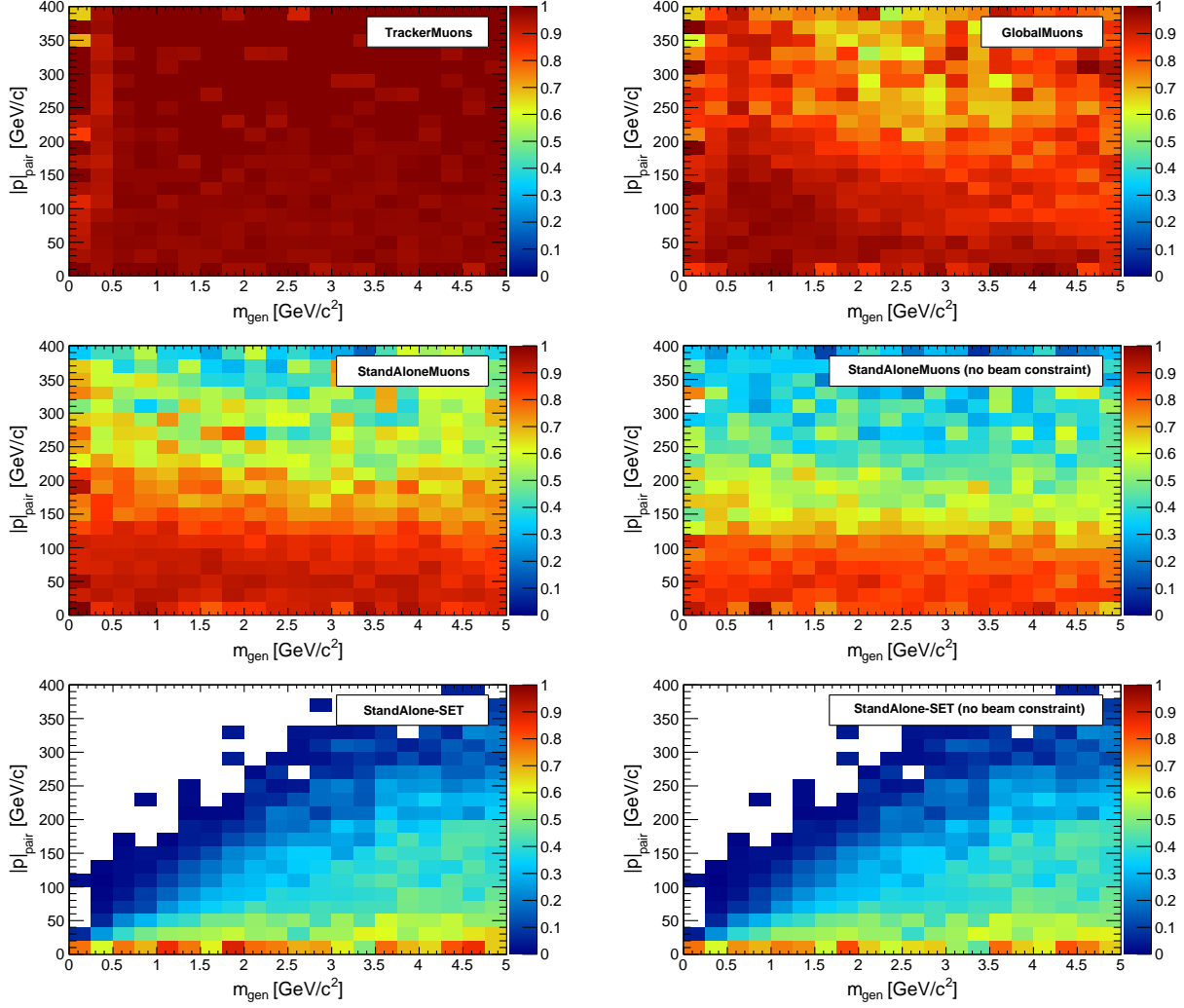


Figure 8: Efficiency as a function of physics-relevant variables: $|\vec{p}|$ and invariant mass of the $\mu^+ \mu^-$ pair. Denominator: generated events with $pT_2 > 5$ GeV/c and $|\eta_1| < 2.4$; numerator: reconstructed and MC-matched μ^+ and μ^- . **FIXME: Vadim recommends higher range in $|\vec{p}|$, say 400 GeV/c.**

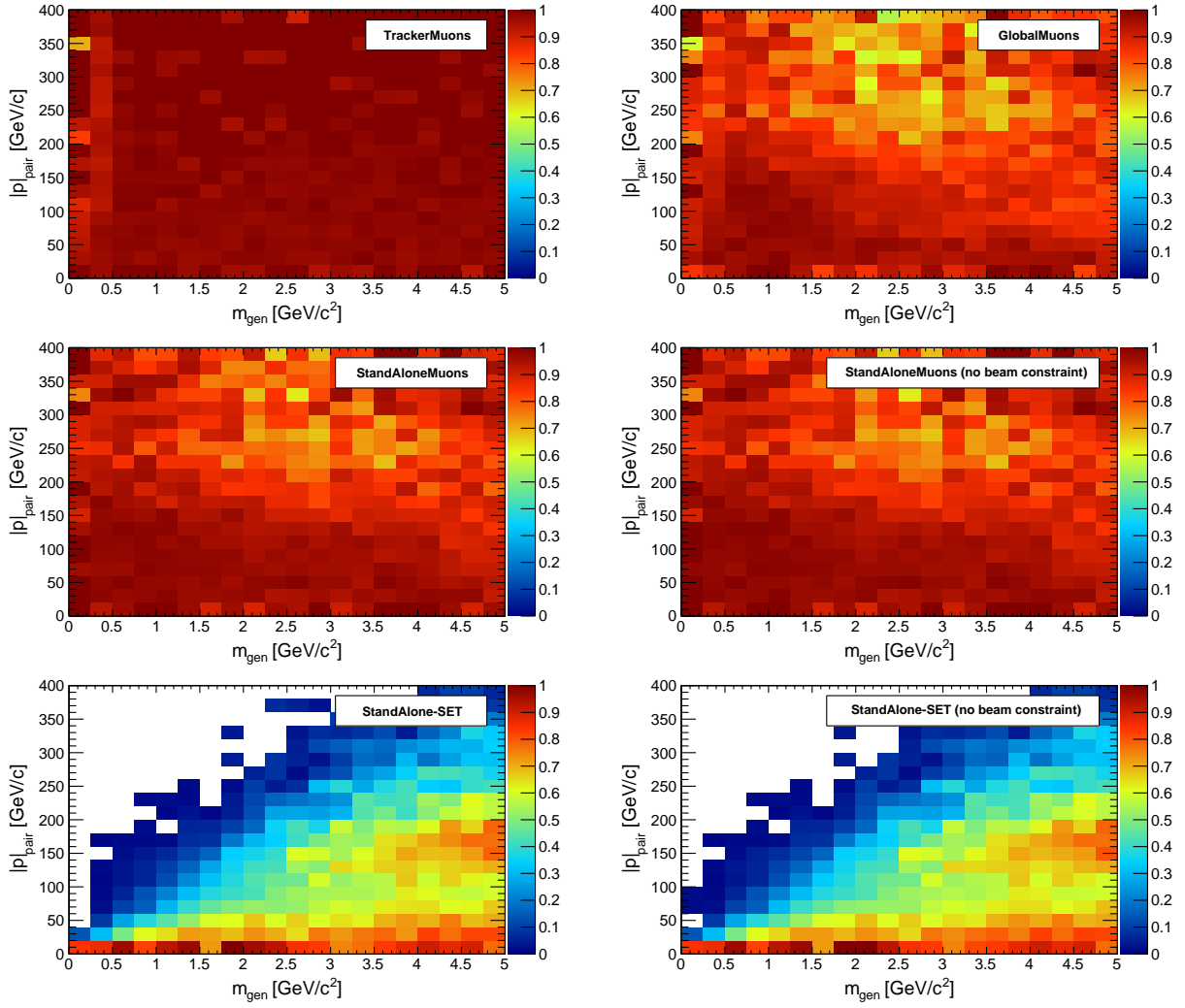


Figure 9: Same as Fig. 8, except that numerator only requires two reconstructed muons (no MC-matching).

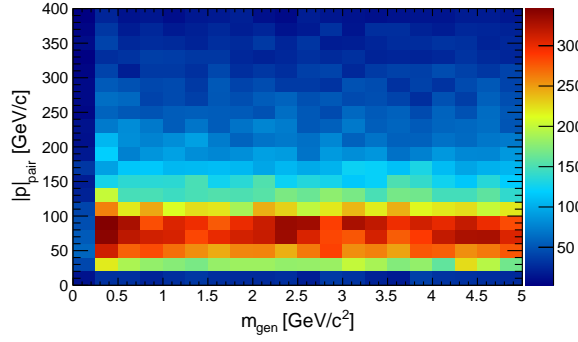


Figure 10: Denominator of plots in Figs. 8 and 9.

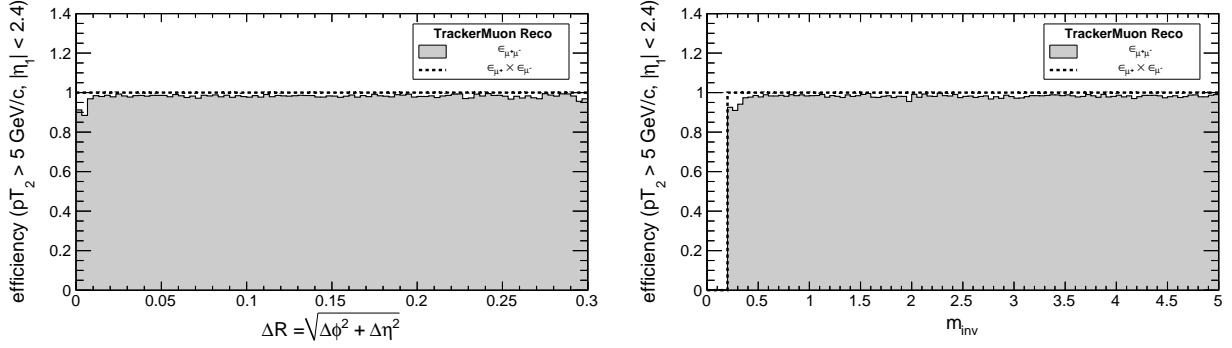


Figure 11: Reconstruction efficiency of TrackerMuons as a function of separation, compared with the product of efficiencies for the μ^+ and μ^- alone.

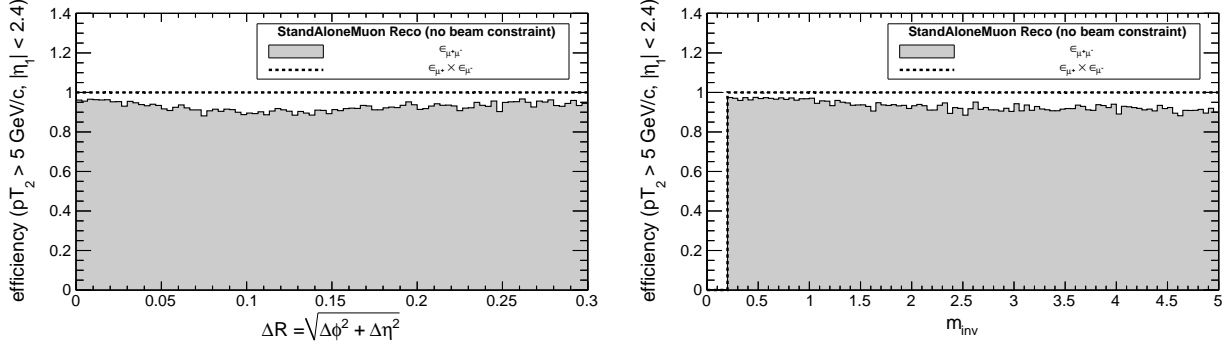


Figure 12: Reconstruction efficiency of StandAloneMuons (no beamline constraint) as a function of separation, compared with the product of efficiencies for the μ^+ and μ^- alone.

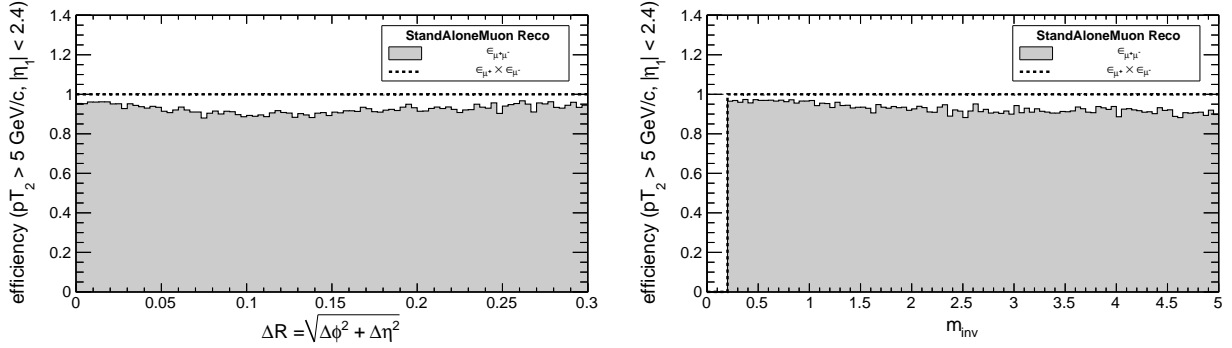


Figure 13: Reconstruction efficiency of StandAloneMuons (with beamline constraint) as a function of separation, compared with the product of efficiencies for the μ^+ and μ^- alone.

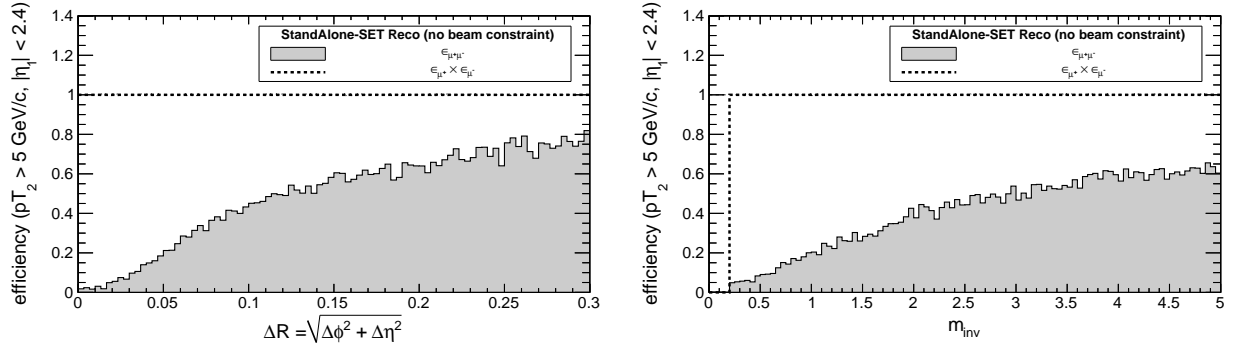


Figure 14: Reconstruction efficiency of StandAlone-SET muons (no beamline constraint) as a function of separation, compared with the product of efficiencies for the μ^+ and μ^- alone.

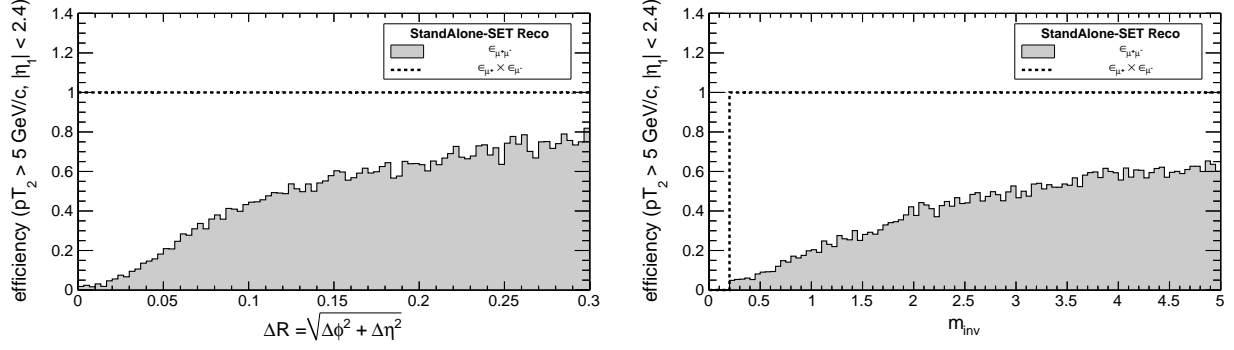


Figure 15: Reconstruction efficiency of StandAlone-SET muons (with beamline constraint) as a function of separation, compared with the product of efficiencies for the μ^+ and μ^- alone.

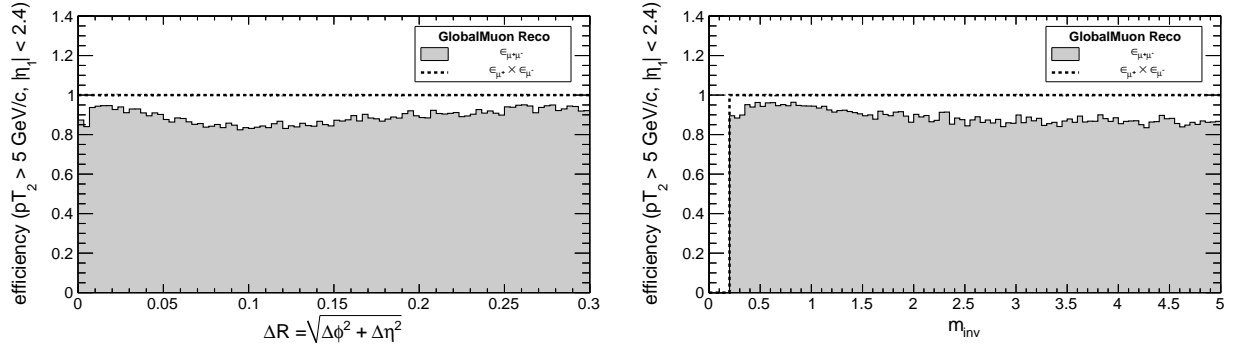


Figure 16: Reconstruction efficiency of GlobalMuons as a function of separation, compared with the product of efficiencies for the μ^+ and μ^- alone.

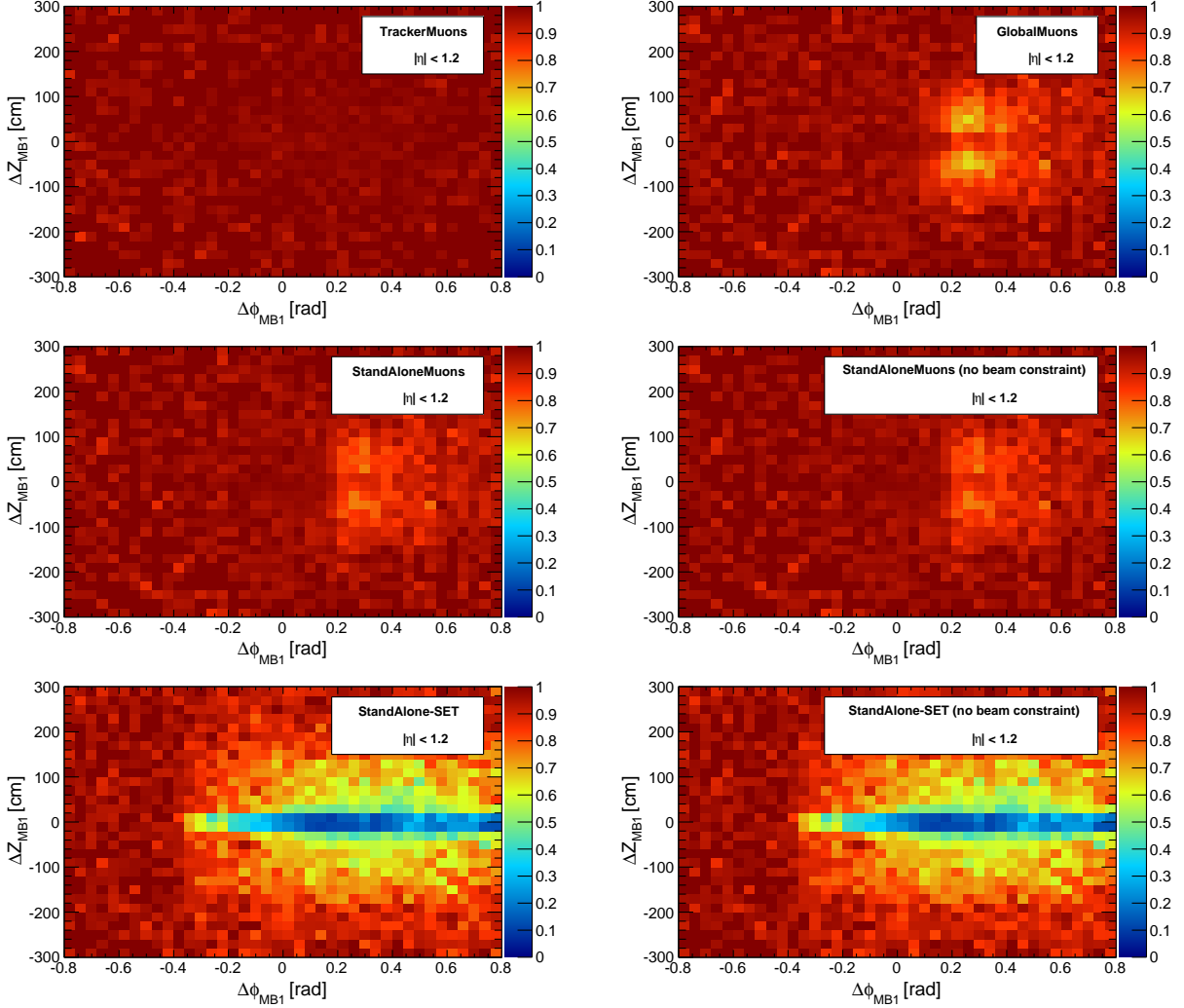


Figure 17: Efficiency as a function of crossing in muon barrel station 1: $\Delta\phi_{MB1}$ and ΔZ_{MB1} are the azimuthal separation angle and longitudinal separation distance of the generator-level muon trajectories on a beam-aligned cylindrical surface with radius 432.946 cm (μ^+ minus μ^-). Denominator: generated events with $pT_2 > 5$ GeV/c and $|\eta_1| < 2.4$ (mass ranges up to 50 GeV/c²); numerator: reconstructed μ^+ and μ^- . **FIXME: Barrel StandAlone/GlobalMuon inefficiencies are always off-center— could this be an indication that the point of confusion in $|\eta| < 1.0$ is not in the muon chambers but somewhere nearby? It looks like an image out-of-focus, like you overshot the location that drives the inefficiency.**

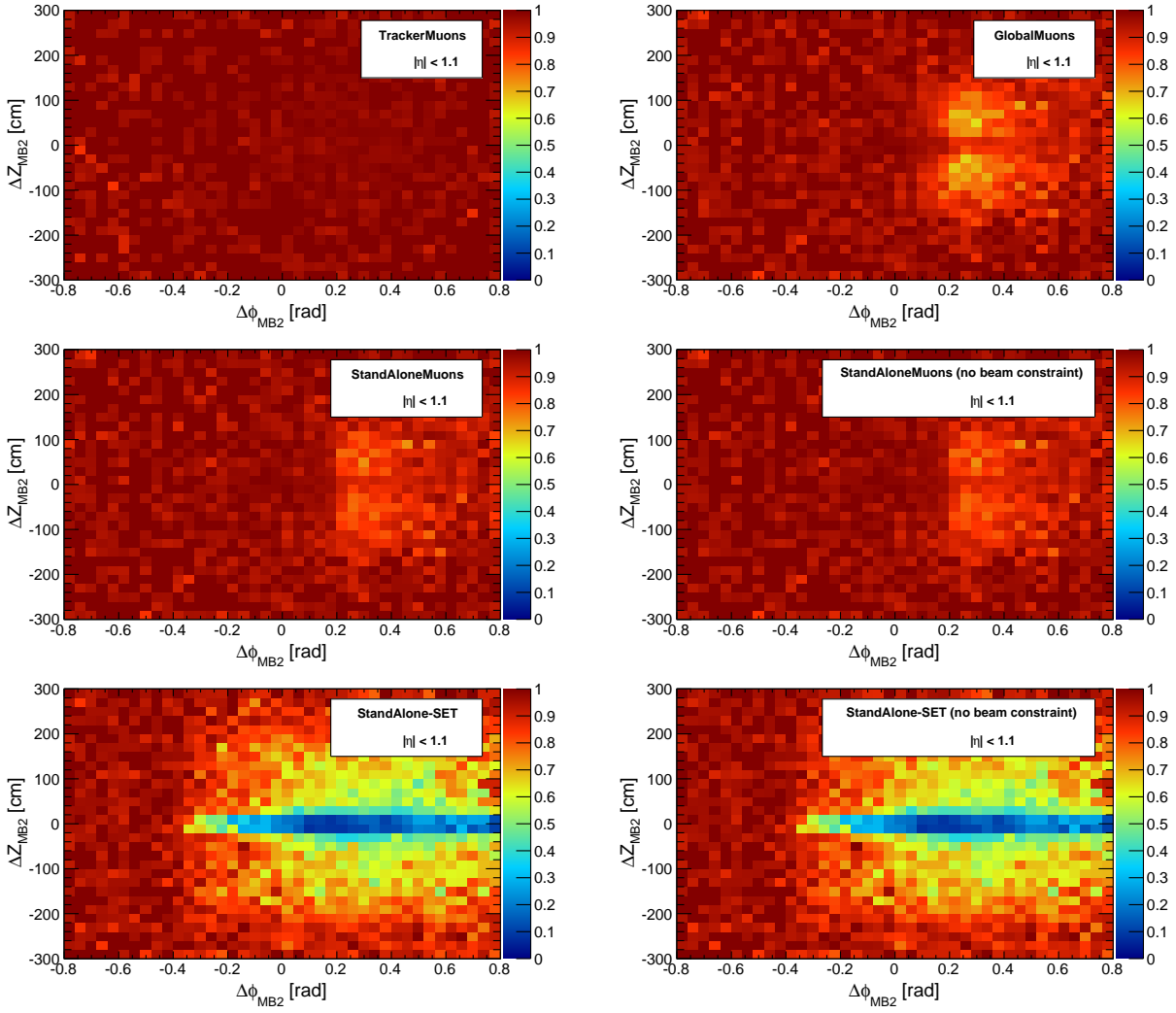


Figure 18: Efficiency as a function of crossing in muon barrel station 2: $\Delta\phi_{MB2}$ and ΔZ_{MB2} are the azimuthal separation angle and longitudinal separation distance of the generator-level muon trajectories on a beam-aligned cylindrical surface with radius 512.923 cm (μ^+ minus μ^-). Denominator: generated events with $pT_2 > 5 \text{ GeV}/c$ and $|\eta_1| < 2.4$ (mass ranges up to $50 \text{ GeV}/c^2$); numerator: reconstructed μ^+ and μ^- .

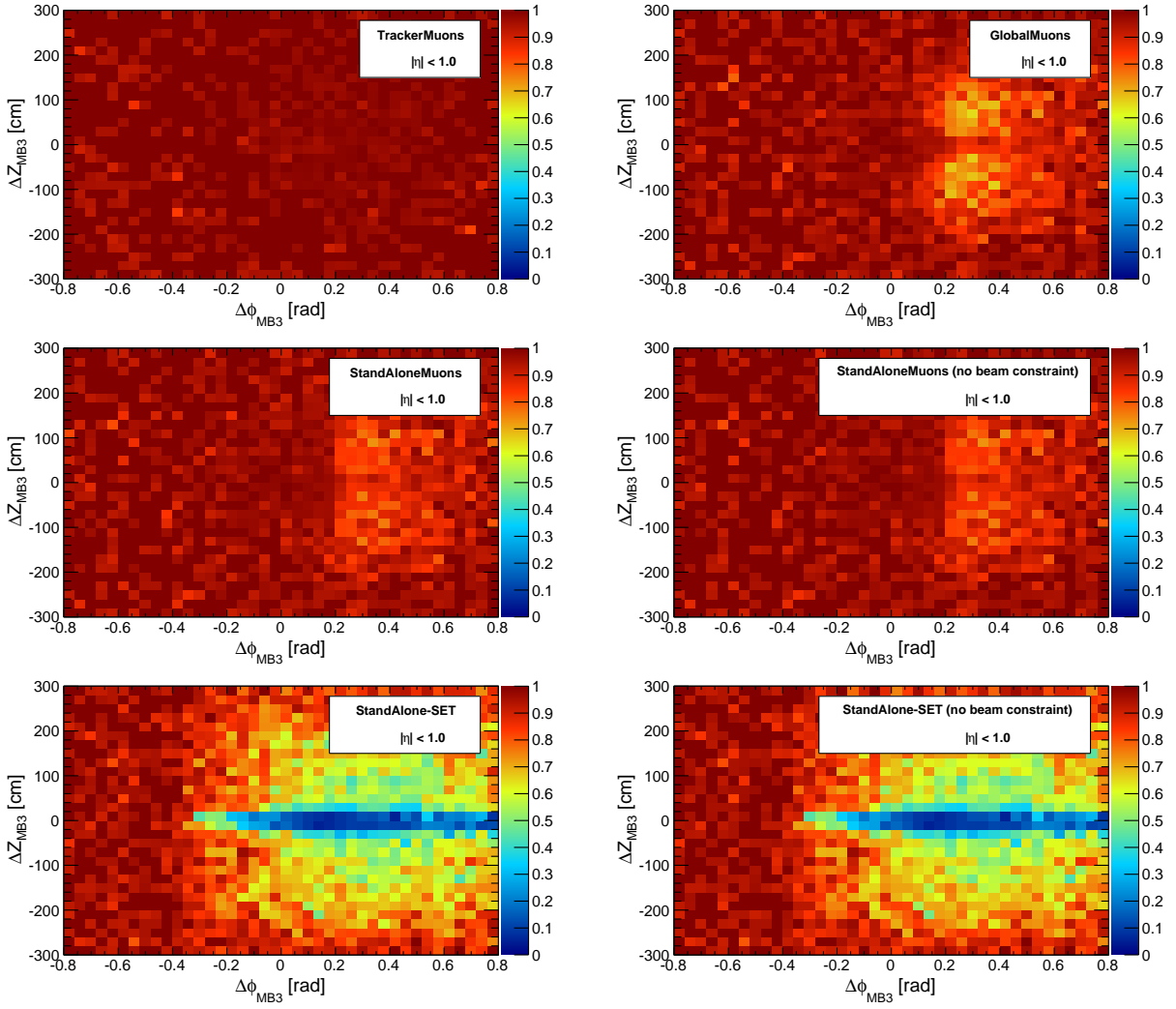


Figure 19: Efficiency as a function of crossing in muon barrel station 3: $\Delta\phi_{MB3}$ and ΔZ_{MB3} are the azimuthal separation angle and longitudinal separation distance of the generator-level muon trajectories on a beam-aligned cylindrical surface with radius 618.269 cm (μ^+ minus μ^-). Denominator: generated events with $pT_2 > 5 \text{ GeV}/c$ and $|\eta_1| < 2.4$ (mass ranges up to $50 \text{ GeV}/c^2$); numerator: reconstructed μ^+ and μ^- .

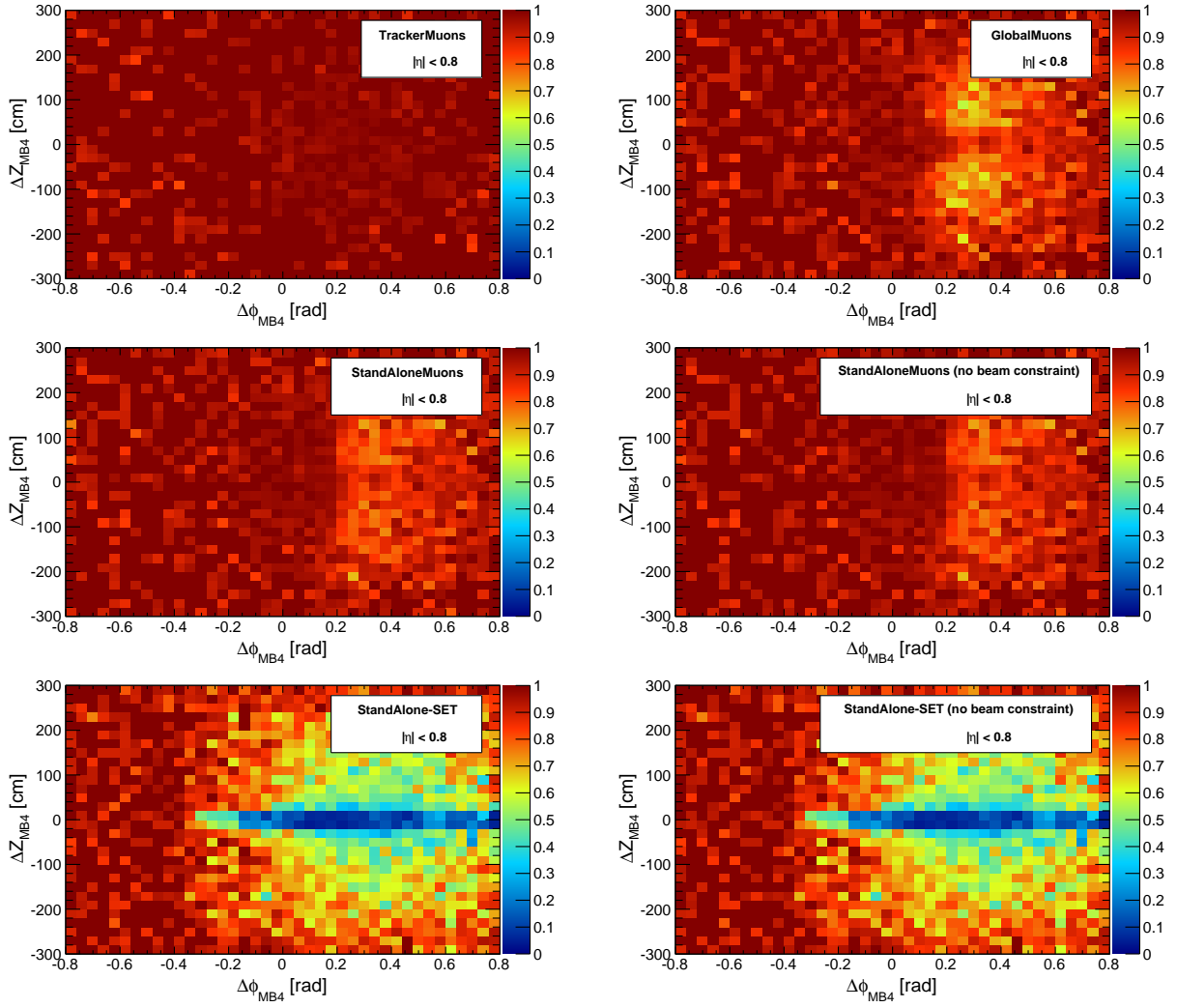


Figure 20: Efficiency as a function of crossing in muon barrel station 4: $\Delta\phi_{MB4}$ and ΔZ_{MB4} are the azimuthal separation angle and longitudinal separation distance of the generator-level muon trajectories on a beam-aligned cylindrical surface with radius 726.425 cm (μ^+ minus μ^-). Denominator: generated events with $pT_2 > 5$ GeV/c and $|\eta_1| < 2.4$ (mass ranges up to 50 GeV/c²); numerator: reconstructed μ^+ and μ^- .

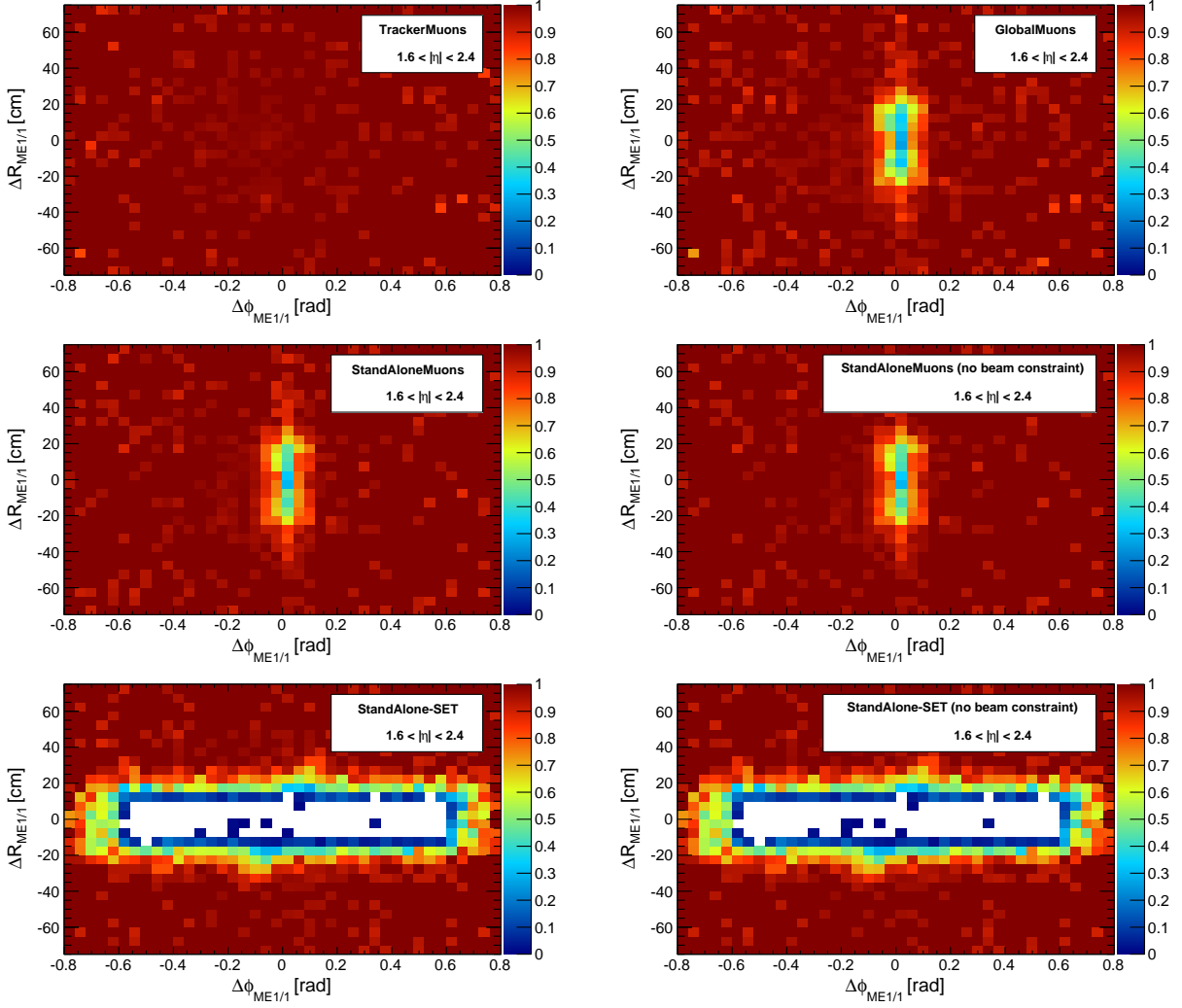


Figure 21: Efficiency as a function of crossing in muon endcap station ME1/1: $\Delta\phi_{ME1/1}$ and $\Delta R_{ME1/1}$ are the azimuthal separation angle and radial separation distance of the generator-level muon trajectories on a plane transverse to the beamline at ± 602.3 cm (μ^+ minus μ^-). Denominator: generated events with $pT_2 > 5$ GeV/c and $|\eta_1| < 2.4$ (mass ranges up to 50 GeV/ c^2); numerator: reconstructed μ^+ and μ^- . **FIXME: Aysen recommends a different symbol than “ ΔR ”.**

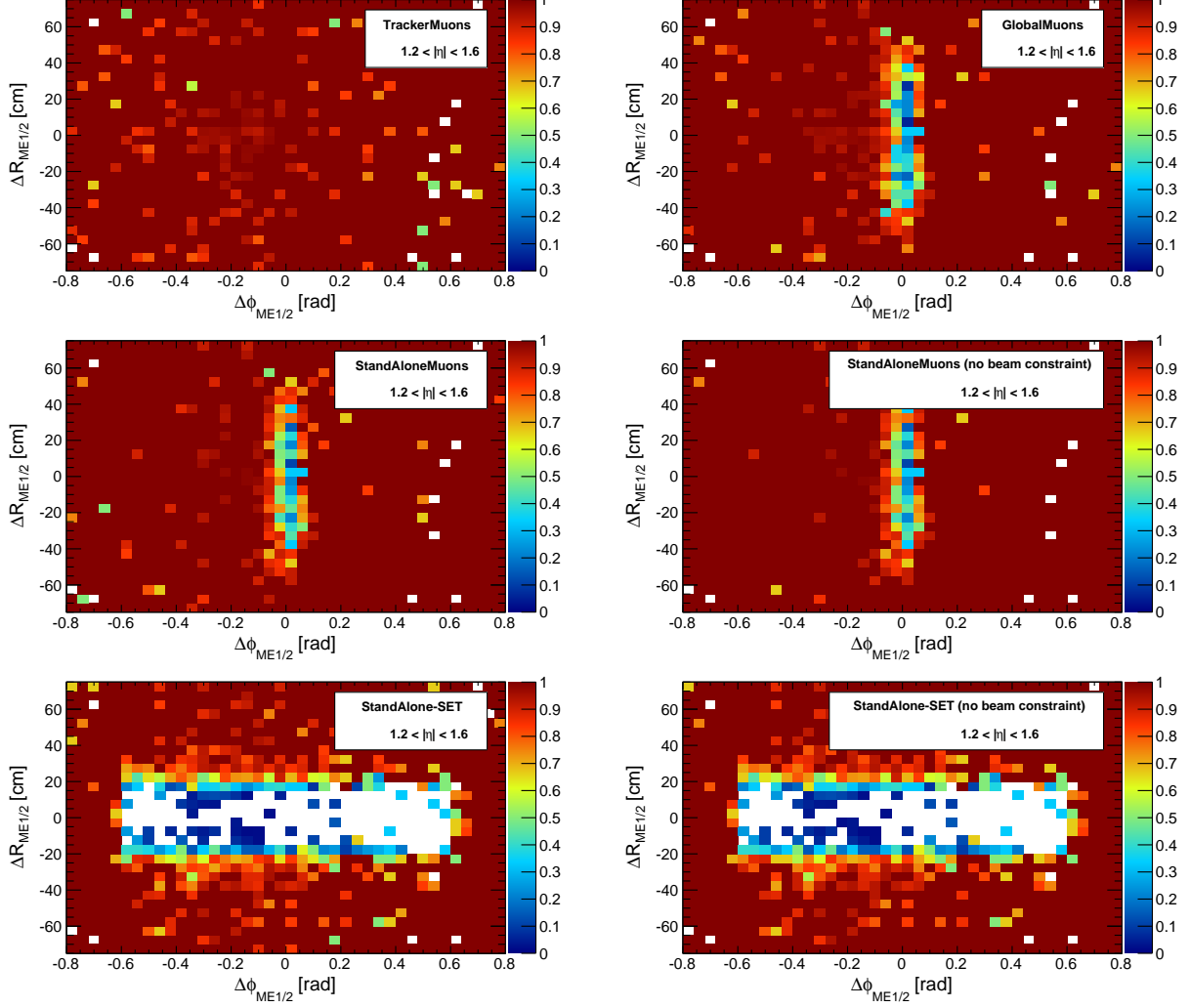


Figure 22: Efficiency as a function of crossing in muon endcap station ME1/2: $\Delta\phi_{ME1/2}$ and $\Delta R_{ME1/2}$ are the azimuthal separation angle and radial separation distance of the generator-level muon trajectories on a plane transverse to the beamline at ± 699.061 cm (μ^+ minus μ^-). Denominator: generated events with $pT_2 > 5$ GeV/c and $|\eta_1| < 2.4$ (mass ranges up to 50 GeV/c²); numerator: reconstructed μ^+ and μ^- .

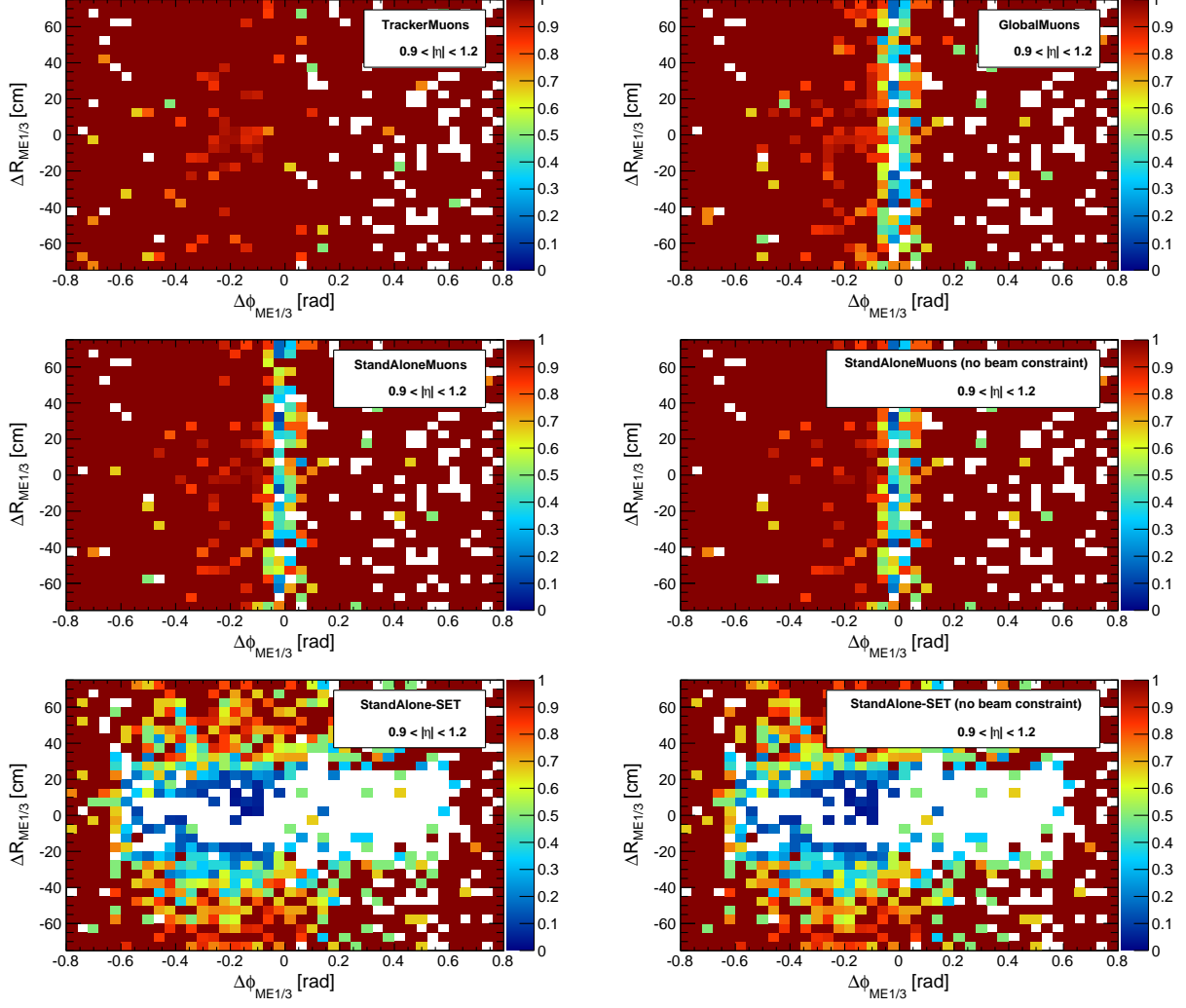


Figure 23: Efficiency as a function of crossing in muon endcap station ME1/3: $\Delta\phi_{ME1/3}$ and $\Delta R_{ME1/3}$ are the azimuthal separation angle and radial separation distance of the generator-level muon trajectories on a plane transverse to the beamline at ± 695.159 cm (μ^+ minus μ^-). Denominator: generated events with $pT_2 > 5$ GeV/c and $|\eta_1| < 2.4$ (mass ranges up to 50 GeV/ c^2); numerator: reconstructed μ^+ and μ^- .

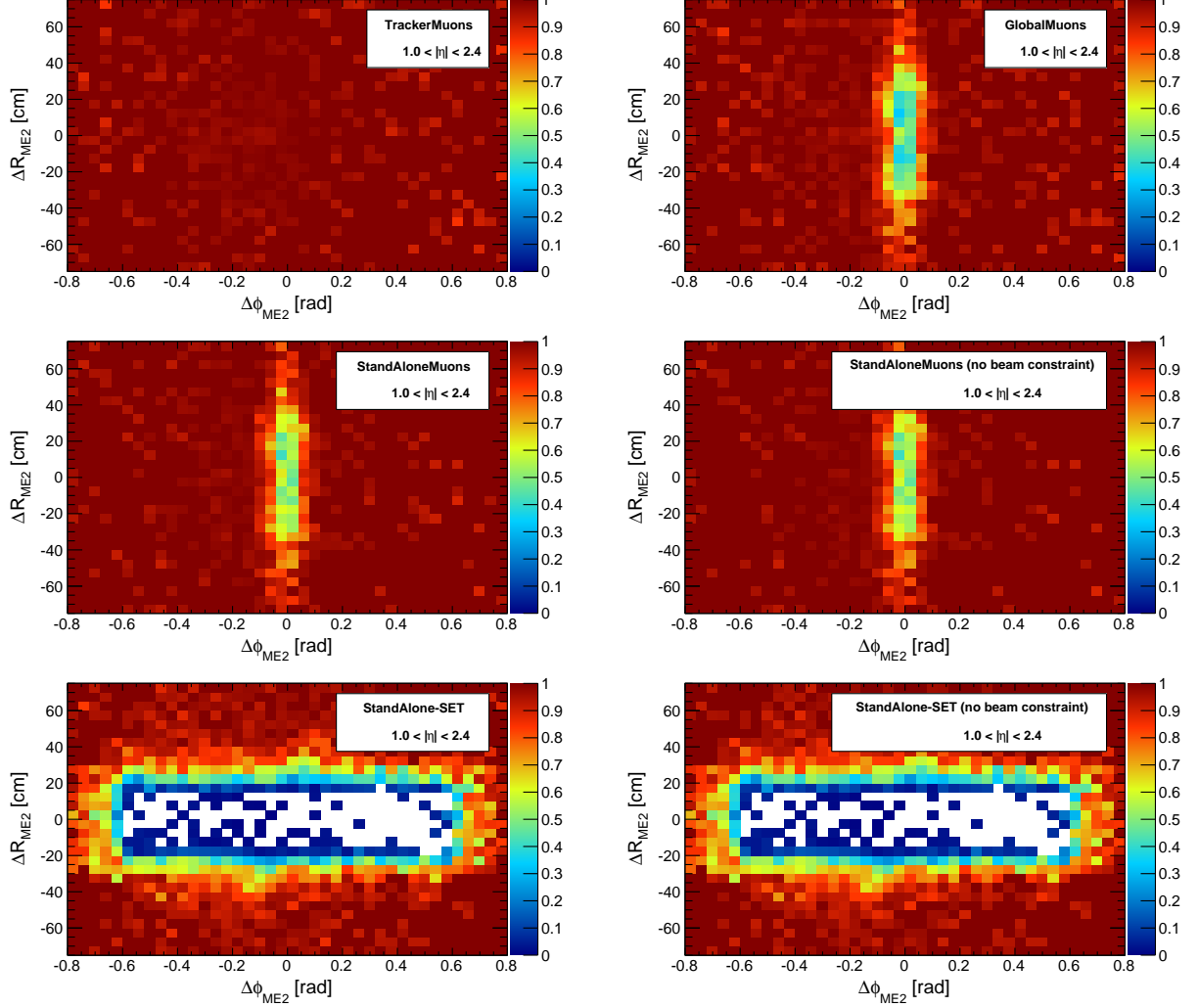


Figure 24: Efficiency as a function of crossing in muon endcap station ME2: $\Delta\phi_{ME2}$ and ΔR_{ME2} are the azimuthal separation angle and radial separation distance of the generator-level muon trajectories on a plane transverse to the beamline at ± 828.561 cm (μ^+ minus μ^-). Denominator: generated events with $pT_2 > 5$ GeV/c and $|\eta_1| < 2.4$ (mass ranges up to 50 GeV/c²); numerator: reconstructed μ^+ and μ^- .

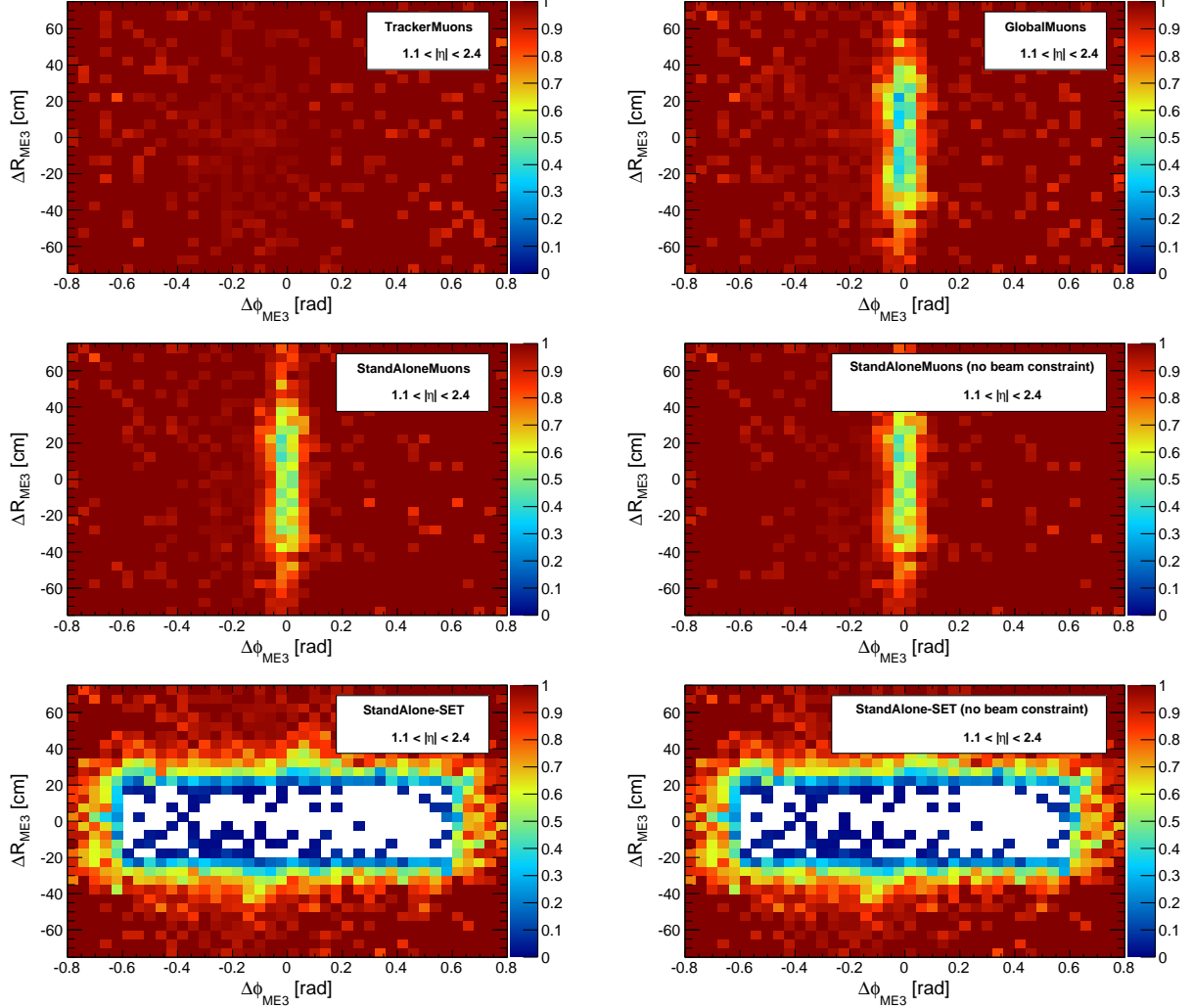


Figure 25: Efficiency as a function of crossing in muon endcap station ME3: $\Delta\phi_{ME3}$ and ΔR_{ME3} are the azimuthal separation angle and radial separation distance of the generator-level muon trajectories on a plane transverse to the beamline at ± 935.439 cm (μ^+ minus μ^-). Denominator: generated events with $pT_2 > 5$ GeV/c and $|\eta_1| < 2.4$ (mass ranges up to 50 GeV/c²); numerator: reconstructed μ^+ and μ^- .

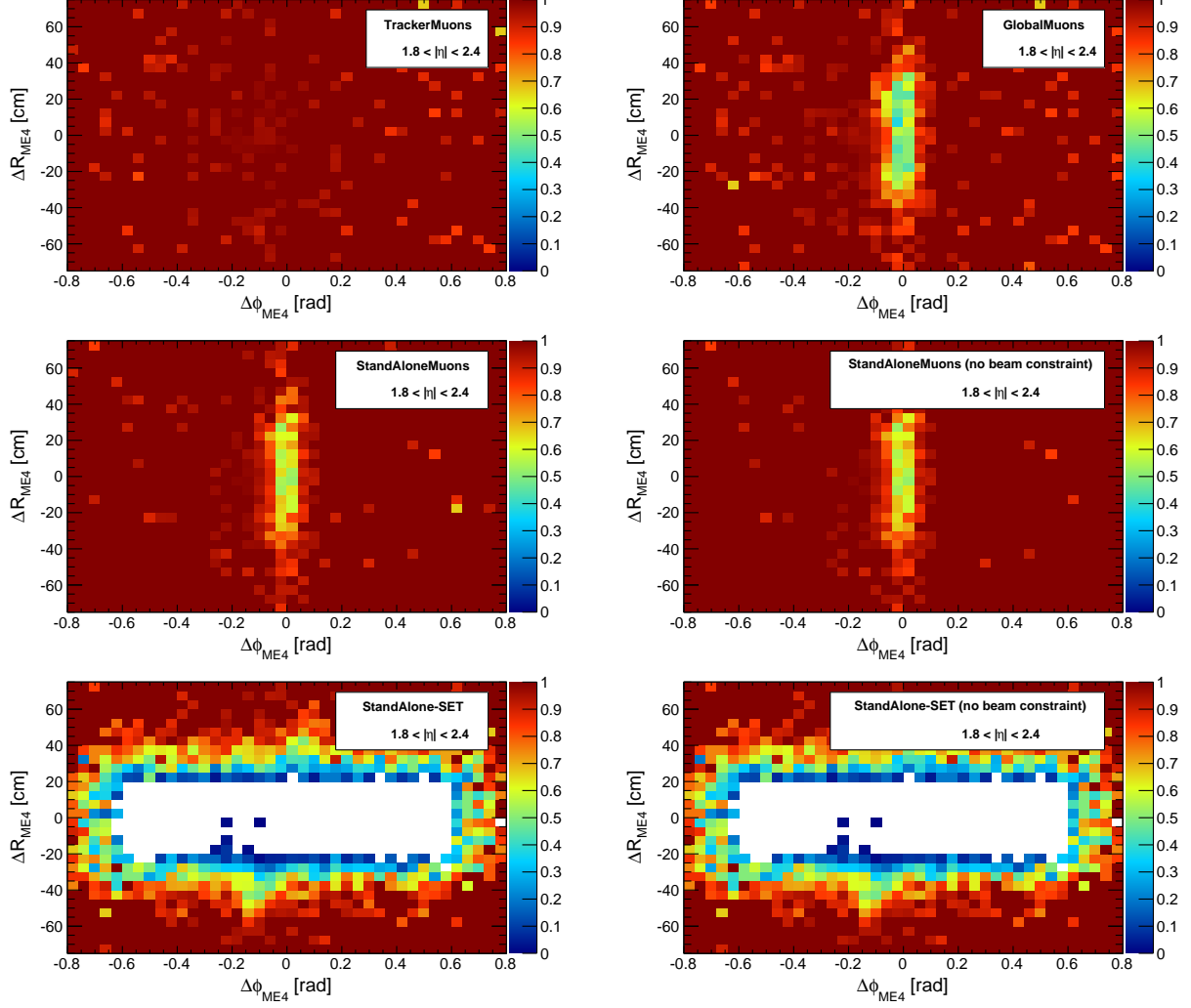


Figure 26: Efficiency as a function of crossing in muon endcap station ME4: $\Delta\phi_{ME4}$ and ΔR_{ME4} are the azimuthal separation angle and radial separation distance of the generator-level muon trajectories on a plane transverse to the beamline at ± 1024.94 cm (μ^+ minus μ^-). Denominator: generated events with $pT_2 > 5$ GeV/c and $|\eta_1| < 2.4$ (mass ranges up to 50 GeV/c²); numerator: reconstructed μ^+ and μ^- .

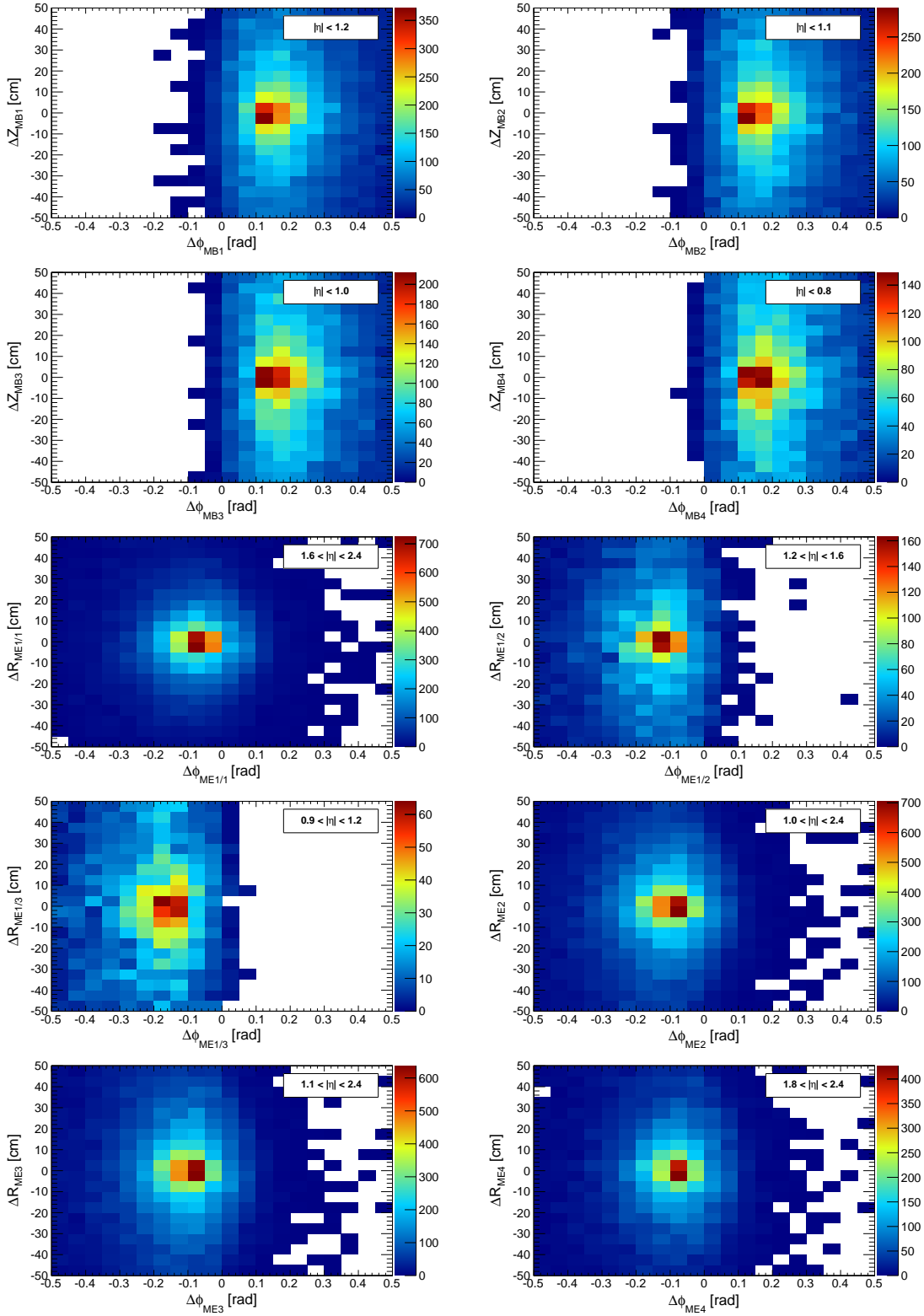


Figure 27: Distribution of muon system crossings for a uniform $0.212\text{--}6 \text{ GeV}/c^2$ mass, $0\text{--}100 \text{ GeV}/c$ muon-pair p_T , and muon-pair $|\eta| < 2.4$ sample.

2.3 Trigger efficiency

FIXME: In addition to trigger efficiency vs. p_T , show trigger efficiency vs. η .

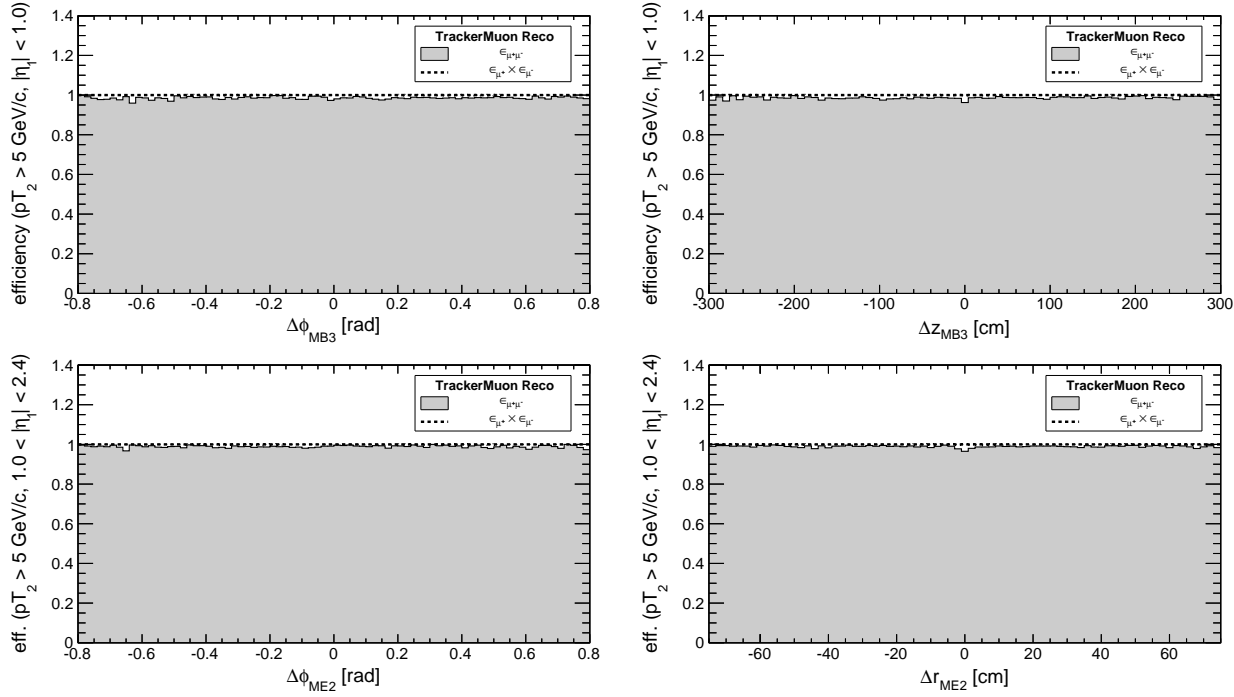


Figure 28: Efficiency as a function of crossing point in muon system for TrackerMuons, compared to product of efficiencies of finding μ^+ and μ^- alone; c.f. Figs 19, 24.

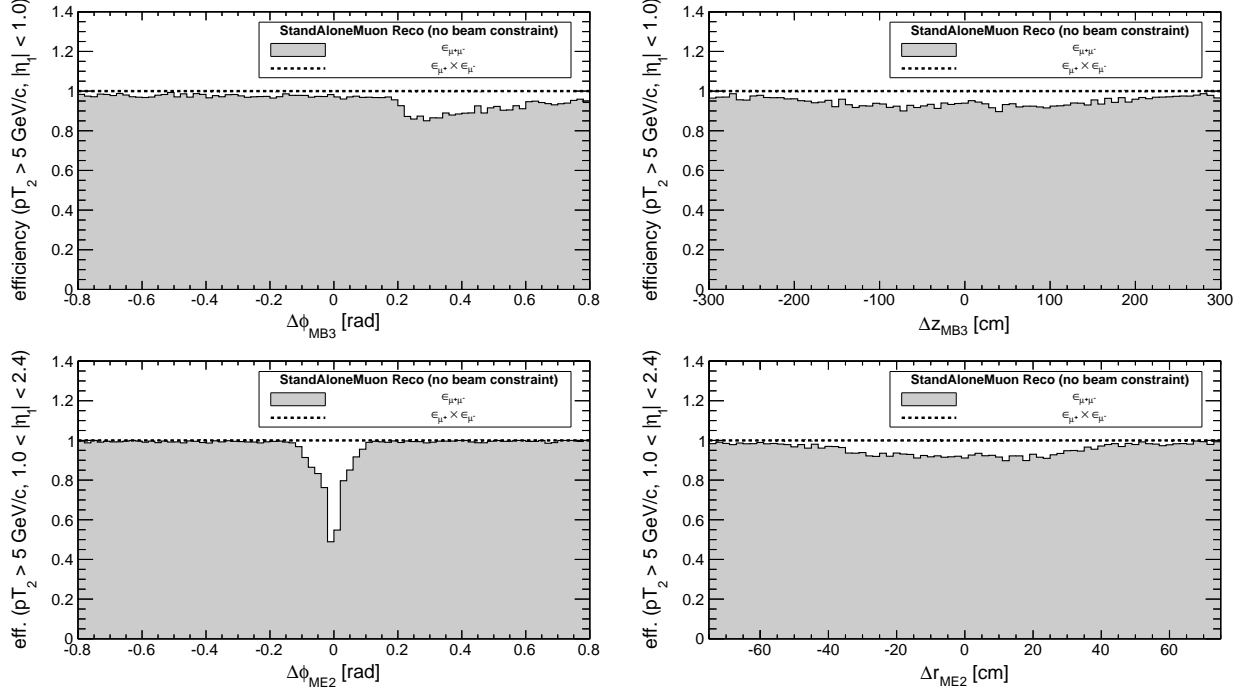


Figure 29: Efficiency as a function of crossing point in muon system for StandAloneMuons (no beamline constraint), compared to product of efficiencies of finding μ^+ and μ^- alone; c.f. Figs 19, 24.

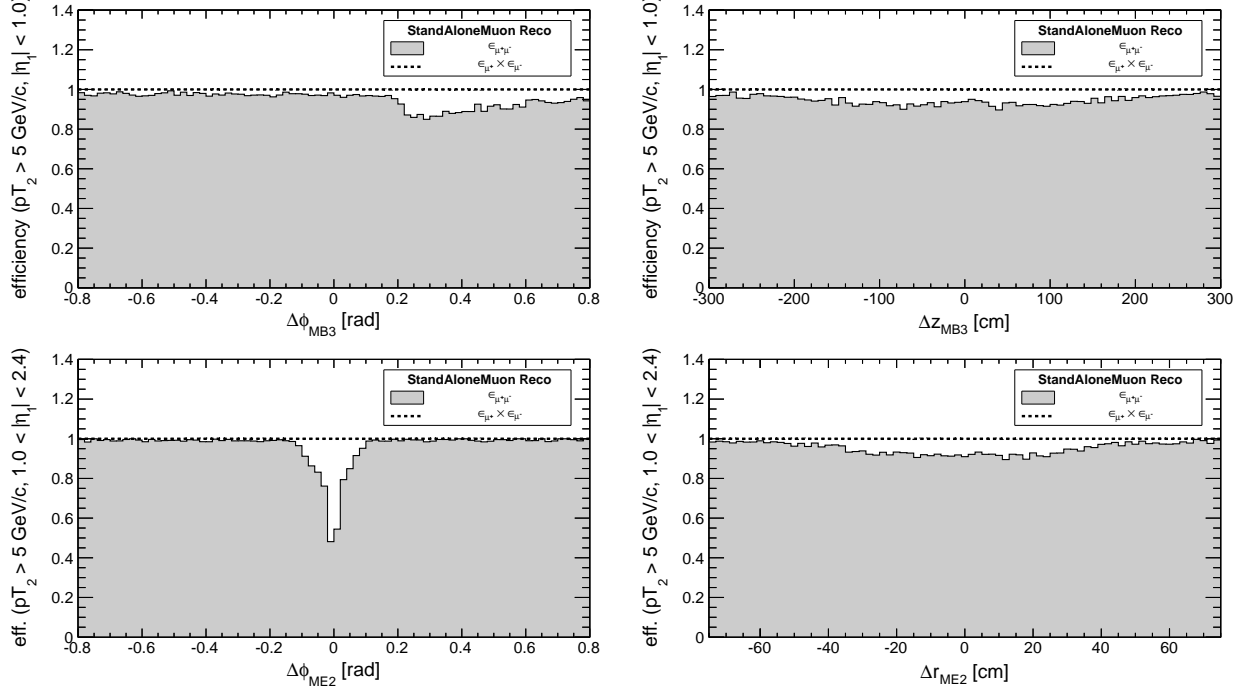


Figure 30: Efficiency as a function of crossing point in muon system for StandAloneMuons (with beamline constraint), compared to product of efficiencies of finding μ^+ and μ^- alone; c.f. Figs 19, 24.

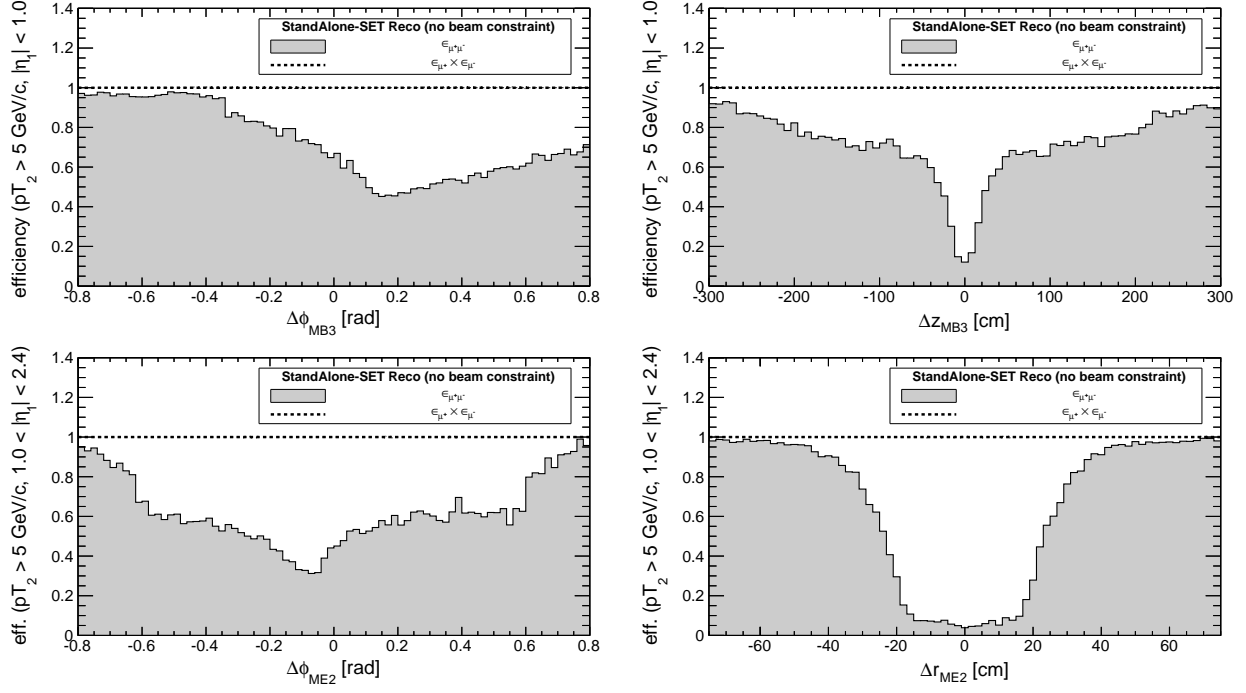


Figure 31: Efficiency as a function of crossing point in muon system for StandAlone-SET muons (no beamline constraint), compared to product of efficiencies of finding μ^+ and μ^- alone; c.f. Figs 19, 24.

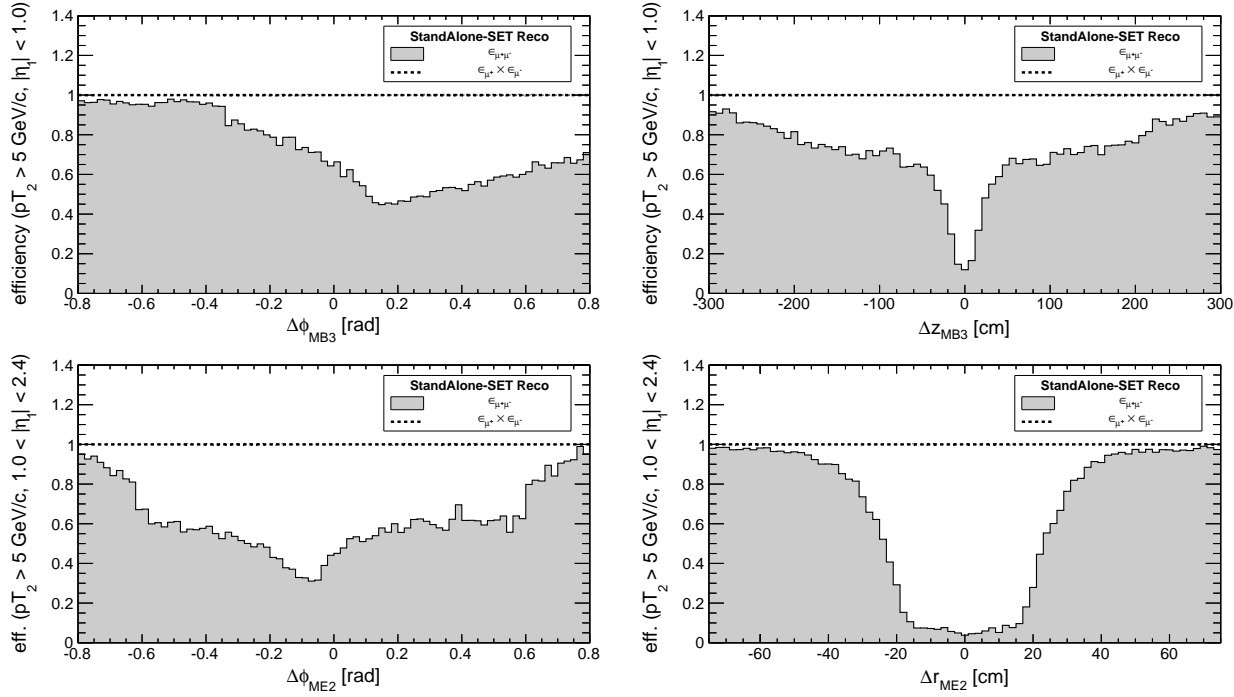


Figure 32: Efficiency as a function of crossing point in muon system for StandAlone-SET muons (with beamline constraint), compared to product of efficiencies of finding μ^+ and μ^- alone; c.f. Figs 19, 24.

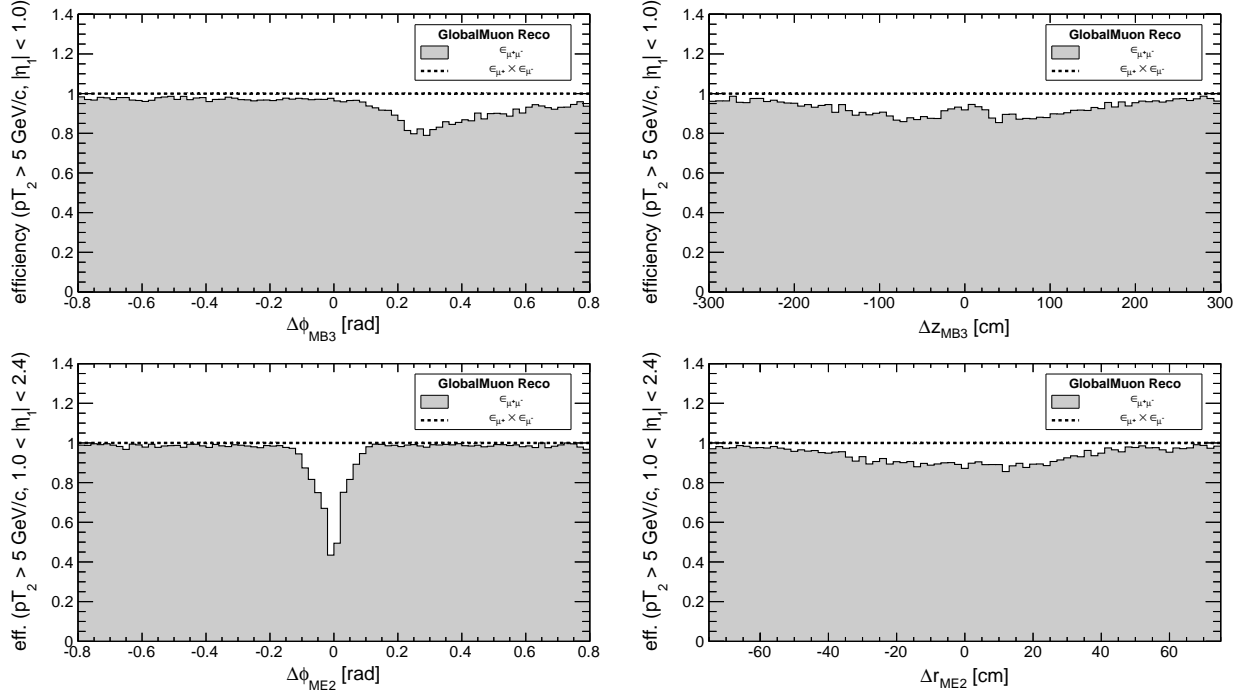


Figure 33: Efficiency as a function of crossing point in muon system for GlobalMuons, compared to product of efficiencies of finding μ^+ and μ^- alone; c.f. Figs 19, 24.

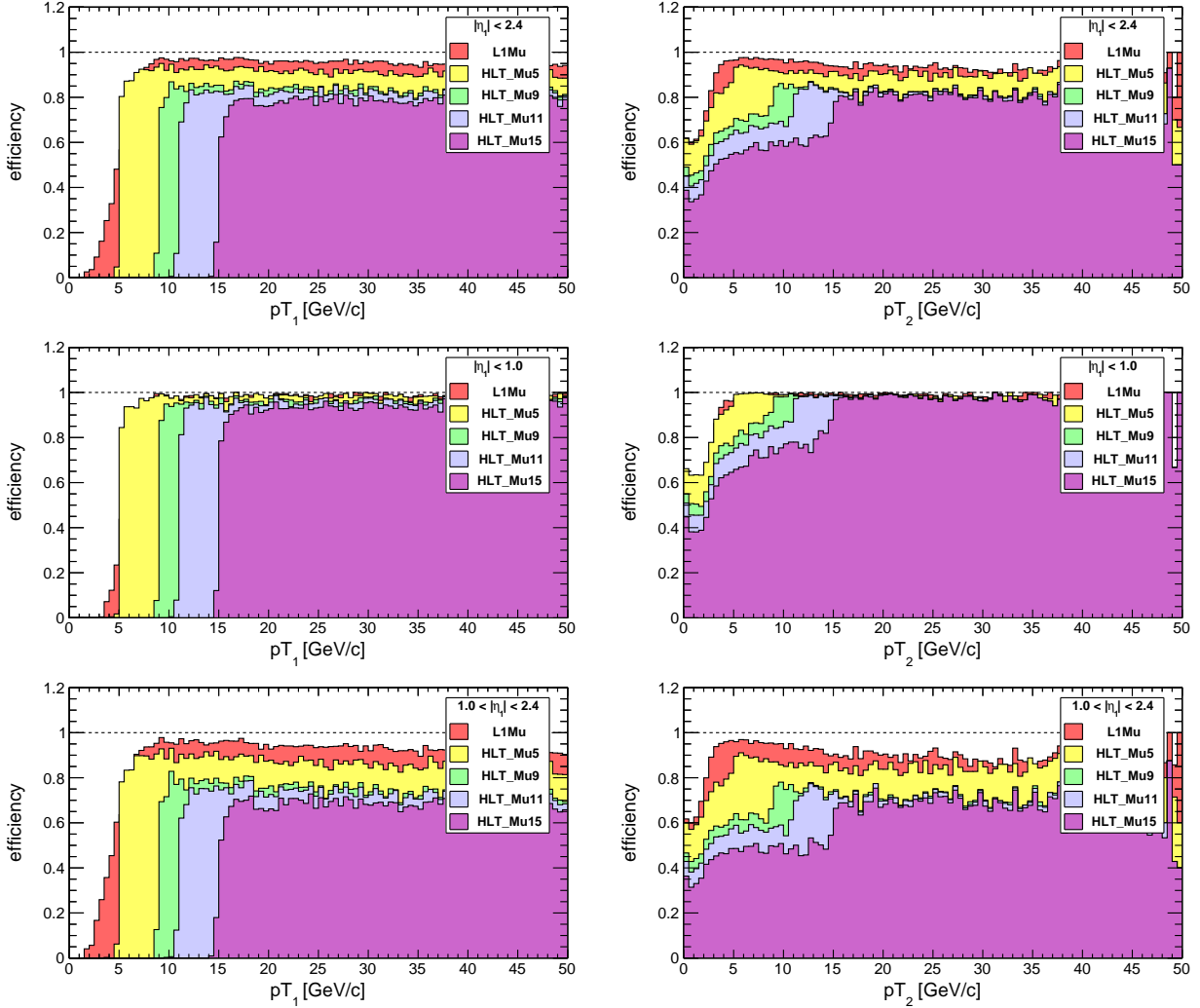


Figure 34: Efficiency of L1 and HLT triggers as a function of highest p_T (which drives trigger efficiency) and second-highest p_T (which drives muon-jet reconstruction efficiency). Denominator: generator-level cut on $|\eta_1|$; numerator: passes various triggers. **FIXME: It looks like L1Mu is not a prerequisite for the HLT paths, as I had expected. Need to find documentation on how these triggers were actually defined in the MC simulation (I might be reading the wrong part of ConfDB).** **FIXME: Barrel L1 efficiency is overestimated? This is known, right? If so, how can I get a reliable estimate?** **FIXME: Vadim knows of parts of the L1 algorithm which are not being emulated... “looks like singles are on in this simulation,” not a long-term situation.**

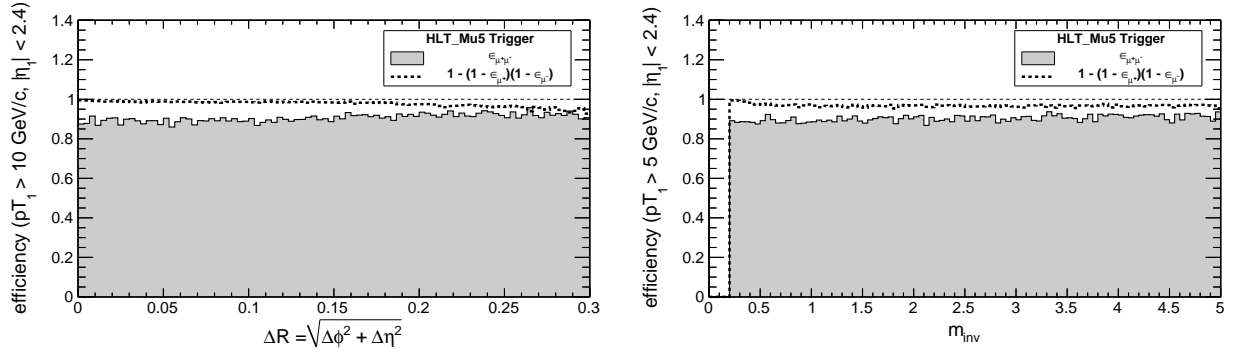


Figure 35: Efficiency of HLT_Mu5 as a function of separation, compared to what would be expected if the response was independent for the μ^+ and μ^- . Denominator: events with a generator-level $pT_1 > 10 \text{ GeV}/c$, $|\eta| < 1.0$ (plateau region of trigger); numerator: event passes trigger.

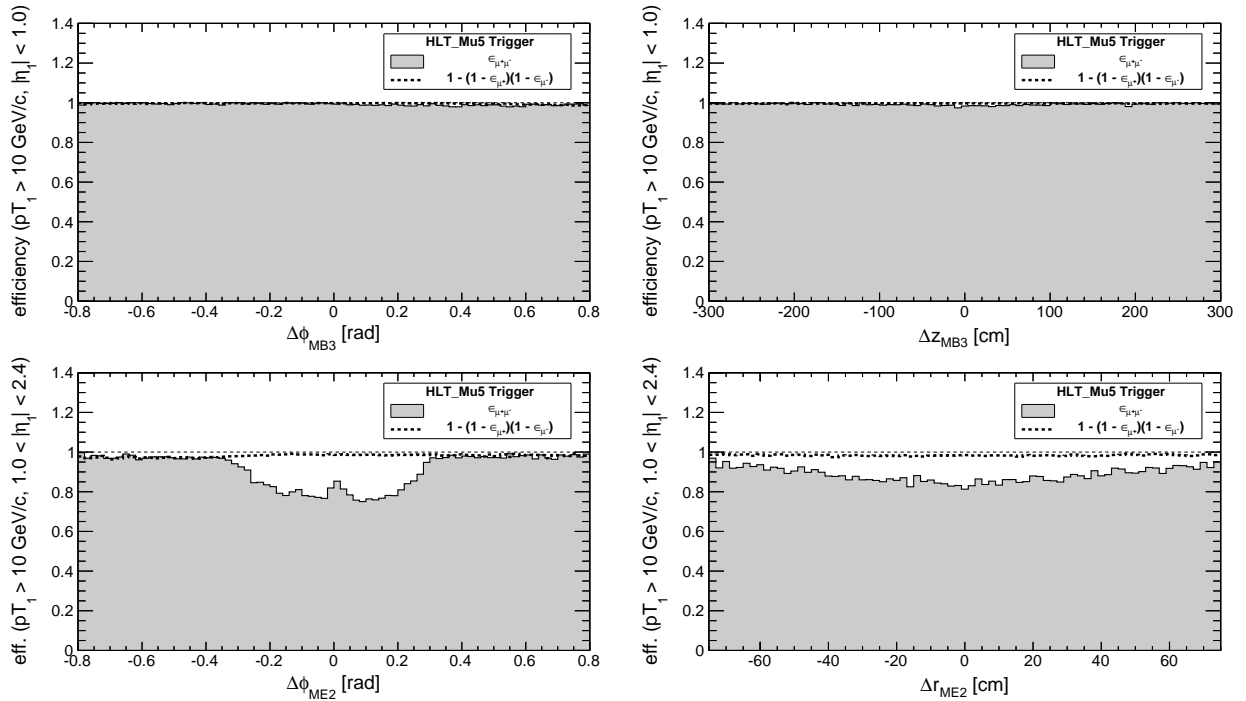


Figure 36: Efficiency of HLT_Mu5 as a function of crossing point in muon system, compared to what would be expected if the response was independent for the μ^+ and μ^- . Same numerator and denominator as Fig. 35.

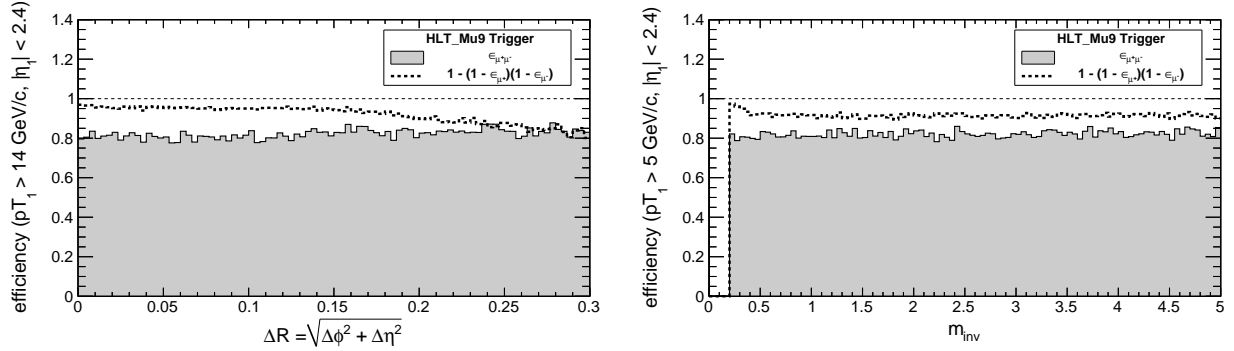


Figure 37: Efficiency of HLT_Mu9 as a function of separation, compared to what would be expected if the response was independent for the μ^+ and μ^- . Denominator: events with a generator-level $pT_1 > 14 \text{ GeV}/c$, $|\eta| < 1.0$ (plateau region of trigger); numerator: event passes trigger.

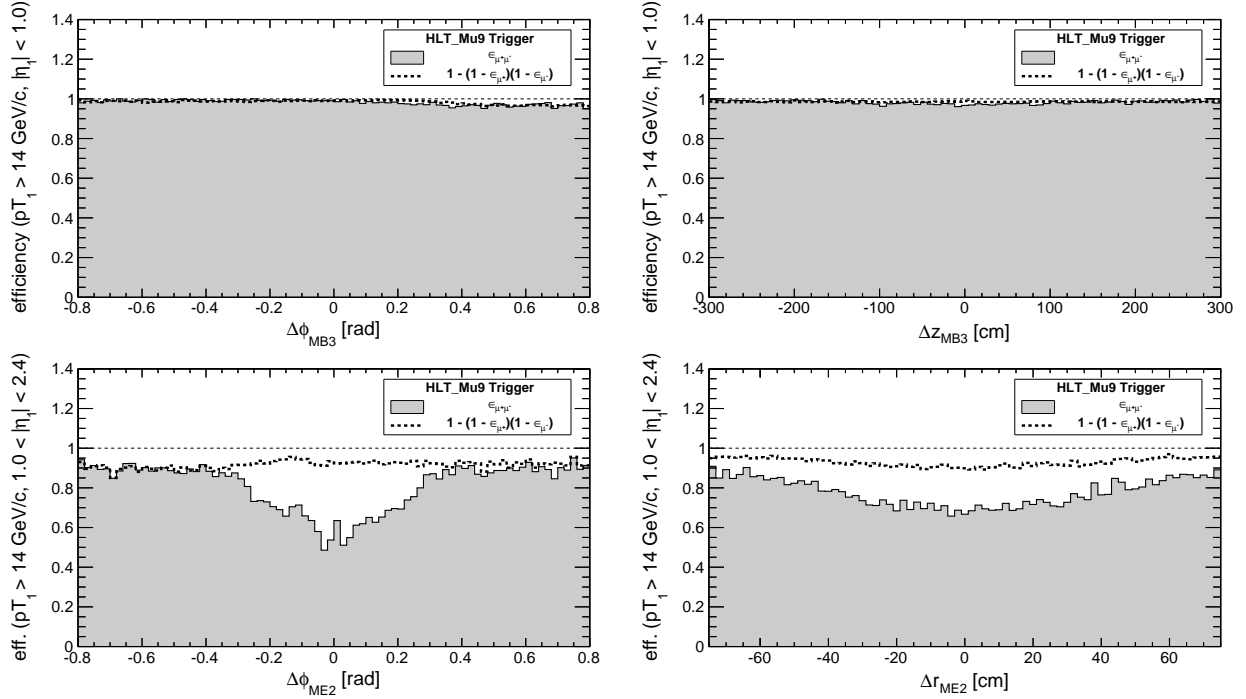


Figure 38: Efficiency of HLT_Mu9 as a function of crossing point in muon system, compared to what would be expected if the response was independent for the μ^+ and μ^- . Same numerator and denominator as Fig. 37. **FIXME: Why is the $1 - (1 - \epsilon_{\mu^+})(\epsilon_{\mu^-})$ curve not perfectly flat?**

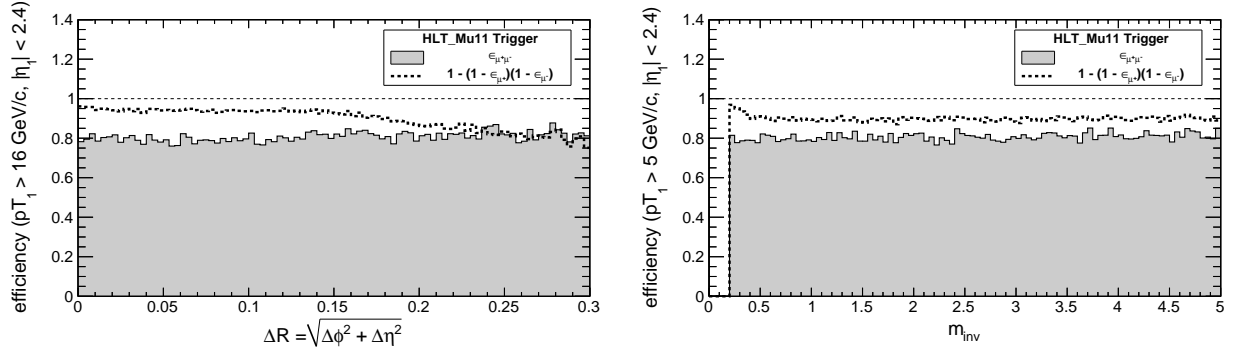


Figure 39: Efficiency of HLT_Mu11 as a function of separation, compared to what would be expected if the response was independent for the μ^+ and μ^- . Denominator: events with a generator-level $pT_1 > 16 \text{ GeV}/c$, $|\eta| < 1.0$ (plateau region of trigger); numerator: event passes trigger.

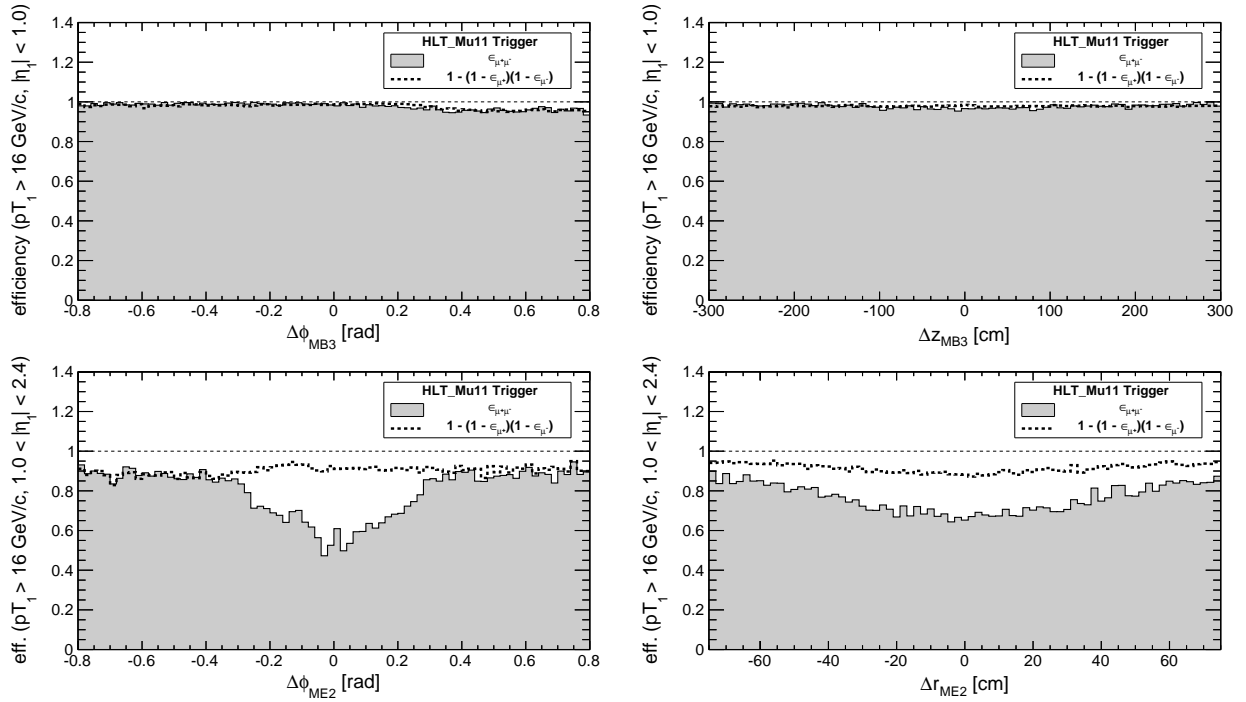


Figure 40: Efficiency of HLT_Mu11 as a function of crossing point in muon system, compared to what would be expected if the response was independent for the μ^+ and μ^- . Same numerator and denominator as Fig. 39. **FIXME: Why is the $1 - (1 - \epsilon_{\mu^+})(\epsilon_{\mu^-})$ curve not perfectly flat?**

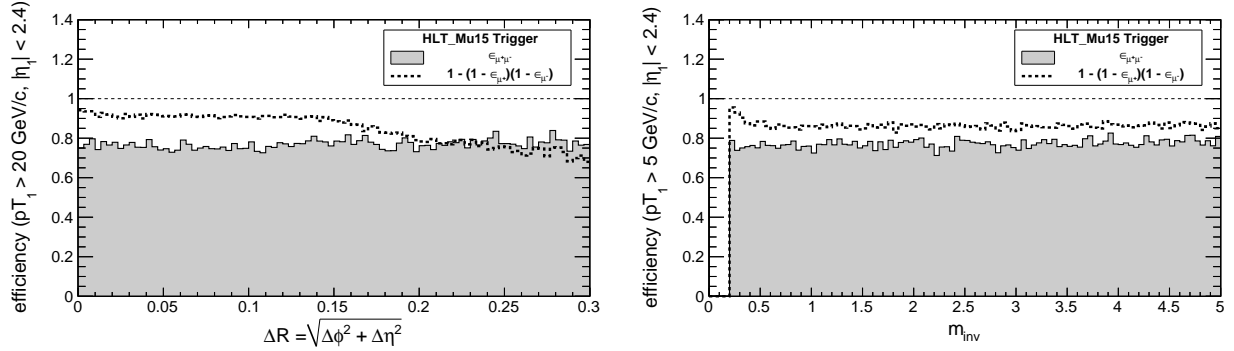


Figure 41: Efficiency of HLT_Mu15 as a function of separation, compared to what would be expected if the response was independent for the μ^+ and μ^- . Denominator: events with a generator-level $pT_1 > 20 \text{ GeV}/c$, $|\eta| < 1.0$ (plateau region of trigger); numerator: event passes trigger.

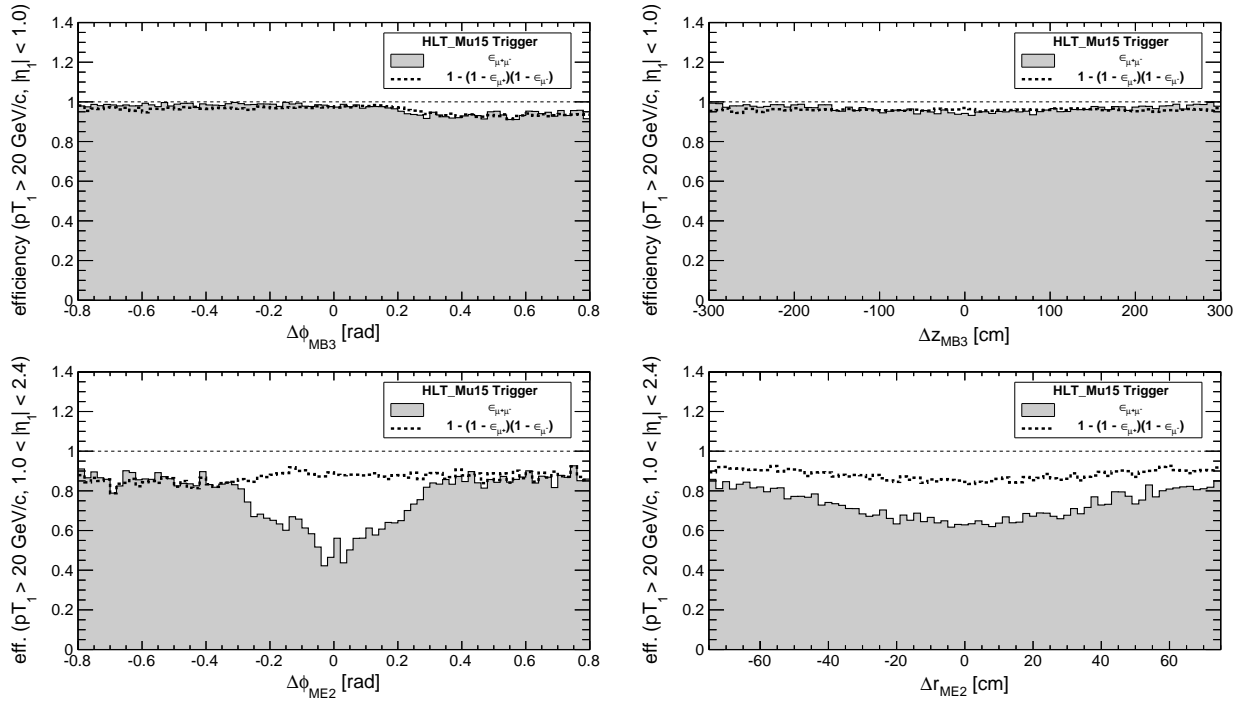


Figure 42: Efficiency of HLT_Mu15 as a function of crossing point in muon system, compared to what would be expected if the response was independent for the μ^+ and μ^- . Same numerator and denominator as Fig. 41. **FIXME: Why is the $1 - (1 - \epsilon_{\mu^+})(\epsilon_{\mu^-})$ curve not perfectly flat?**

2.4 Efficiency of track cuts

Tracker-track quality cuts

- $p_T > 5 \text{ GeV}/c$
- $N_{\text{tracker hits}} \geq 8$
- $\chi^2_{\text{tracker}}/N_{\text{dof}} < 5$
- $\sigma_\phi < 0.03$
- $\sigma_\eta < 0.01$
- $\sigma_{d_{xy}} < 0.05 \text{ cm}$
- $\sigma_{d_z} < 0.1 \text{ cm}$
- $N_{\text{segment matches}} \geq 2$ (this is the important one for suppressing backgrounds in prompt muons)

GlobalMuons can have one additional cut:

- tracker-track/StandAloneMuon consistency $\chi^2/N_{\text{dof}} < 5$

Named muon selection algorithms are taken from `MuonSelectors.h`:

- TMOneStationLoose
- TMOneStationTight
- TMLastStationLoose
- TMLastStationTight
- TMOneStationAngLoose
- TMOneStationAngTight
- TMLastStationAngLoose
- TMLastStationAngTight

2.5 Efficiency for displaced muon-jets

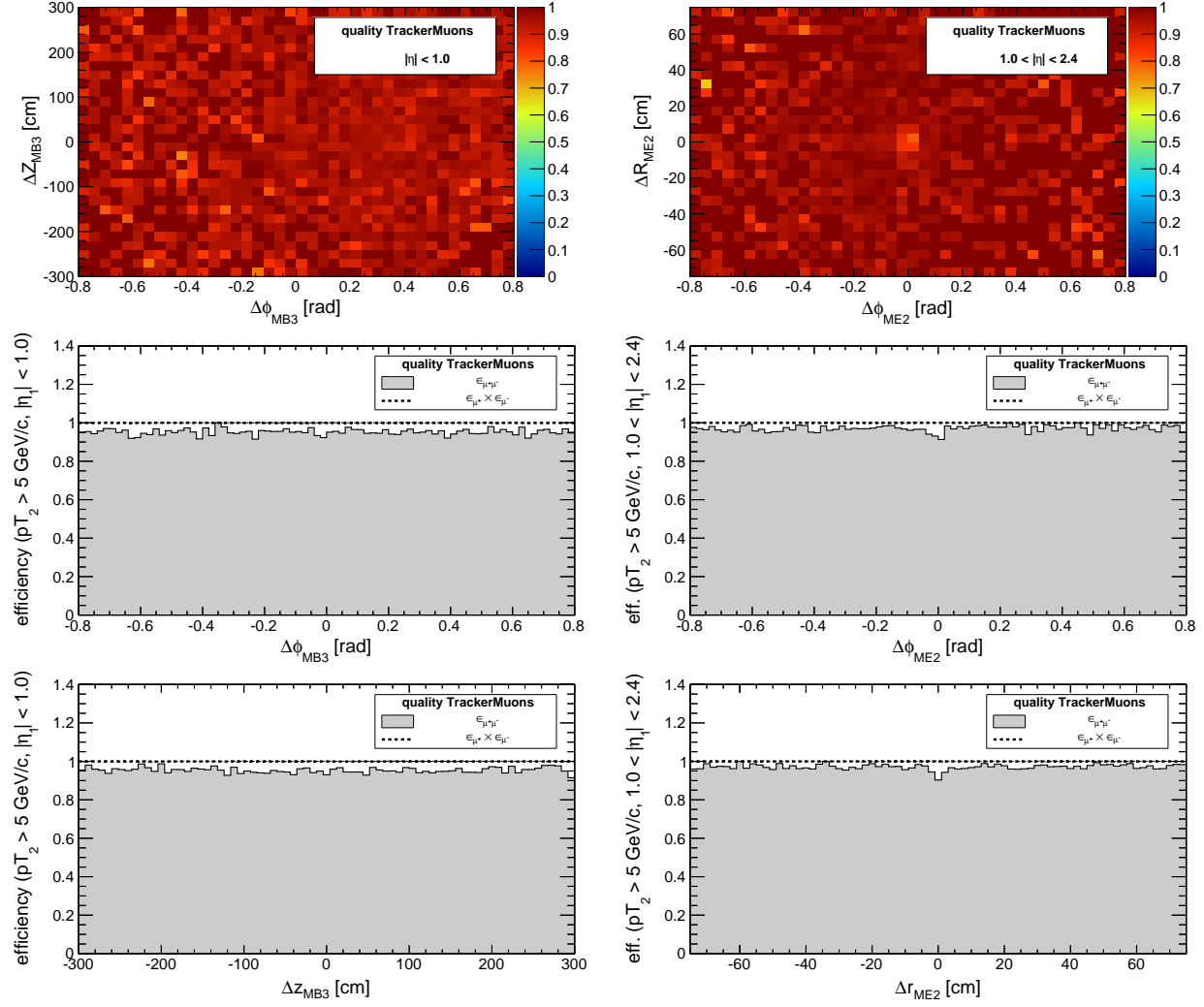


Figure 43: Efficiency of TrackerMuons with quality cuts (see text). Denominator: all muon pairs with $pT_2 > 5 \text{ GeV}/c$, $|\eta_1| < 2.4$; numerator: both muons reconstructed and pass quality cuts. **FIXME:** $\epsilon_{\mu^+} \times \epsilon_{\mu^-}$ indicates that two-muon efficiency is smaller than the product of one-muon efficiencies, but it clearly is not due to overlap in the muon system. Could it be somewhere else?

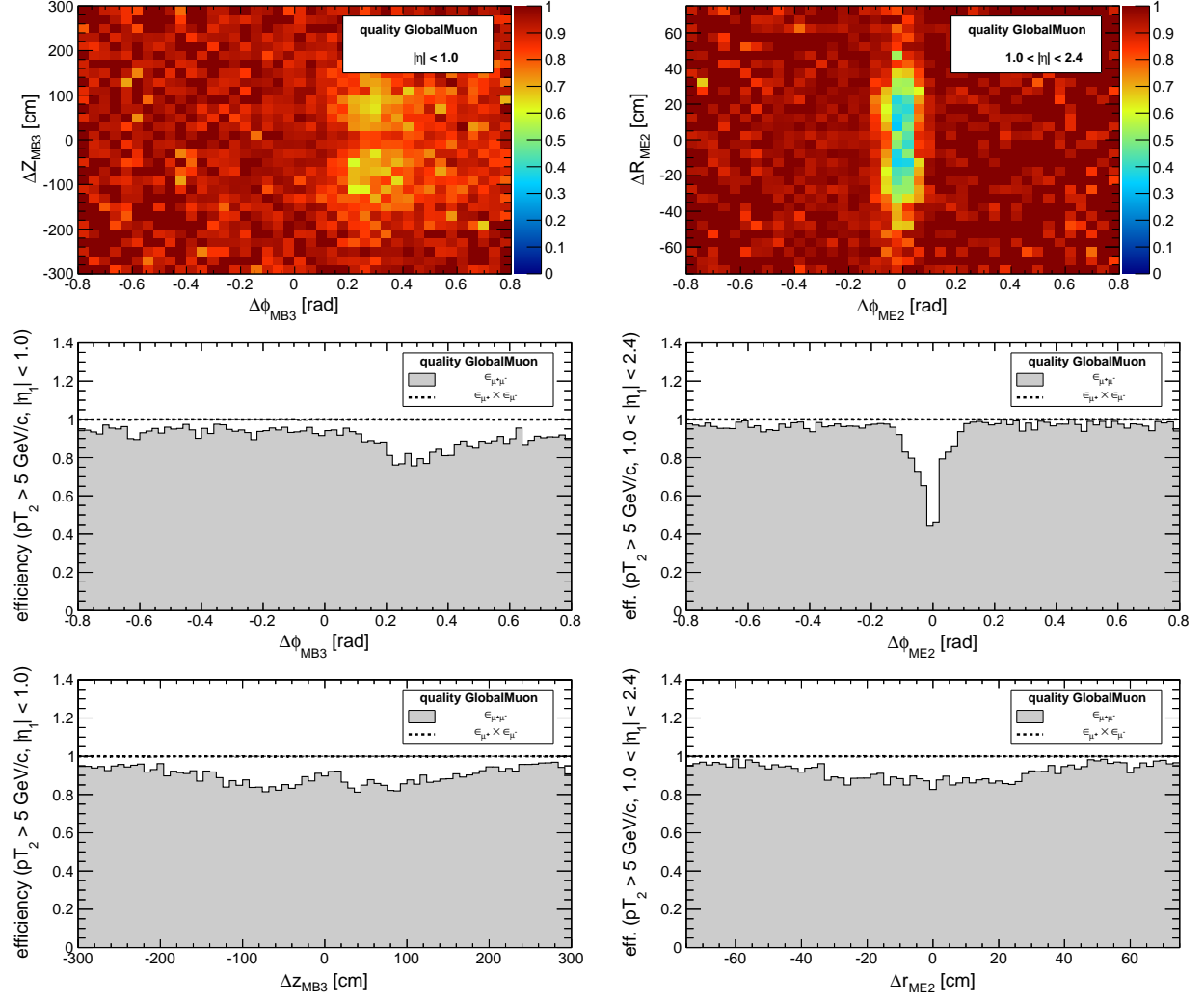


Figure 44: Efficiency of GlobalMuons with quality cuts (see text). Denominator: all muon pairs with $pT_2 > 5 \text{ GeV}/c$, $|\eta_1| < 2.4$; numerator: both muons reconstructed and pass quality cuts.

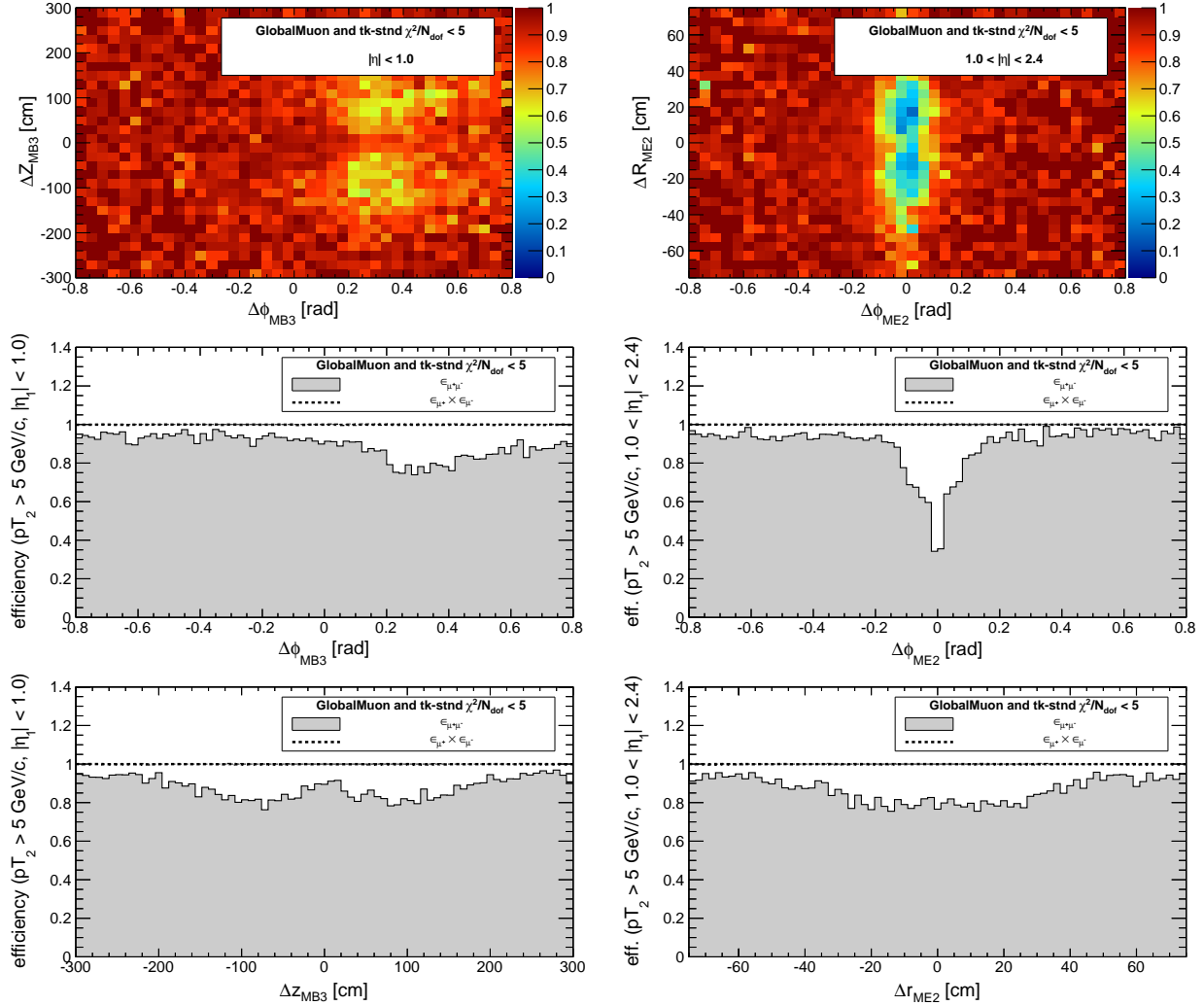


Figure 45: Efficiency of GlobalMuons with quality cuts and tracker-track/StandAloneMuon $\chi^2/N_{\text{dof}} < 5$ (see text). Denominator: all muon pairs with $pT_2 > 5 \text{ GeV}/c$, $|\eta_1| < 2.4$; numerator: both muons reconstructed and pass quality cuts.

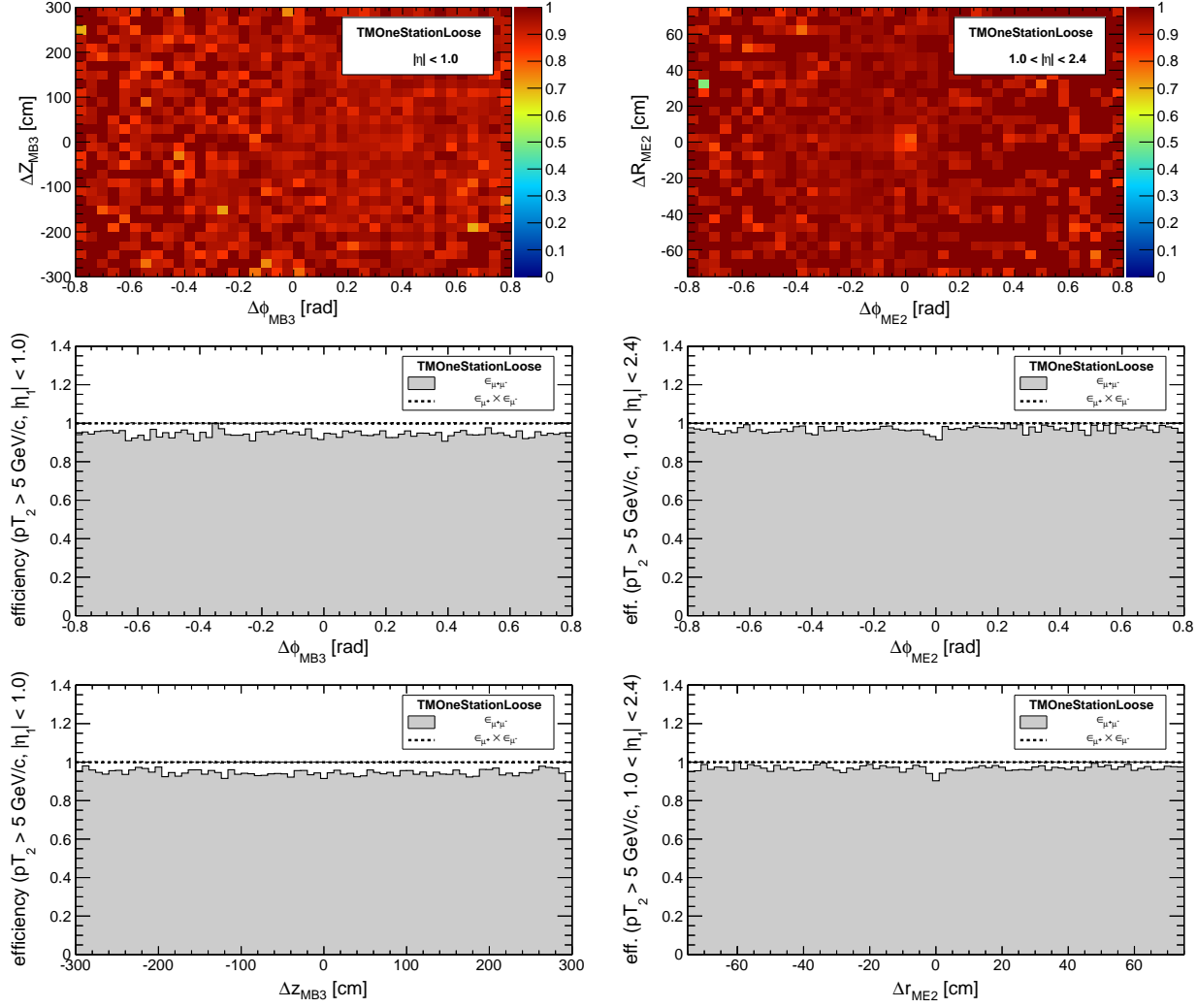


Figure 46: Efficiency of TrackerMuons with “TMOneStationLoose” requirement and quality cuts (see text). Denominator: all muon pairs with $pT_2 > 5 \text{ GeV}/c$, $|\eta_1| < 2.4$; numerator: both muons reconstructed and pass quality cuts. **FIXME:** $\epsilon_{\mu^+} \times \epsilon_{\mu^-}$ indicates that two-muon efficiency is smaller than the product of one-muon efficiencies, but it clearly is not due to overlap in the muon system. Could it be somewhere else?

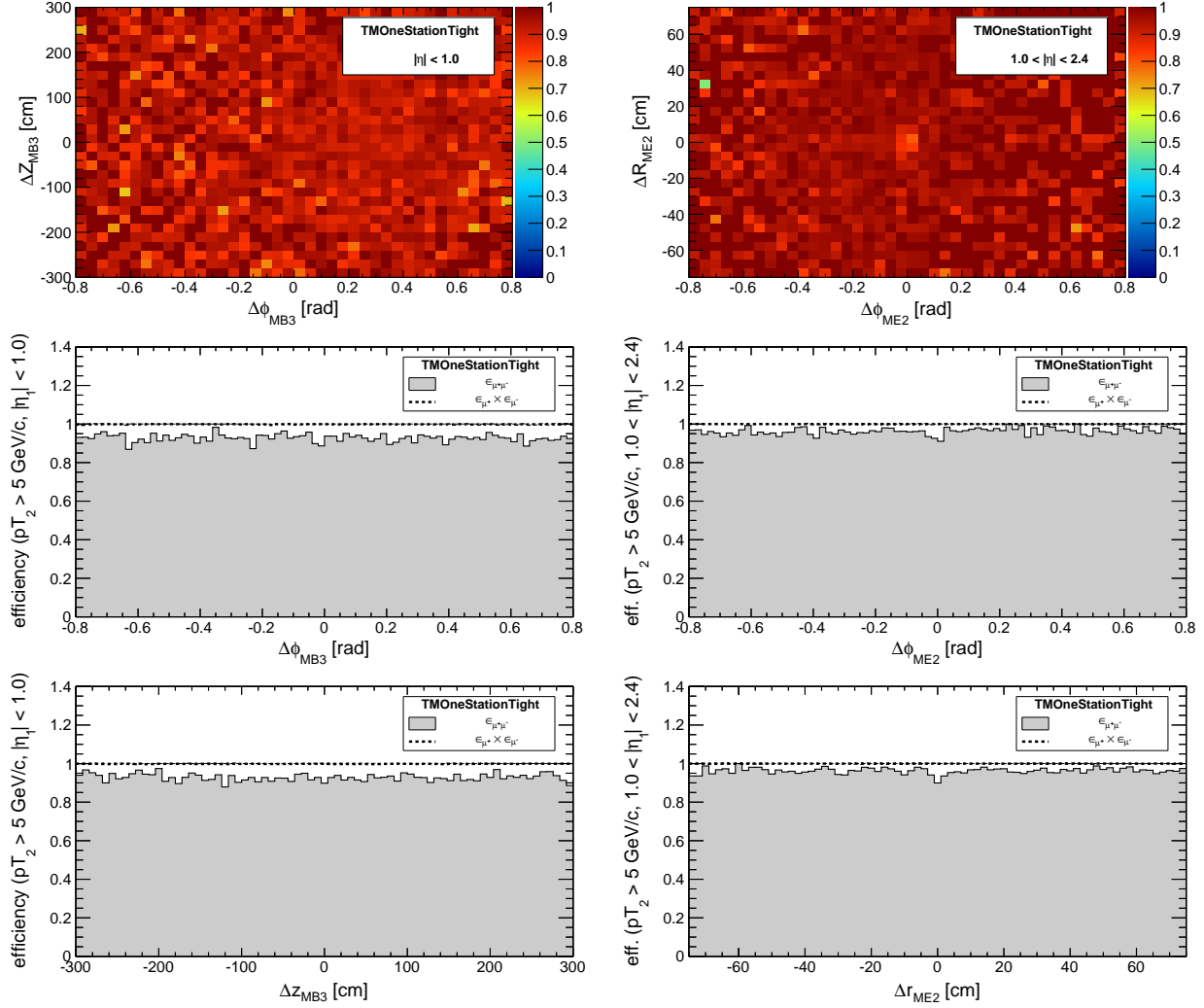


Figure 47: Efficiency of TrackerMuons with “TMOneStationTight” requirement and quality cuts (see text). Denominator: all muon pairs with $pT_2 > 5 \text{ GeV}/c$, $|\eta_1| < 2.4$; numerator: both muons reconstructed and pass quality cuts. **FIXME:** $\epsilon_{\mu^+} \times \epsilon_{\mu^-}$ indicates that two-muon efficiency is smaller than the product of one-muon efficiencies, but it clearly is not due to overlap in the muon system. Could it be somewhere else?

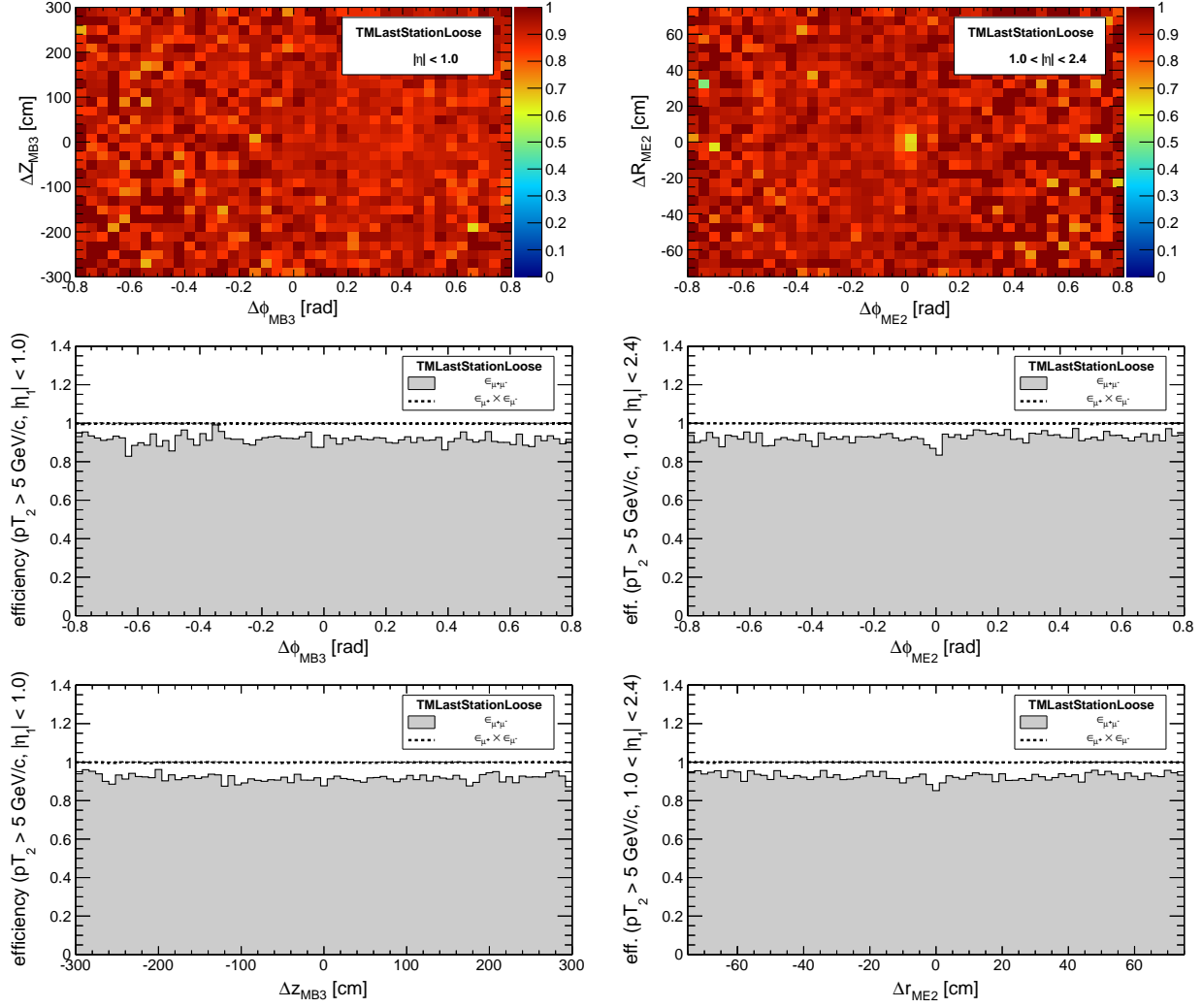


Figure 48: Efficiency of TrackerMuons with “TMLastStationLoose” requirement and quality cuts (see text). Denominator: all muon pairs with $pT_2 > 5 \text{ GeV}/c, |\eta_1| < 2.4$; numerator: both muons reconstructed and pass quality cuts. **FIXME: $\epsilon_{\mu^+} \times \epsilon_{\mu^-}$ indicates that two-muon efficiency is smaller than the product of one-muon efficiencies, but it clearly is not due to overlap in the muon system. Could it be somewhere else?**

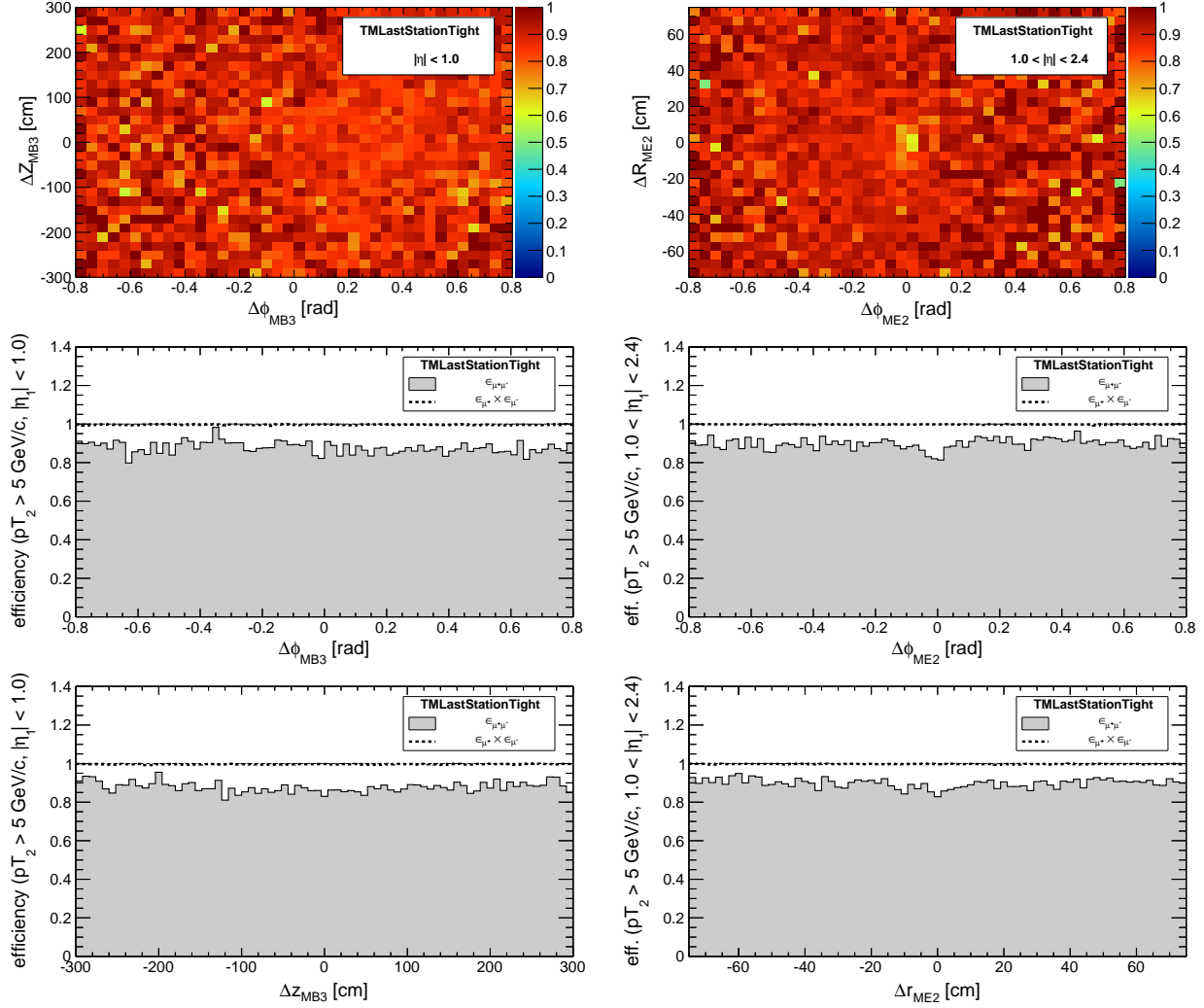


Figure 49: Efficiency of TrackerMuons with “TMLastStationTight” requirement and quality cuts (see text). Denominator: all muon pairs with $pT_2 > 5 \text{ GeV}/c$, $|\eta_1| < 2.4$; numerator: both muons reconstructed and pass quality cuts. **FIXME:** $\epsilon_{\mu^+} \times \epsilon_{\mu^-}$ indicates that two-muon efficiency is smaller than the product of one-muon efficiencies, but it clearly is not due to overlap in the muon system. Could it be somewhere else?

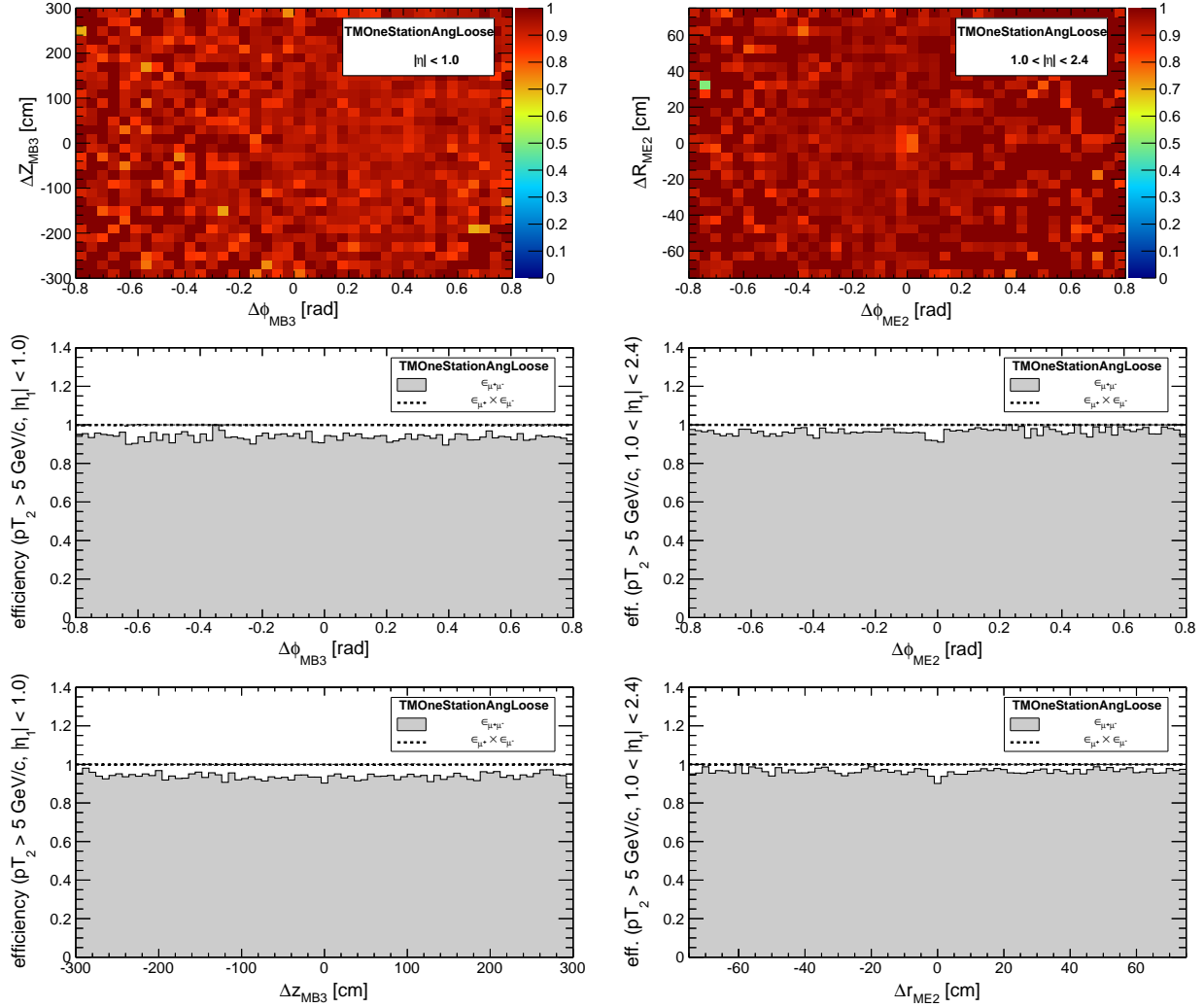


Figure 50: Efficiency of TrackerMuons with “TMOneStationAngLoose” requirement and quality cuts (see text). Denominator: all muon pairs with $pT_2 > 5 \text{ GeV}/c$, $|\eta_1| < 2.4$; numerator: both muons reconstructed and pass quality cuts. **FIXME:** $\epsilon_{\mu^+} \times \epsilon_{\mu^-}$ indicates that two-muon efficiency is smaller than the product of one-muon efficiencies, but it clearly is not due to overlap in the muon system. Could it be somewhere else?

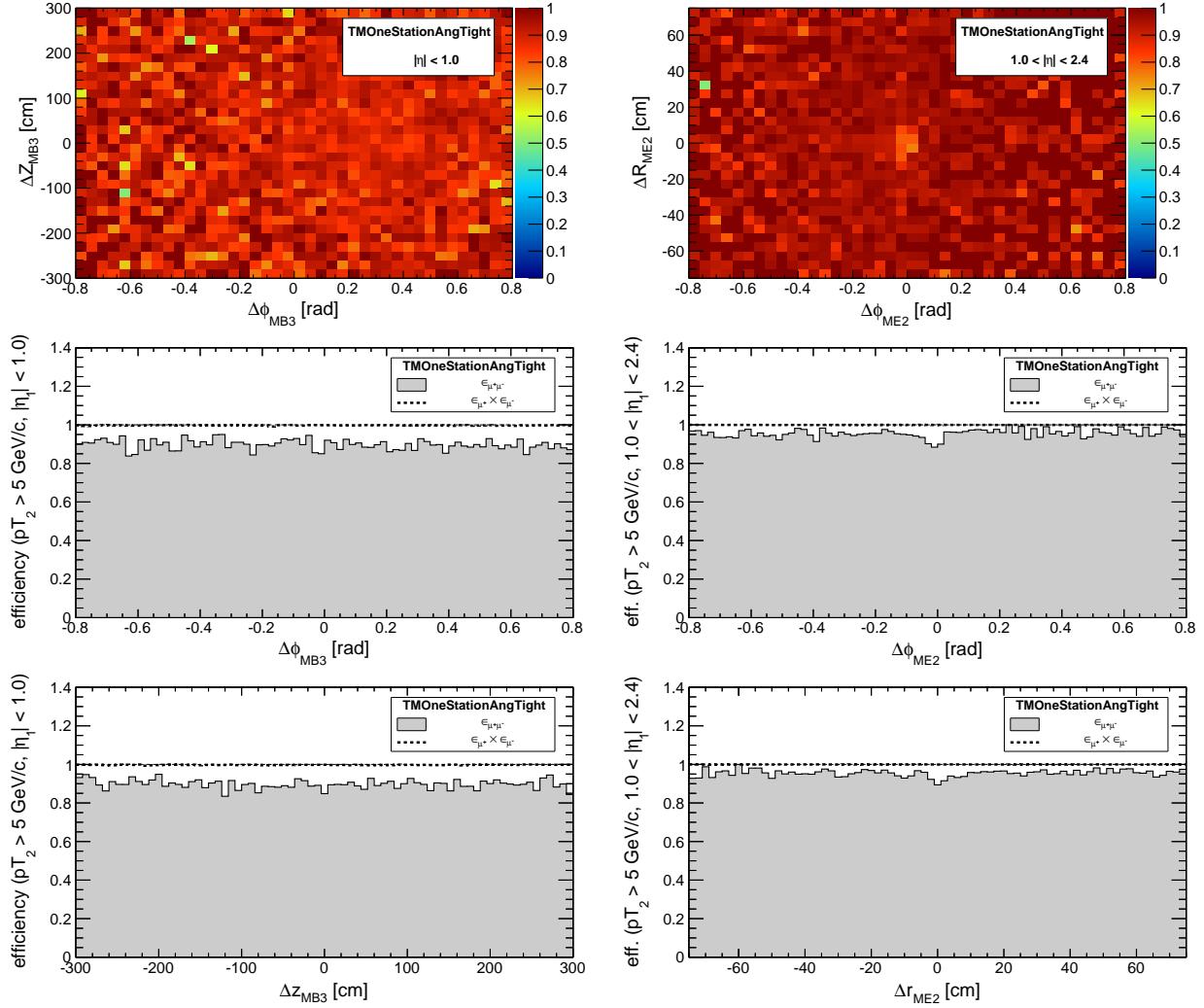


Figure 51: Efficiency of TrackerMuons with “TMOneStationAngTight” requirement and quality cuts (see text). Denominator: all muon pairs with $pT_2 > 5 \text{ GeV}/c$, $|\eta_1| < 2.4$; numerator: both muons reconstructed and pass quality cuts. **FIXME:** $\epsilon_{\mu^+} \times \epsilon_{\mu^-}$ indicates that two-muon efficiency is smaller than the product of one-muon efficiencies, but it clearly is not due to overlap in the muon system. Could it be somewhere else?

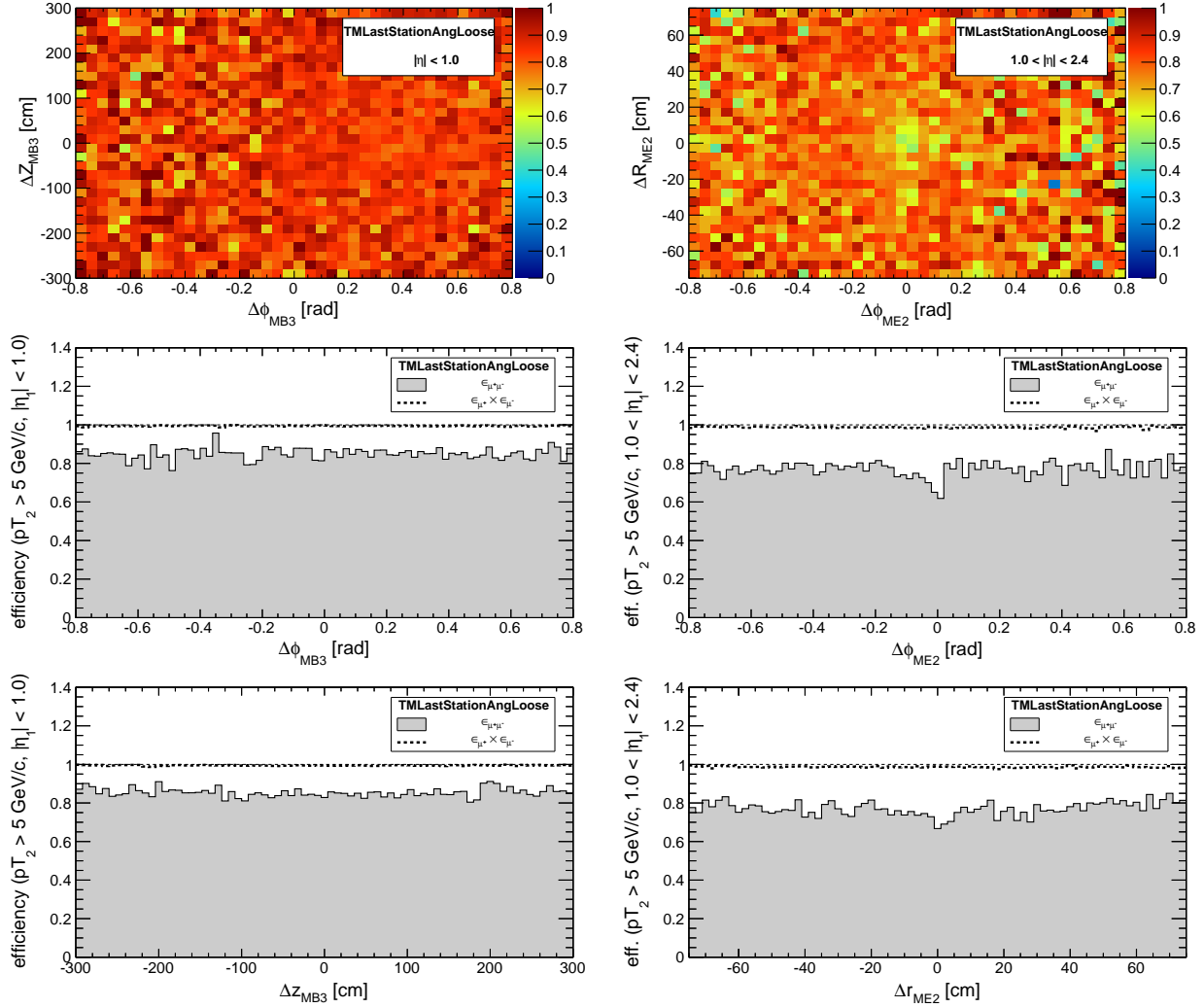


Figure 52: Efficiency of TrackerMuons with “TMLastStationAngLoose” requirement and quality cuts (see text). Denominator: all muon pairs with $pT_2 > 5 \text{ GeV}/c$, $|\eta_1| < 2.4$; numerator: both muons reconstructed and pass quality cuts. **FIXME:** $\epsilon_{\mu^+} \times \epsilon_{\mu^-}$ indicates that two-muon efficiency is smaller than the product of one-muon efficiencies, but it clearly is not due to overlap in the muon system. Could it be somewhere else?

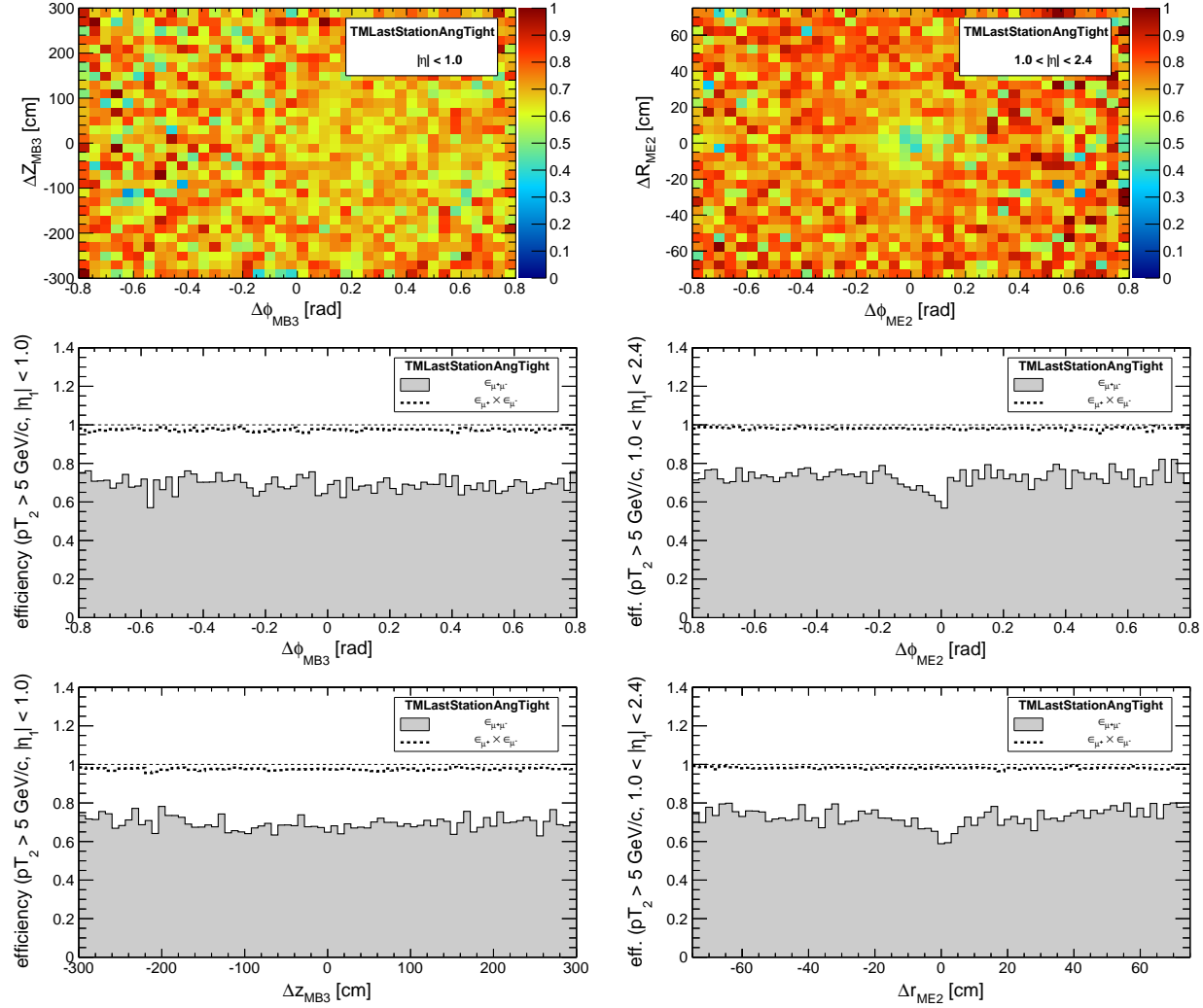


Figure 53: Efficiency of TrackerMuons with “TMLastStationAngTight” requirement and quality cuts (see text). Denominator: all muon pairs with $pT_2 > 5 \text{ GeV}/c$, $|\eta_1| < 2.4$; numerator: both muons reconstructed and pass quality cuts. **FIXME:** $\epsilon_{\mu^+} \times \epsilon_{\mu^-}$ indicates that two-muon efficiency is smaller than the product of one-muon efficiencies, but it clearly is not due to overlap in the muon system. Could it be somewhere else?

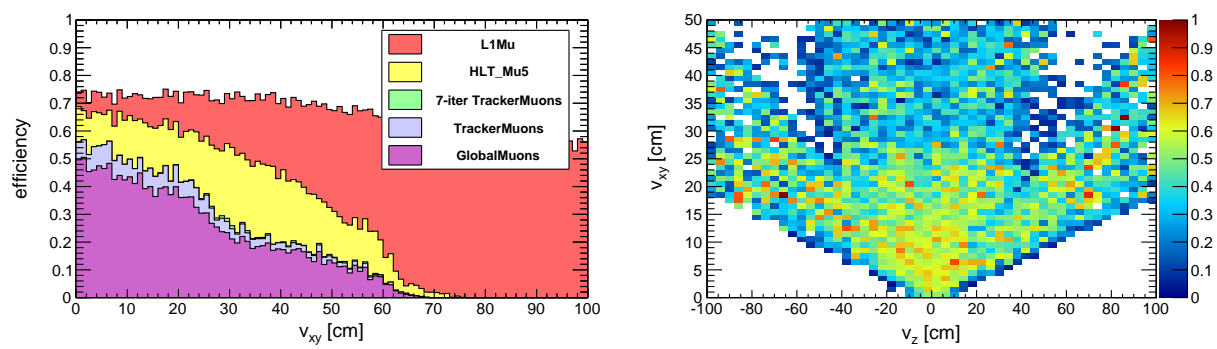


Figure 54: Trigger and reconstruction efficiency for displaced dimuons.

3 Grouping muons

FIXME: Is χ^2_{vertex} highly correlated with $\left(\frac{\Delta z_{\text{vertex}}}{\sigma_{\Delta z}}\right)^2$? That is, does all of the vertex identification come from z -significance? If so, then z -significance may be a more robust variable to cut on than P_{vertex} .

3.1 Muon-grouping efficiency

3.2 Muon-jet merging

By tuning the matching parameter, we can turn multi-muon-jets into mega-muon-jets and vice-versa.

3.3 Extra muons in muon-jets

An “extra muon” is a muon that has nothing to do with the resonance decay, and is a function of pile-up.

The P_{vertex} criterion in muon grouping is effective at controlling extra muons in high pile-up environments.

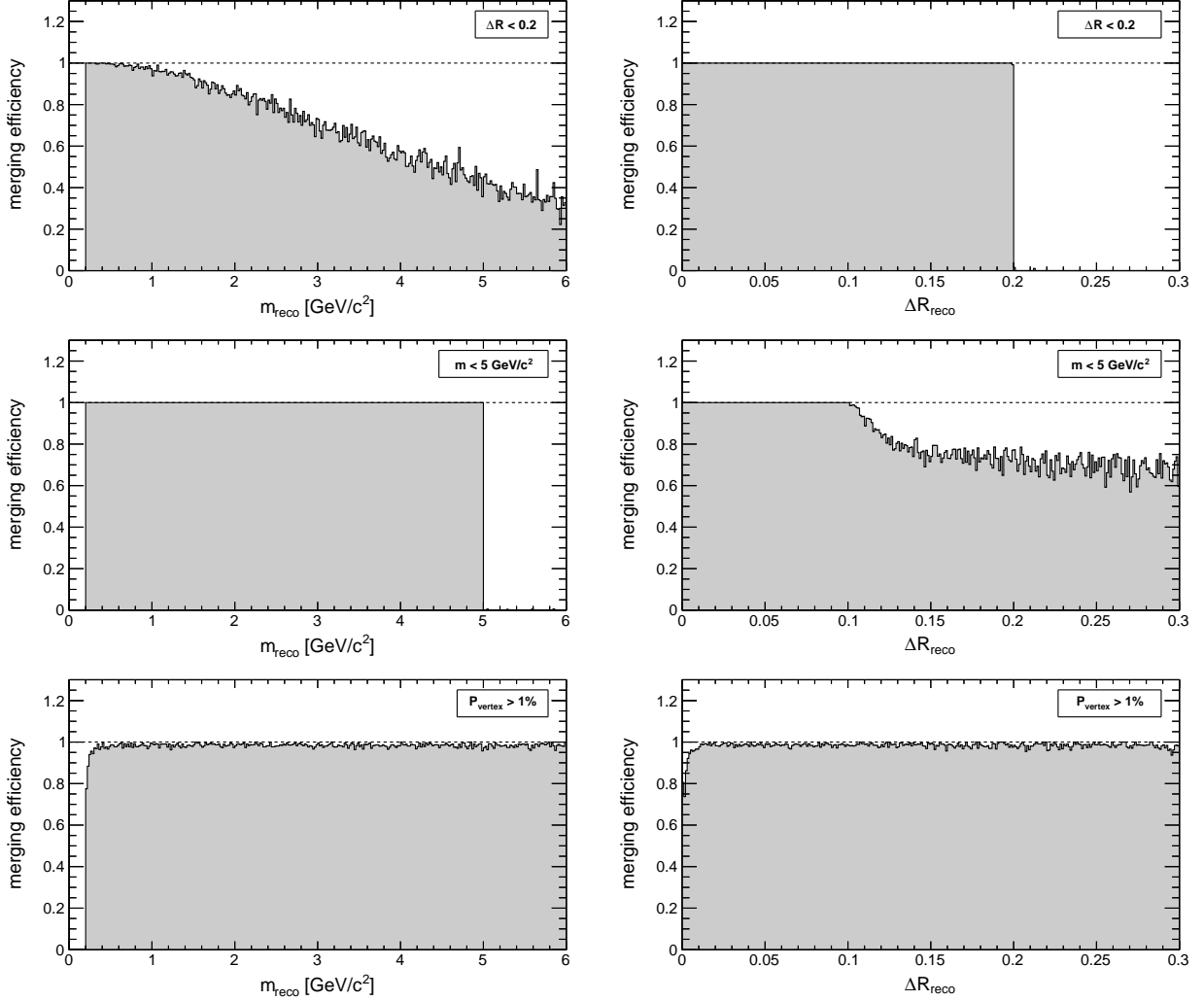


Figure 55: Muon grouping efficiency as a function of reconstructed mass and ΔR for different “closeness” criteria (see Figs. 56 and 57 for more combinations). Denominator: events in which both muons were reconstructed; numerator: events in which they were grouped in the same muon-jet.

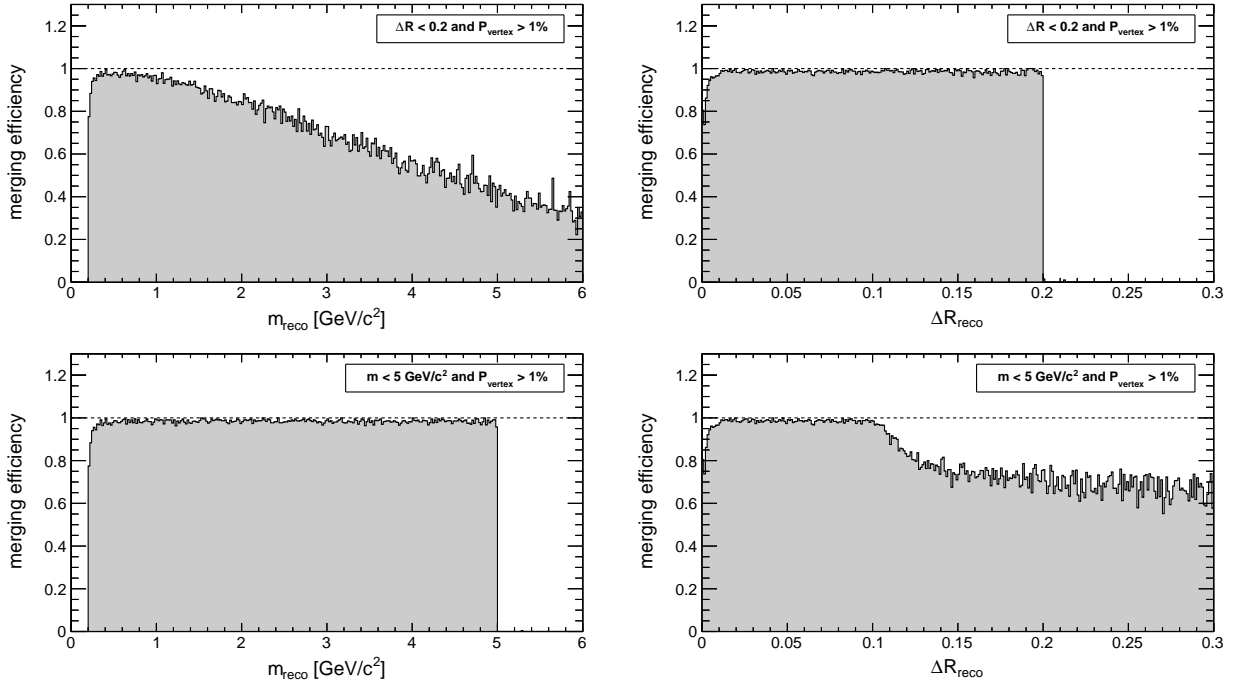


Figure 56: Muon grouping efficiency as a function of reconstructed mass and ΔR for different “closeness” criteria (see Figs. 55 and 57 for more combinations). Denominator: events in which both muons were reconstructed; numerator: events in which they were grouped in the same muon-jet.

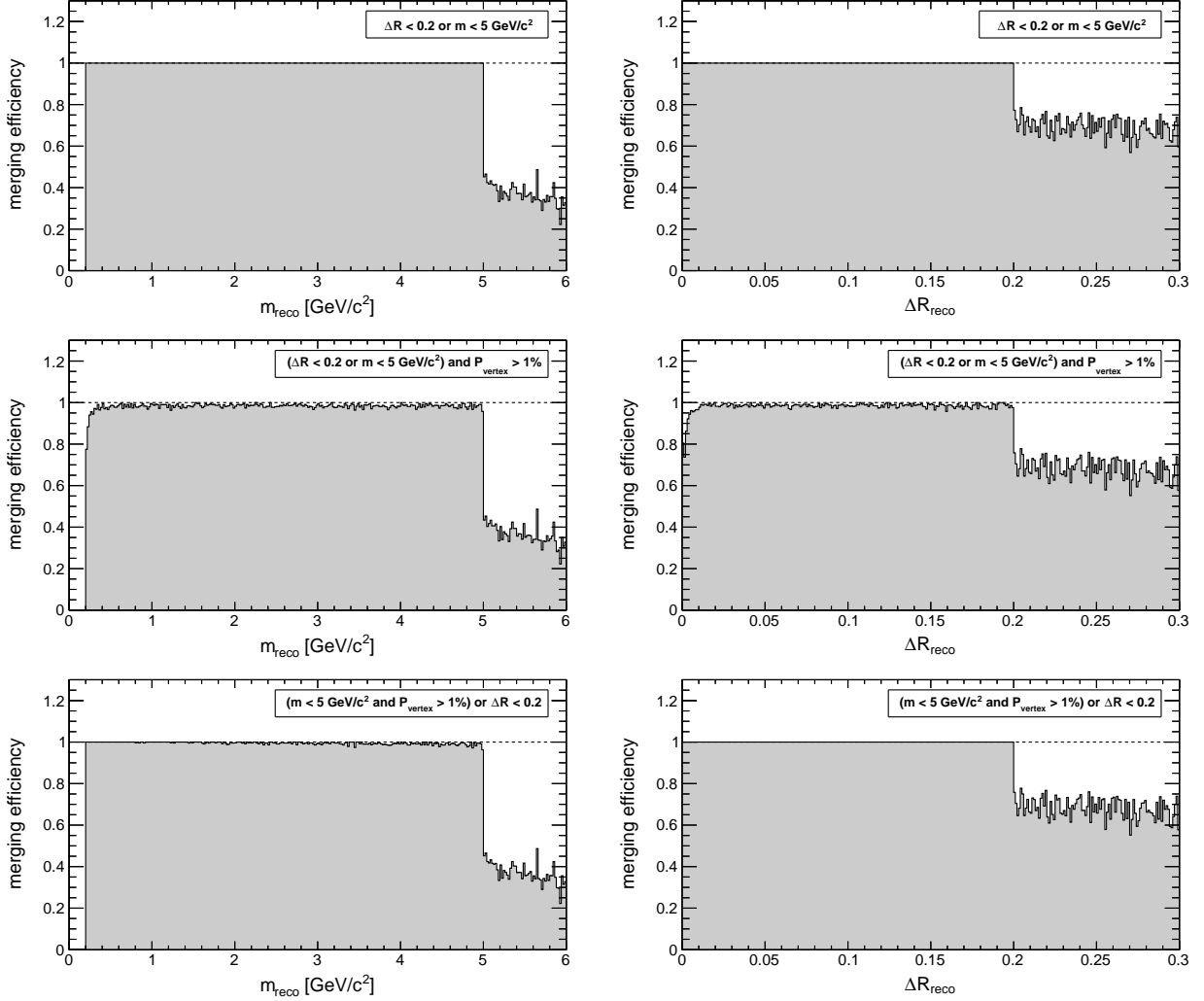


Figure 57: Muon grouping efficiency as a function of reconstructed mass and ΔR for different “closeness” criteria (see Figs. 55 and 56 for more combinations). Denominator: events in which both muons were reconstructed; numerator: events in which they were grouped in the same muon-jet.

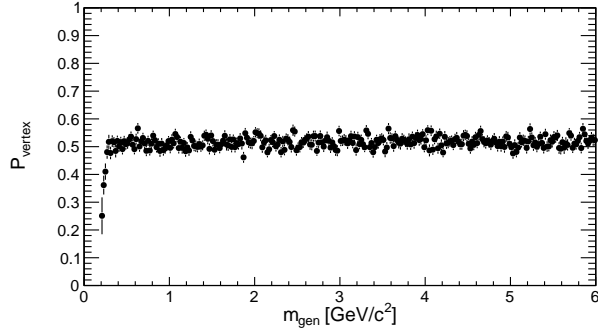


Figure 58: Average vertex probability in bins of dimuon mass. The probability is only non-uniformly distributed for masses below $0.4 \text{ GeV}/c^2$, where vertex reconstruction fails for nearly collinear tracks.

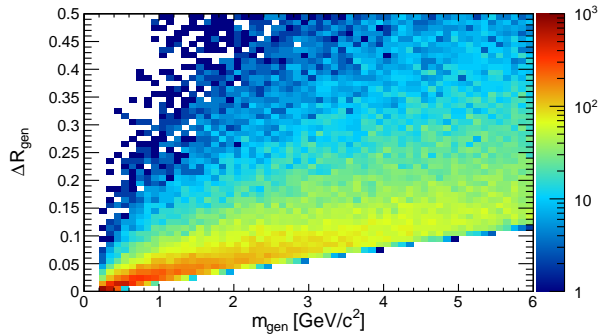


Figure 59: Geometric separation of μ^+ and μ^- as a function of dimuon mass (generator-level in both cases). The shape of this distribution depends on the momentum distribution of the sample, which is uniform in pT_{pair} between 0 and $100 \text{ GeV}/c$.

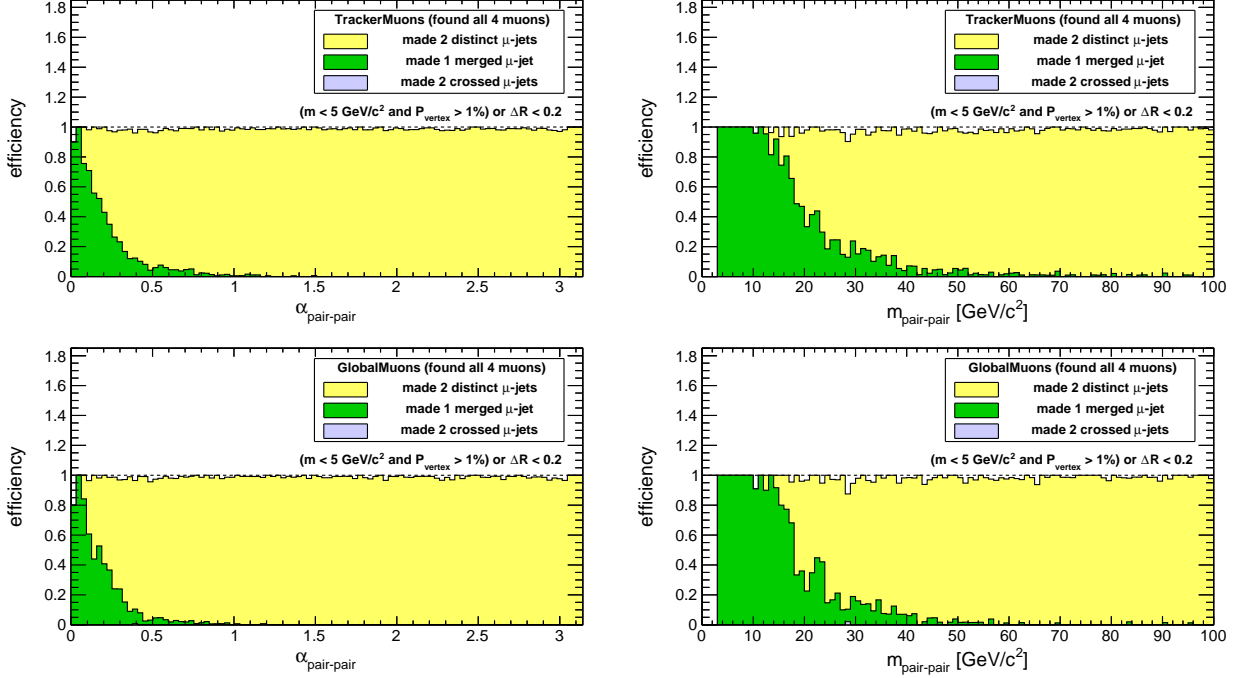


Figure 60: Efficiency for finding two distinct muon-jets, one merged muon-jet, or two wrong-combination muon-jets, in a sample of four muons: $\alpha_{\text{pair-pair}}$ is the angle between the two dimuon axes and $m_{\text{pair-pair}}$ is the mass of the four-muon mass. Denominator: events with four reconstructed muons; numerator: events grouped as two correct pairs of muons, one four-muon group, or two incorrect pairs of muons, respectively. **FIXME: The shape of these distributions probably depend on the kinematics of the decay, and the “decay” is really two uncorrelated dimuons that are both uniform in p_T and η .** Perhaps you should try it with fully-simulated cascade decays: scalar case, vector case. **FIXME: Also, this plot would be interesting to see for different matching criteria, to see if you can scan from grouping nearly everything to grouping hardly anything.**

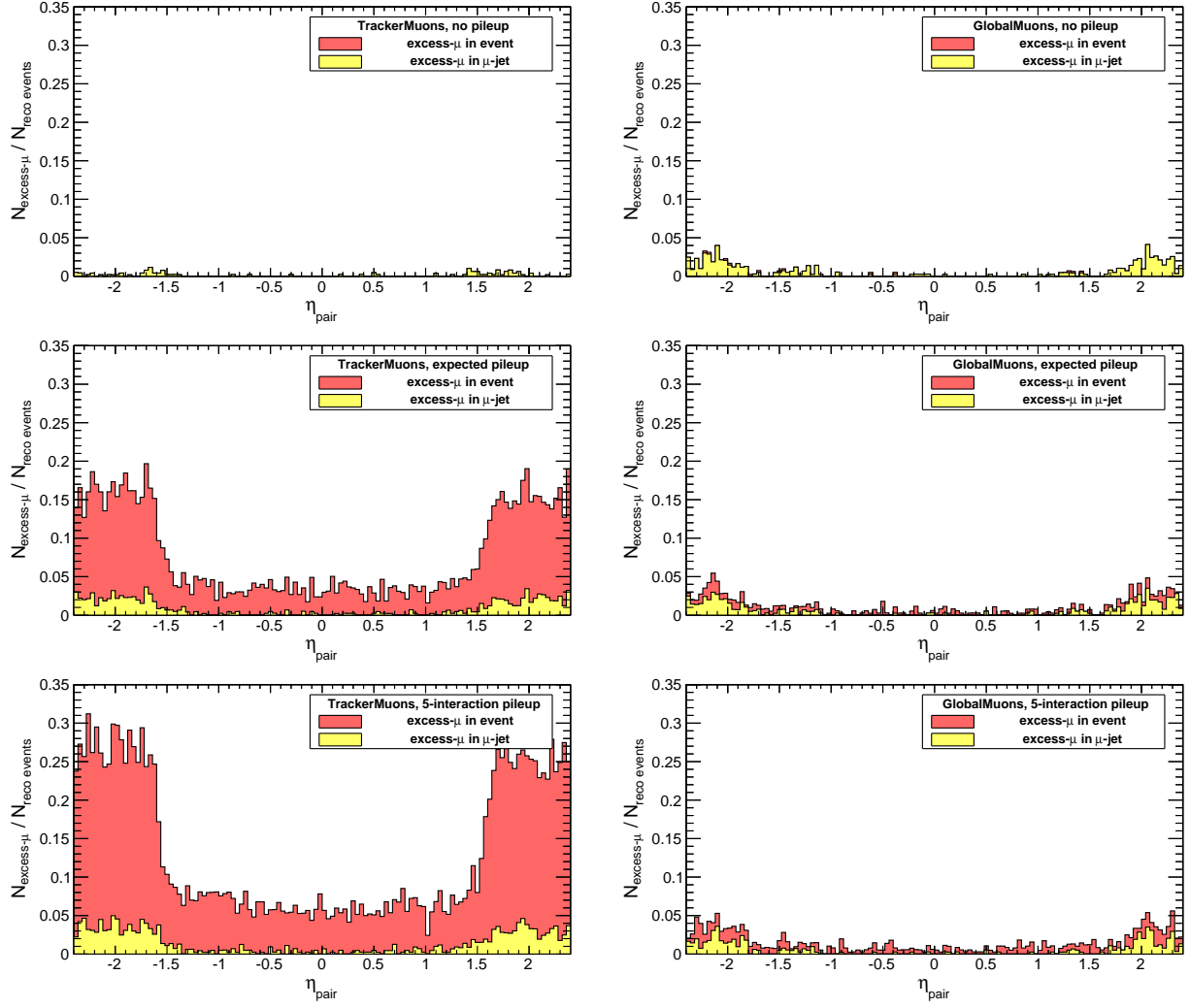


Figure 61: Probability that an extra muon will be reconstructed in the event and probability that it will be included in the muon-jet for dimuon guns with varying levels of pile-up. Denominator: signal muons reconstructed and MC-matched; numerator: more than two muons reconstructed and more than two muons included in muon-jet, respectively. “Expected pileup” is the 7 TeV collision-energy, $6.9 \times 10^{30} \text{ cm}^{-2}\text{s}^{-1}$ integrated luminosity with 156 bunch-crossings working point **FIXME: reference?**, and “5-interaction pileup” is an extreme with an average of 5 interactions per event.

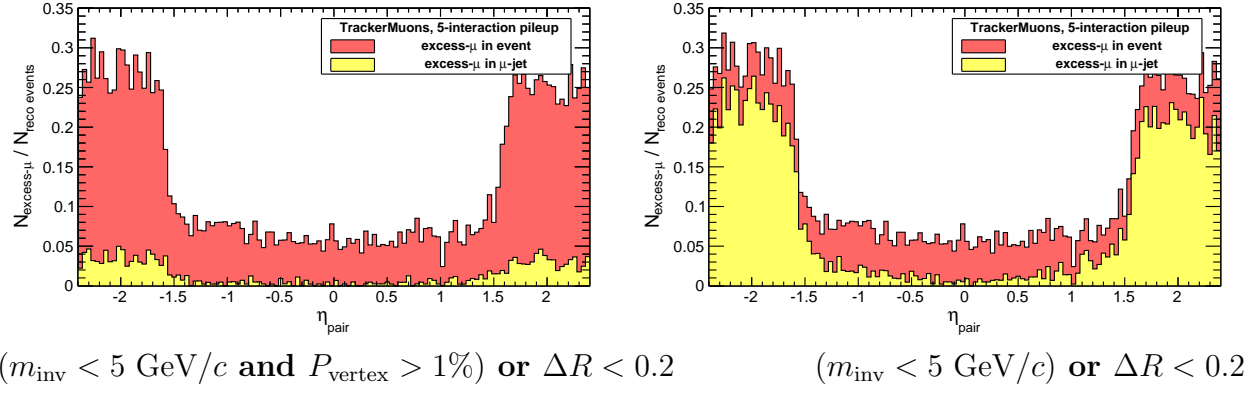


Figure 62: Probability of an extra muon with and without $P_{\text{vertex}} > 1\%$ in the muon grouping criteria. **FIXME: Include the muon grouping criteria in the auto-generated plot.** **FIXME: Also, you should probably put thr three curves on one plot.**

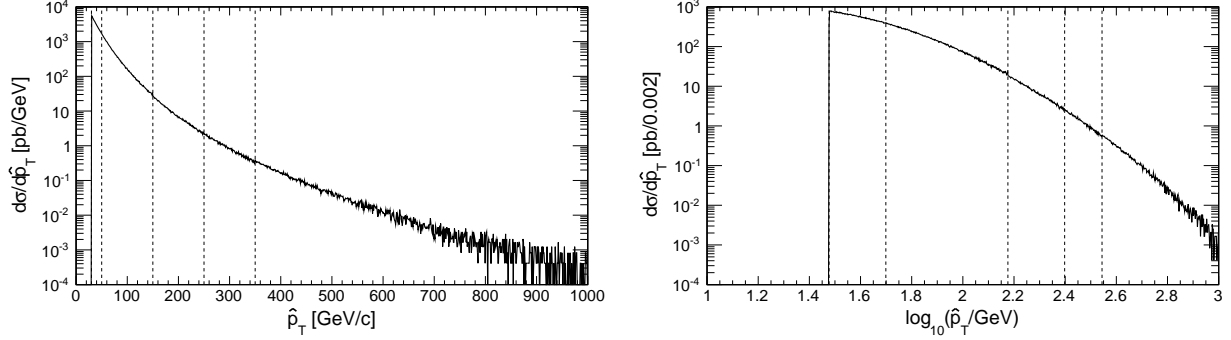


Figure 63: QCD scale (\hat{p}_T) of the five InclusiveMu_PtXXX samples after normalization to integrated luminosity (Continuous means properly weighted).

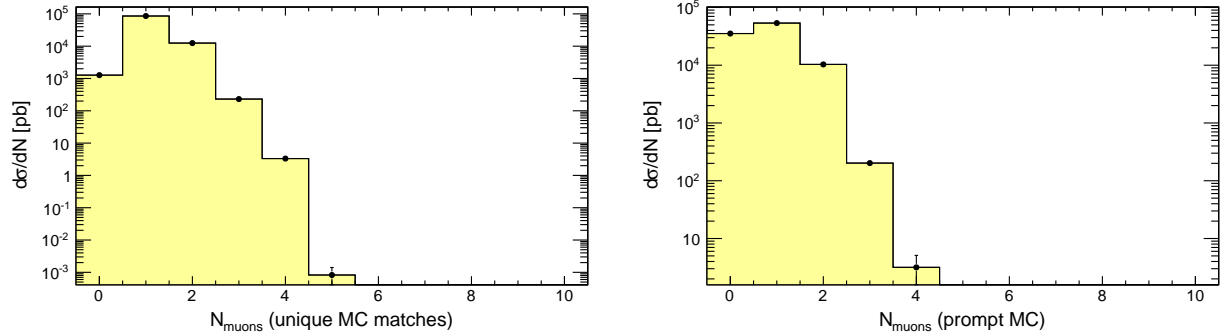


Figure 64: Number of generator-level muons in each event: (a) by determining the number of unique MC muons matched to an inclusive set of reconstructed muons, (b) by counting the number of generator-level muons which did not come from a π^\pm , K^\pm , or K_L decay (“prompt”). For all subsequent plots, we define the “number of real (reconstructable) muons” using method (a).

4 Backgrounds

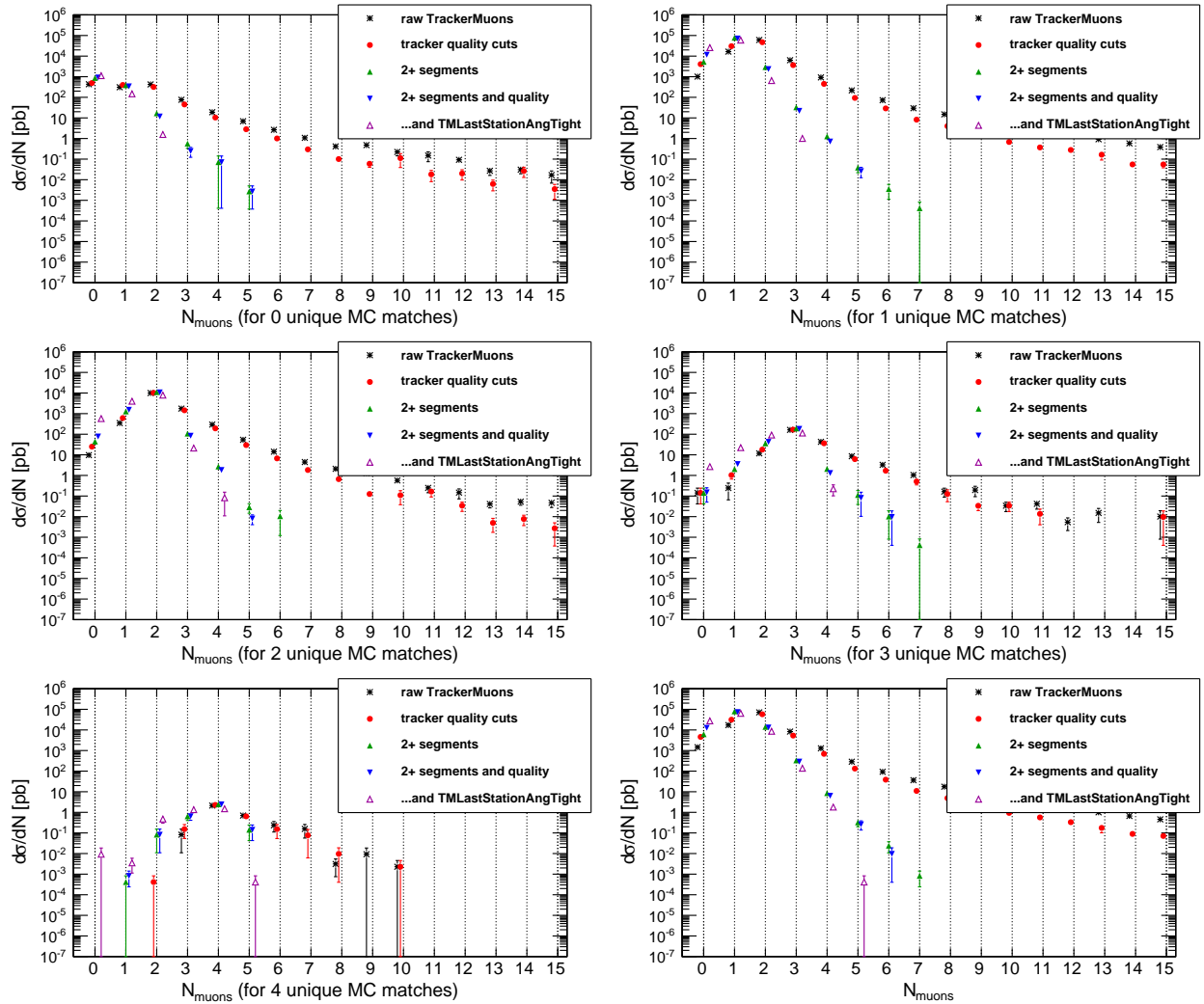


Figure 65: Number of TrackerMuons with different track-quality cuts, split by number of real muons (see Fig. 64(a)), and all-inclusive (bottom-right).

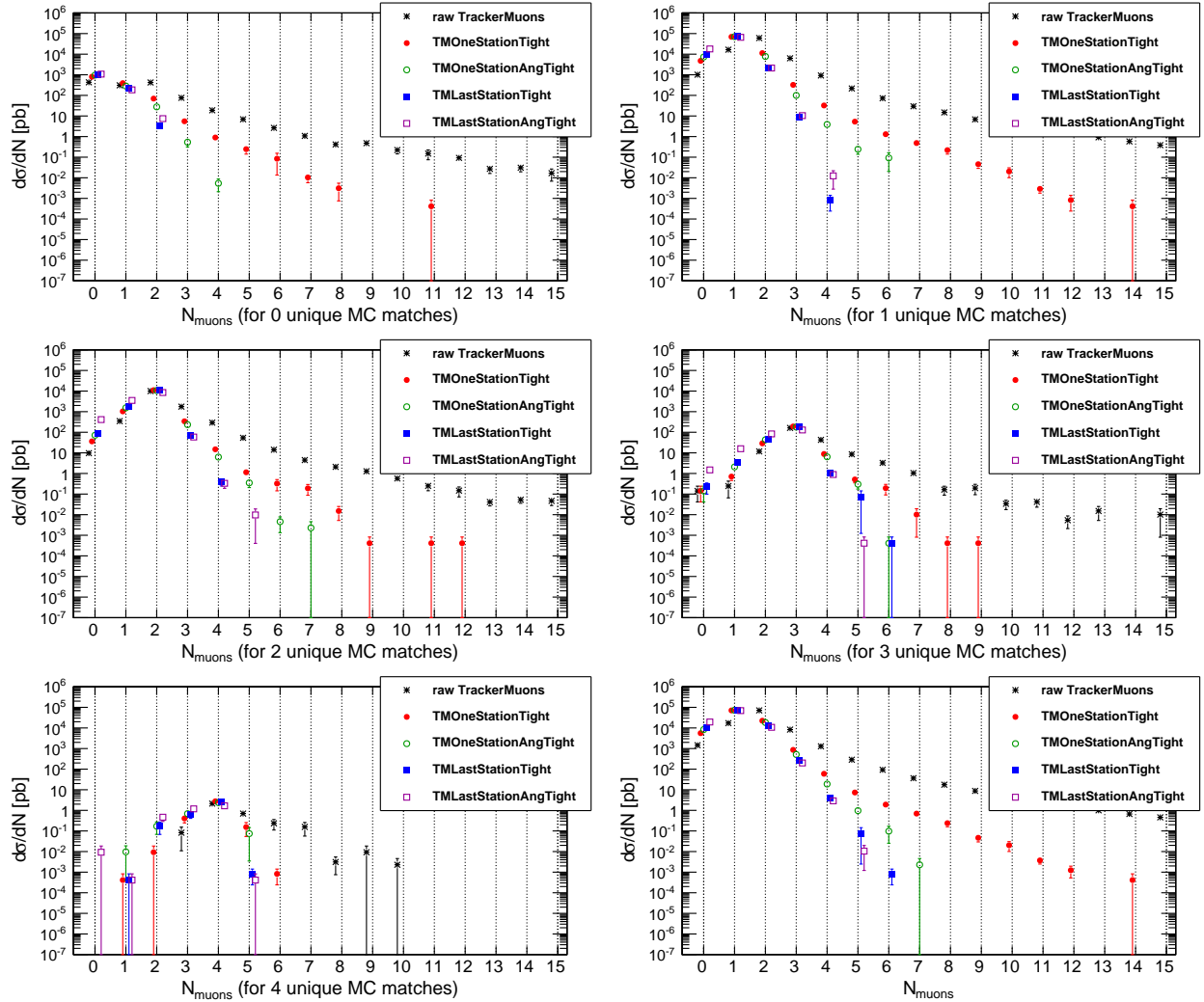


Figure 66: Number of TrackerMuons with different MuonSelectors.h cuts, split by number of real muons (see Fig. 64(a)), and all-inclusive (bottom-right).

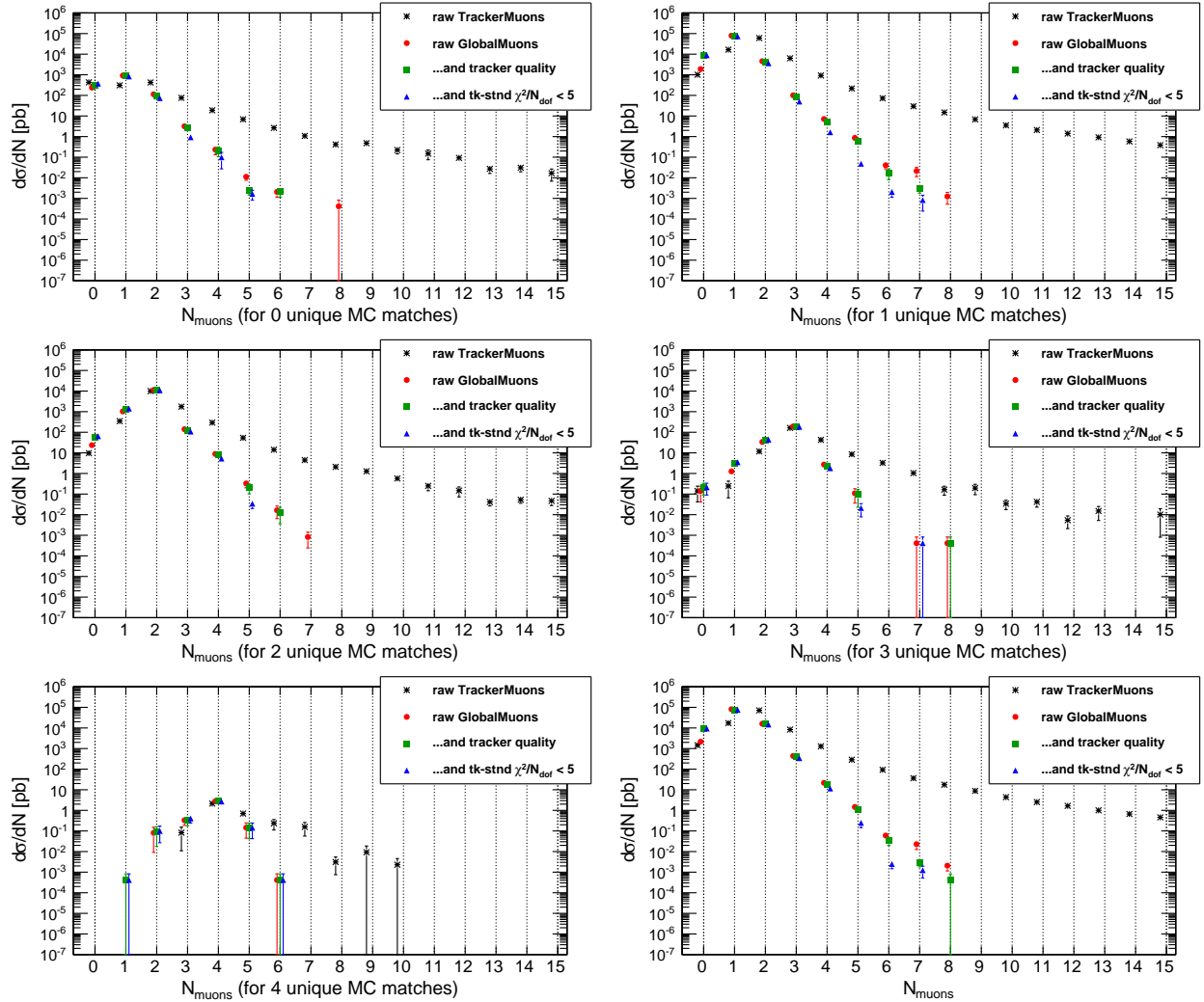


Figure 67: Number of GlobalMuons with different quality cuts, split by number of real muons (see Fig. 64(a)), and all-inclusive (bottom-right).

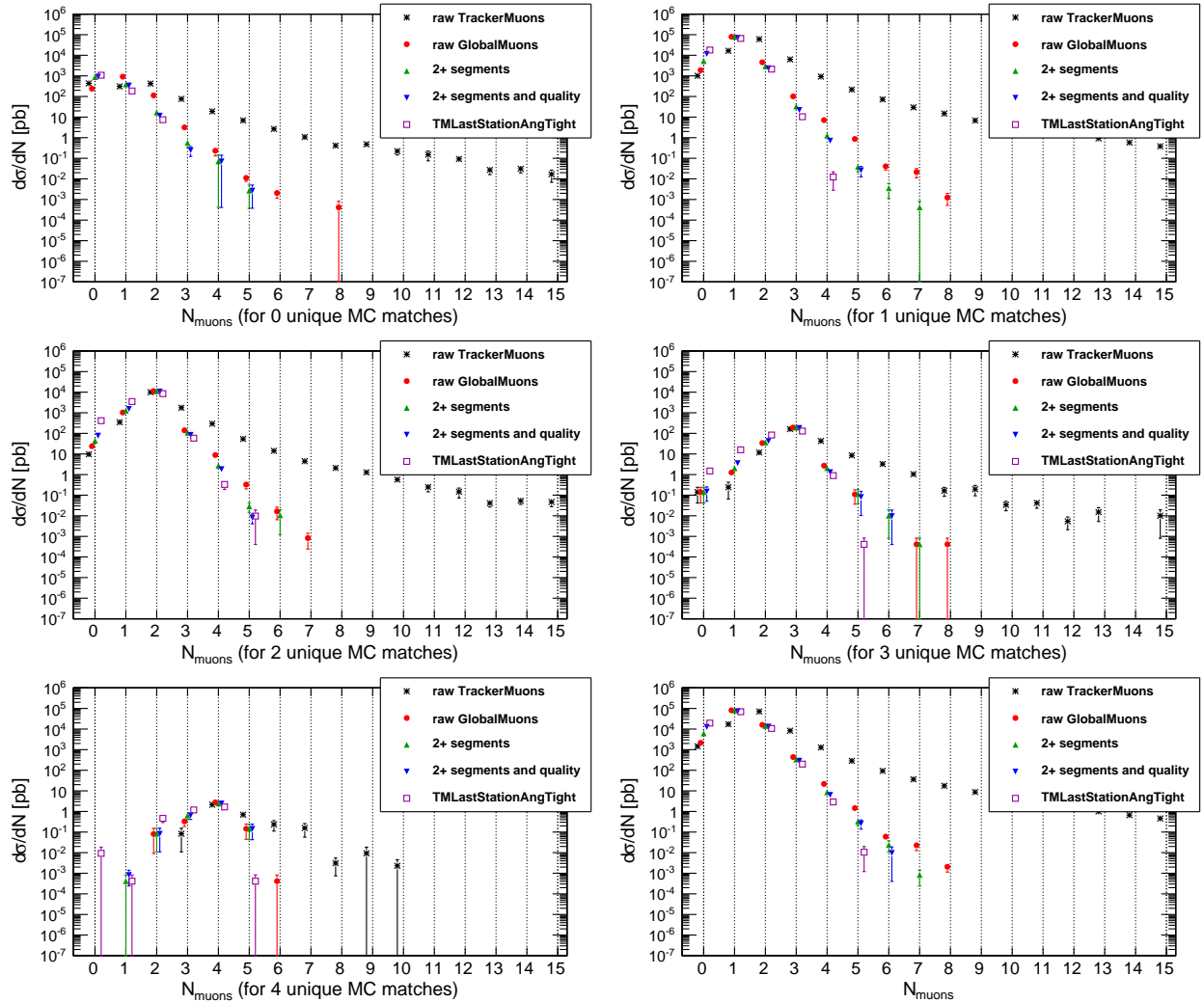


Figure 68: A digest of Figs. 65, 66, and 67 on one page.

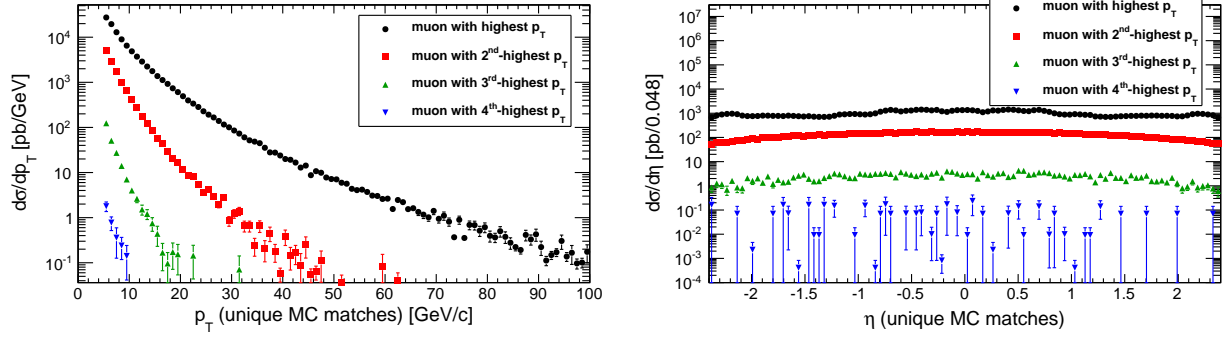


Figure 69: Distribution of p_T and η for the four highest-momentum muons (generator-level).

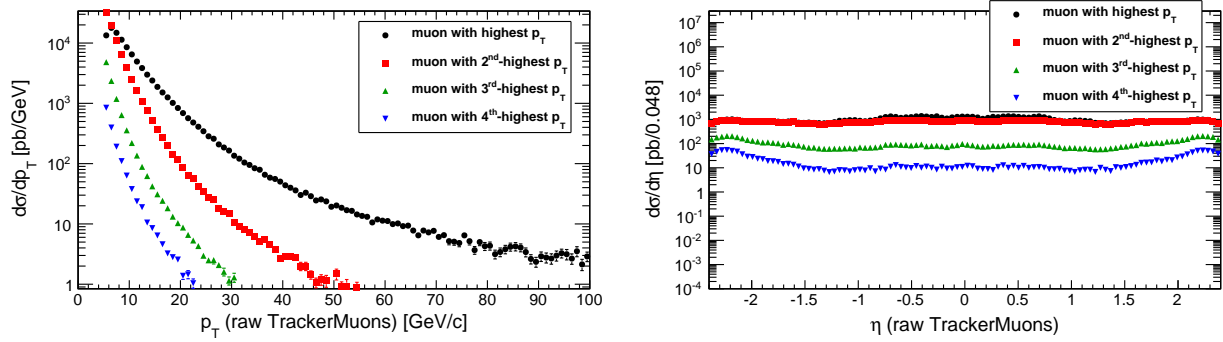


Figure 70: Distribution of p_T and η for the four highest-momentum TrackerMuons.

4.1 Pair-pair mass constraint

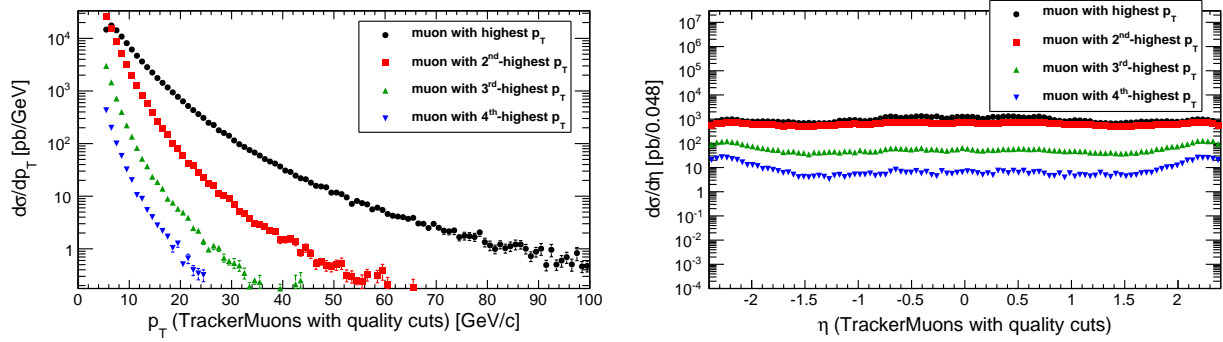


Figure 71: Distribution of p_T and η for the four highest-momentum TrackerMuons with tracker-track quality cuts.

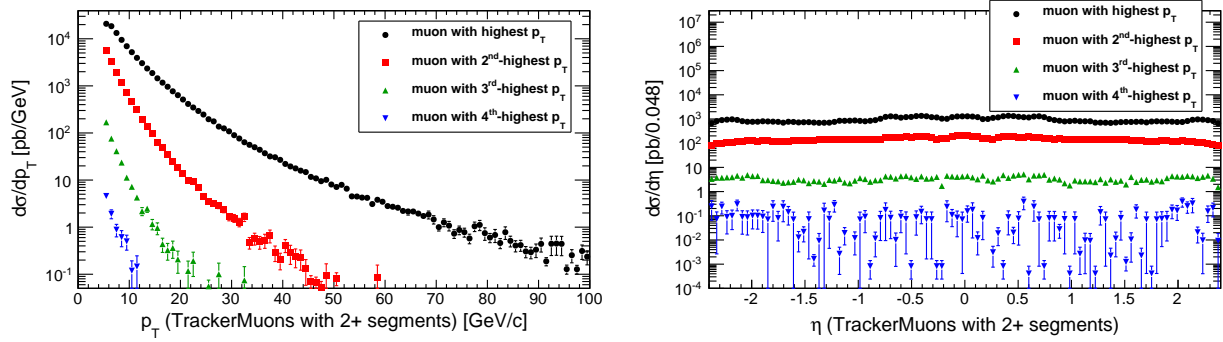


Figure 72: Distribution of p_T and η for the four highest-momentum TrackerMuons with two or more associated muon segments.

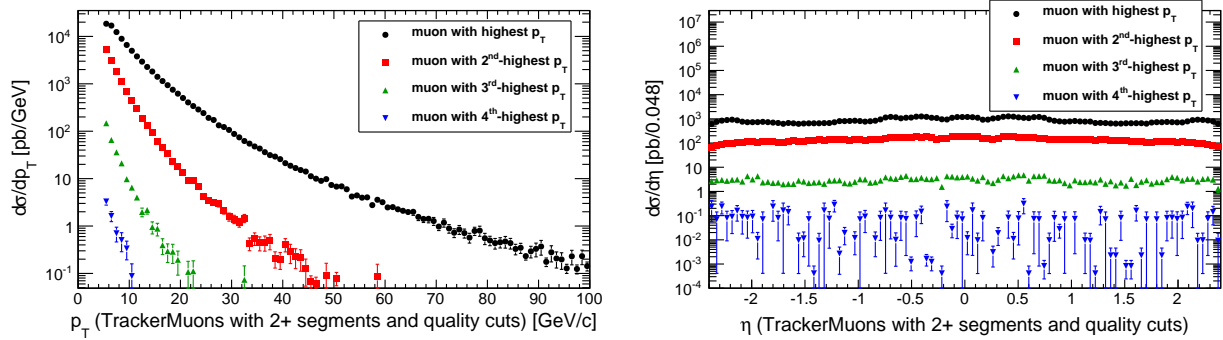


Figure 73: Distribution of p_T and η for the four highest-momentum TrackerMuons with two or more associated muon segments and tracker-track quality cuts.

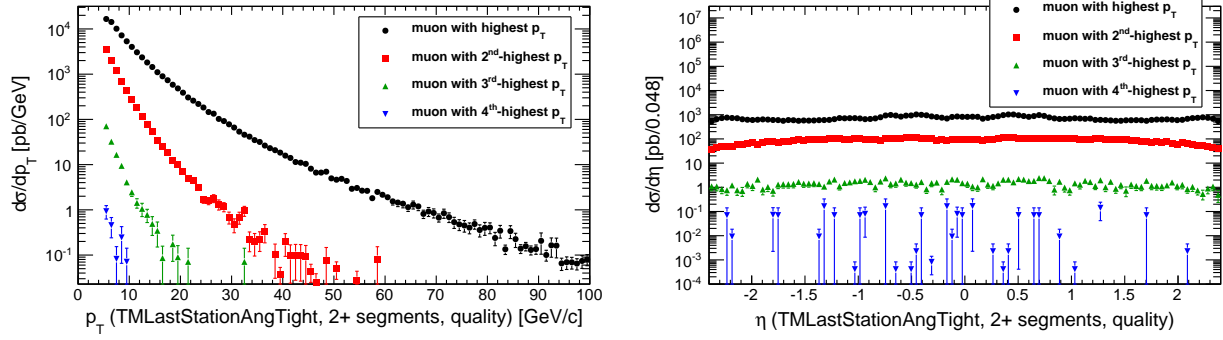


Figure 74: Distribution of p_T and η for the four highest-momentum TrackerMuons with two or more associated muon segments, tracker-track quality cuts, and the TMLastStationAngTight selector.

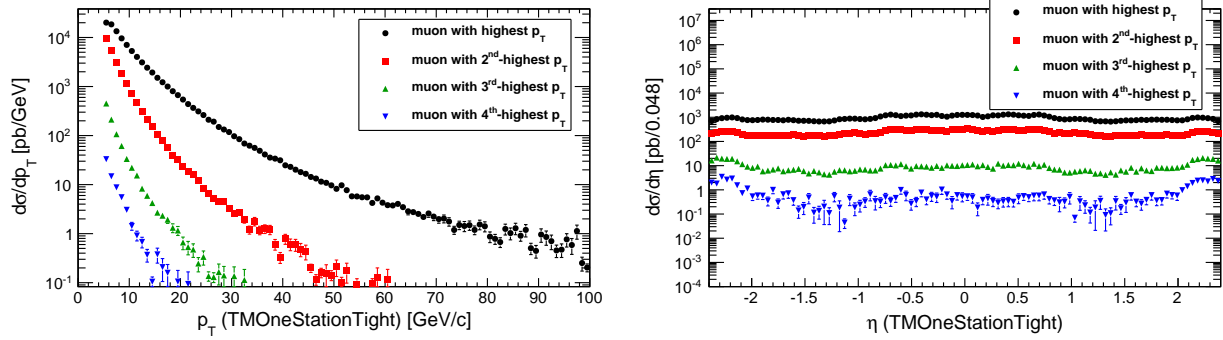


Figure 75: Distribution of p_T and η for the four highest-momentum TrackerMuons with the TMOneStationTight selector.

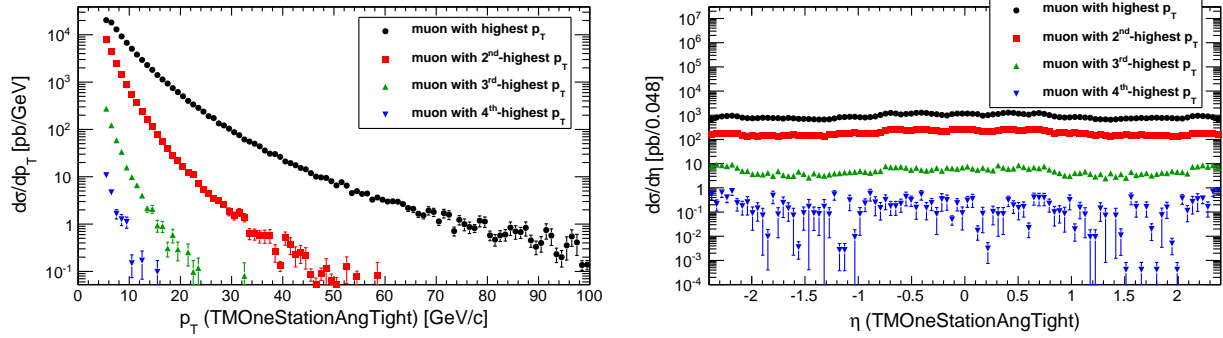


Figure 76: Distribution of p_T and η for the four highest-momentum TrackerMuons with the TMOneStationAngTight selector.

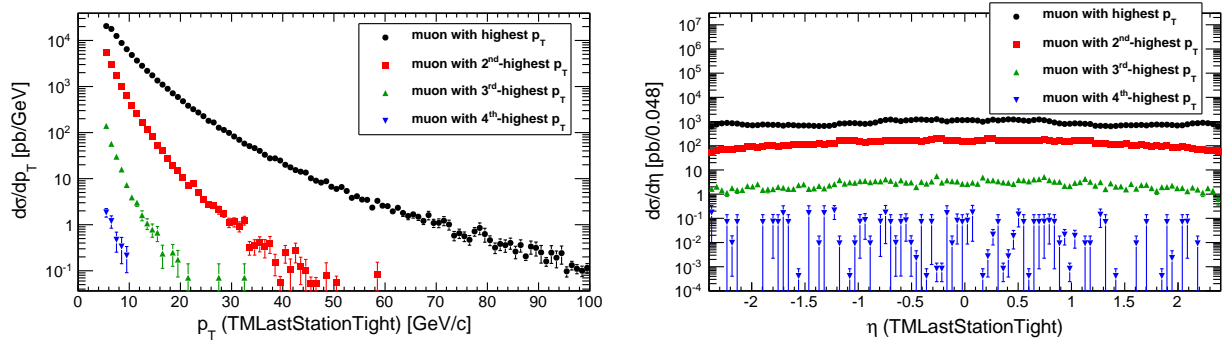


Figure 77: Distribution of p_T and η for the four highest-momentum TrackerMuons with the TMLastStationTight selector.

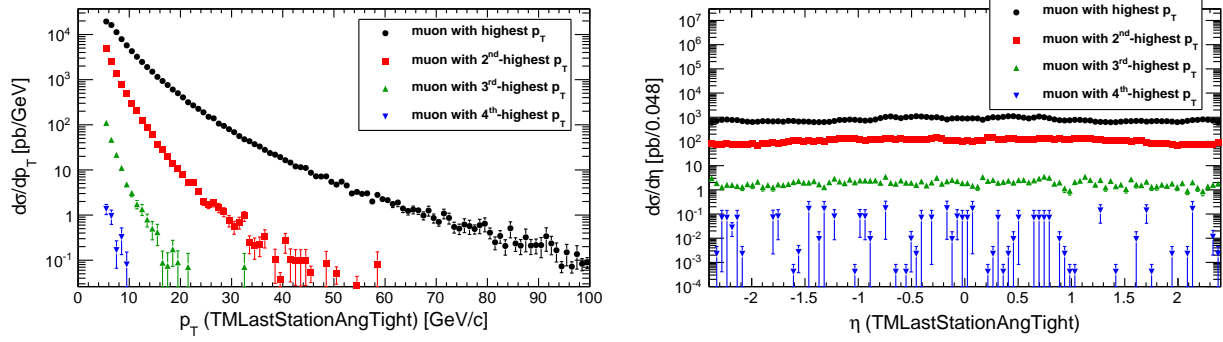


Figure 78: Distribution of p_T and η for the four highest-momentum TrackerMuons with the TMLastStationAngTight selector.

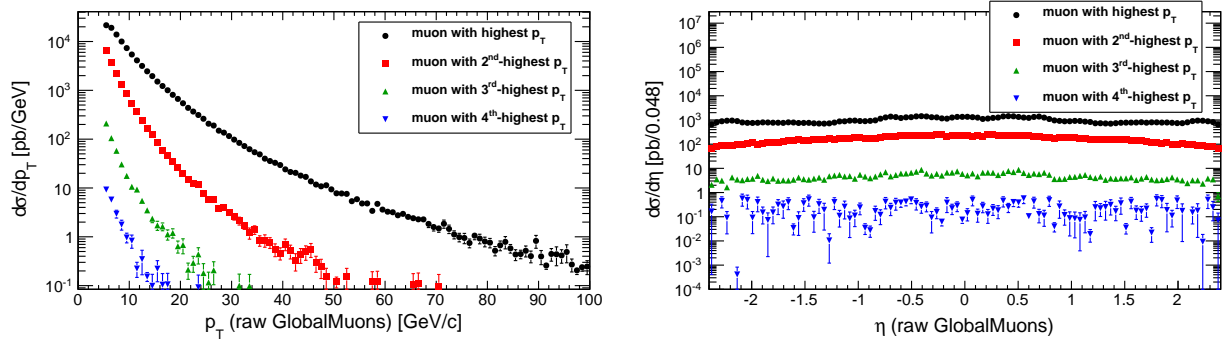


Figure 79: Distribution of p_T and η for the four highest-momentum GlobalMuons.

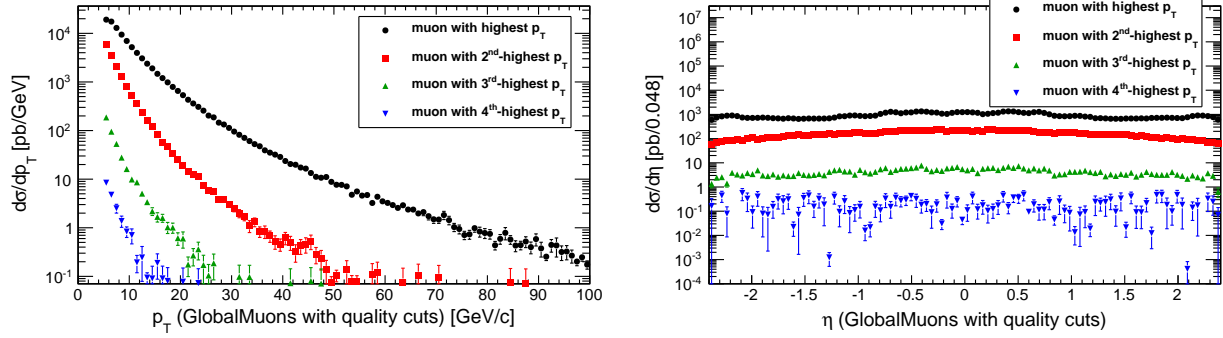


Figure 80: Distribution of p_T and η for the four highest-momentum GlobalMuons with tracker-track quality cuts.

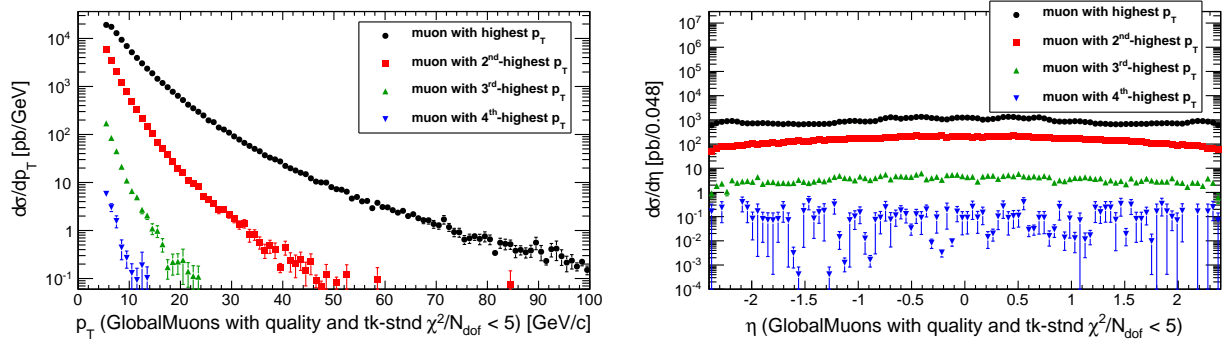


Figure 81: Distribution of p_T and η for the four highest-momentum GlobalMuons with tracker-track quality cuts and tracker-track/StandAloneMuon $\chi^2/N_{\text{dof}} < 5$.

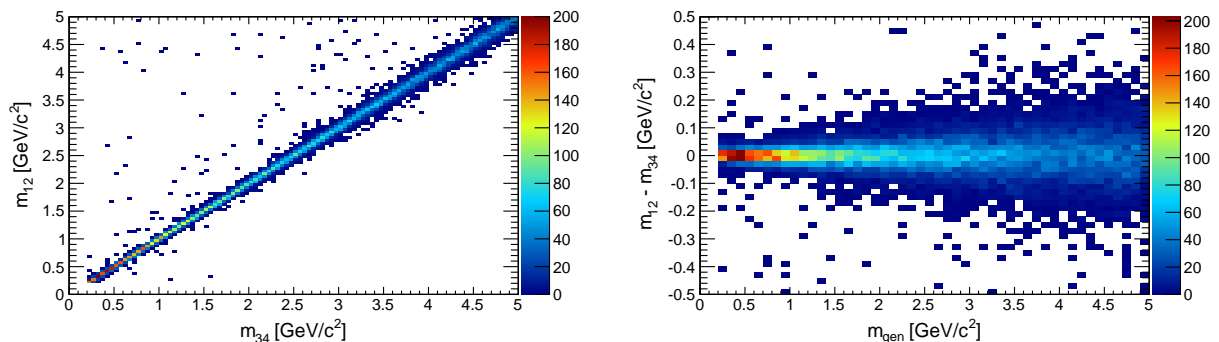


Figure 82: Reconstructed mass resolution from a jet-gun sample with two independently-generated dimuons of the same mass m_{gen} . The muon-jets have reconstructed masses m_{12} and m_{34} , respectively.